SOME ASPECTS OF GYROSCOPE STABILITY AND DYNAMIC RESPONSE

Thesis presented to the

UNIVERSITY OF GLASGOW

Faculty of Engineering

For the Degree of Doctor of Philosophy

by

E. J. JOSS, B. Sc., A. M. I. Mech. E.

ProQuest LLC.
789 East Eisenhower Parkway
P.O. Box 1346
Ann Arbor, MI 48106 – 1346

Some Aspects of Gyroscope Stability and Dynamic Response

Summary

The thesis describes the results of some investigations into the causes of instability in free gimbal-mounted gyroscopes. Considerable use has been made of analogue and digital computation to isolate the effects of various types of reaction forces which may occur in the spin axis bearings, and the effect of rotor asymmetry is also considered.

Rotor asymmetry and variation of radial stiffness in the spin axis bearings were both found to give rise to linear differential equations with periodic coefficients, and an analytical procedure of general applicability has been developed for obtaining the width of the unstable zones and the degree of instability at the parametric resonances. This procedure gives excellent agreement with the results of direct computer solution of the equations of motion.

Slackness in the spin axis bearings of a gyroscope did not appear, per se, to produce instability. It may do so, however, as a secondary effect since forces which otherwise would be negligible become significant when other restraints on shaft displacement are removed.

Tangential forces in the spin axis bearings in either direction were

found to produce instability but different modes of vibration were excited according to the direction of the forces.

The effect of cage accelerations in the spin axis bearings has been considered and has been shown to be small. Likewise, transverse couples which arise due to non uniformity of the motor magnetic field when the rotor tilts relative to the stator, have been shown to be negligible.

Shaft and bearing compliance has also been considered, mainly from the point of view of natural frequency and frequency response to externally applied torques.

Bearing eccentricity has been shown to cause a forced nutation at the frequency of rotation of the ball cage, giving rise to a simple resonance if this frequency should coincide with a natural frequency of the gyro.

Experimental work has been carried out with a view to establishing the nature of the dynamic forces and deflections in the spin axis bearings. Because these are of such small amplitude and of such a complex waveform, analysis of the experimental results has proved difficult. Sinusoidal forcing of a casing containing a gyro rotor in order to obtain the frequency response of the shaft and bearing deflections was moderately successful while the rotor was stationary but no readings were possible with the rotor running because of a seemingly random variation in the response.

CONTENTS

CHAPTER 1.

INTRODUCTION.

1.1. Description of the Problem

This work was initiated following the publication of a paper by Quartley[1] in which is described a series of experiments on a model gyroscope with the effective gimbal inertia artificially increased.

This model work was carried out because of the occurrence of self sustained nutation in a gyro forming part of a radar device. For security reasons no details of this gyro could be released but the self sustained nutation at, or very near to, the natural frequency is said to have appeared after modification of a previously satisfactory gyroscope. The modifications consisted of the addition of torque motors and pick offs to the gimbals, lowering the natural frequency of the gyro by a factor of two to three. The instability was also associated with slackness in the spin axis bearings, but even with the bearings tight the damping of a nutational oscillation was less than would be expected from measurements of friction at the gimbal bearings.

The existence of such a problem was confirmed during discussions between the writer and members of staff at Messrs. Ferranti Ltd., Edinburgh where similar trouble had been experienced during the "Anglicisation" of

a Kearfott gyro of American design.

In this case the natural frequency of nutation was considerably lower than expected, by some 25%. During the discussion this gyro was referred to several times as having an angular momentum of 5 million c.g.s. units at 400 rev/sec. but calculation of the polar moment of inertia of the rotor gave this result only if the recess for the stator coils was neglected. The reduction in inertia due to the recess was of the order of 25%. Since the nutation frequency is proportional to rotor angular momentum it seems possible (but scarcely credible) that the discrepancy in natural frequency was due to an error in calculating the polar moment of inertia of the motor.

On the basis of these interesting, but rather vague, descriptions of a problem it was decided to study the behaviour of the gimbal mounted gyroscope under a variety of conditions.

1.2. General Approach

The first approach to the problem was to build simulations of the problem, of various degrees of complexity, on an analogue computer. Although this work was restricted by lack of computing equipment it gave invaluable help in visualising the behaviour of the system and illustrating the interaction of the different variables involved.

Once an appreciation of the behaviour of a given system had been obtained more detailed work was usually done by digital computation. This

proved rather time consuming but gave more reliable results.

In the analysis of the problem the equations of motion of the system could be simplified considerably since the vibrations to be studied were of small amplitude - ($\frac{1}{4}$ degree was quoted as a bad case for the Kearfott-Ferranti Mk VI gyro). Hence moments of inertia could be regarded as constants, and the equations linearised by the usual small angle approximations sin $\theta \doteq \theta$ and cos $\theta \doteq 1$. A further simplification was made by assuming the oscillations to take place about a zero position in which the spin axis and gimbal axes were mutually at right angles. The rotor centre of gravity and that of the inner gimbal were assumed to be at the intersection of the gimbal axes, and products of inertia were assumed to be zero.

1.3 Definition of axes and basic equations.

Allowance is made in the analysis for displacement of the rotor axis relative to its equilibrium position in the inner gimbal. It is assumed, however, that this displacement consists of rotation only with no translation of the rotor centre of gravity from the intersection of the gimbal axes. This introduces two more degrees of freedom into the usual simple equations describing nutation and permits the introduction of various non linearities and disturbances in the interaction between rotor and inner gimbal. Fig. 1. shows the configuration

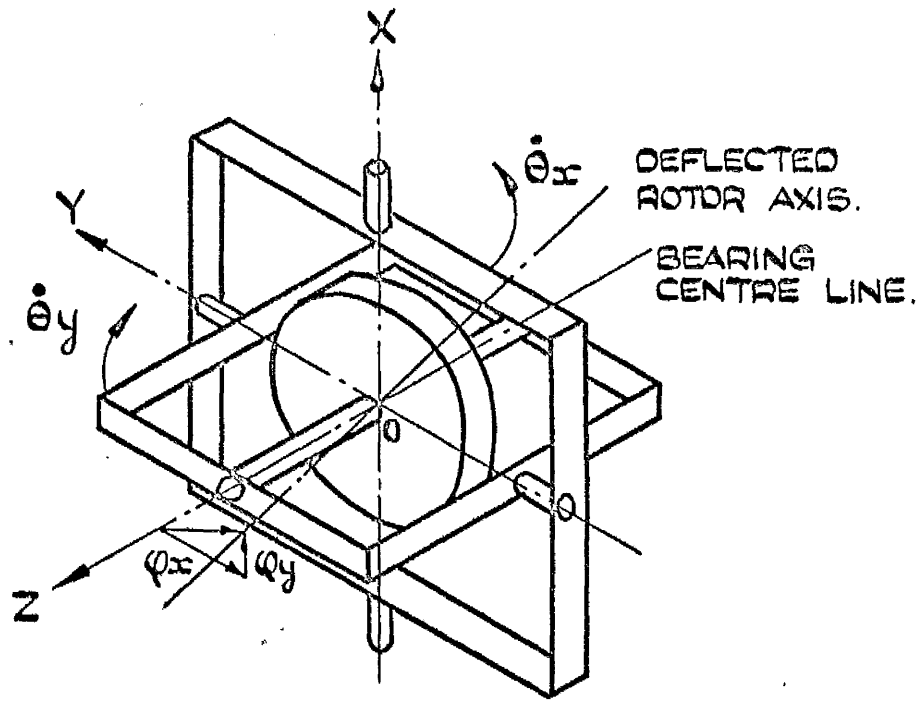

DEFINITION OF AXES & VARIABLES.

FIG. 1

of the gyro and the axes OX, OY, OZ which are fixed in space. Axis OX is the outer gimbal axis and in the zero displacement condition OY and OZ coincide with the inner gimbal axis and spin axis respectively. Θ_x and Θ_y are displacements of the gimbals about OX and OY respectively, while φ_x and φ_y are displacements of the rotor spin axis relative to the gimbals. The absolute displacements of the rotor spin axis are therefore $\Theta_x + \varphi_x$, and $\Theta_y + \varphi_y$.

The equations of motion in a general form are:-

$$I[\ddot{\Theta}_x + \ddot{\varphi}_x] + J\Omega[\dot{\Theta}_y + \dot{\varphi}_y] + T_{1x}(t, \varphi_x, \dot{\varphi}_x, \varphi_y, \dot{\varphi}_y) + T_{2x}(t) = 0$$

$$I[\ddot{\Theta}_y + \ddot{\varphi}_y] - J\Omega[\dot{\Theta}_x + \dot{\varphi}_x] + T_{1y}(t, \varphi_x, \dot{\varphi}_x, \varphi_y, \dot{\varphi}_y) + T_{2y}(t) = 0 \qquad (1.1)$$

$$M_x \ddot{\Theta}_x - T_{1x}(t, \varphi_x, \dot{\varphi}_x, \varphi_y, \dot{\varphi}_y) + T_{3x}(t, \Theta_x, \dot{\Theta}_x) = 0$$

$$M_y \ddot{\Theta}_y - T_{1y}(t, \varphi_x, \dot{\varphi}_x, \varphi_y, \dot{\varphi}_y) + T_{3y}(t, \Theta_y, \dot{\Theta}_y) = 0$$

where I = transverse moment of inertia of the rotor

J = polar moment of inertia of the rotor

M_x = moment of inertia of inner and outer gimbal about OX

M_y = moment of inertia of inner gimbal about OY

Ω = angular velocity of spin of the rotor (assumed constant)

$T_{1x,y}$ = torques about OX, OY transmitted from rotor to gimbals via the spin axis bearings and magnetic field of motor.

$T_{2x,y}$ = out of balance torque on rotor about OX, OY

$T_{3x,y}$ = torques at gimbal bearings and external forcing torques.

The symbols in round brackets indicate the variables on which T_1, T_2, T_3 may depend.

All the subsequent analyses relate to particular cases of the equations set down above, except for the cases in which the rotor is unsymmetrical.

1.4 Review of literature.

There is very little literature directly concerned with the particular problem of self sustained oscillations in gyroscopes.

Only the papers of Quartley[1] and Prentis[2] deal with the influence of the spin axis bearings on stability, while that of Magnus[3] deals with instability due to an unsymmetrical rotor. An interesting paper by Kharlamov[4] discusses the effects of different forms of rotor drive in an astatic three gimbal gyroscope, but the question of stability is not considered.

However, if the gimbal suspension of the gyroscope is disregarded and attention is focussed on the vibration of a rotating body in bearings there is a vast amount of literature available, some concerned with whirling due to shaft elasticity, and some concerned with the influence of bearing reactions on shaft vibration.

In this latter group the majority of the work has been done on journal

bearings, both oil and gas lubricated, but a certain amount of literature exists concerned with the effect of ball bearings on shaft vibration.

Since this thesis is concerned primarily with ball bearing gyroscopes, discussion will be limited to those papers concerned with ball bearings, or the vibrations of shafts supported by ball bearings.

The author who has made the largest contribution in this field is probably Yamamoto[5,6]

In his 1954 paper[5] he deals mainly with the vibration of a simple vertical shaft carrying a single large diameter rotor and supported in double row self aligning bearings.

Five main topics are discussed, viz.

(1) Synchronous backward whirl.

(2) Forward whirl at the ball cage frequency.

(3) Backward whirl due to radial stiffness variation in the bearings.

(4) Various small amplitude vibrations due to manufacturing errors in the bearings.

(5) The effect of bearing clearance in producing jump phenomena.

Yamamoto showed that synchronous backward precession, or reverse whirl at the rotational speed of the shaft, occurred only when the rotor was offset axially from midspan and the bearing pedestals had different stiffnesses in two directions at right angles.

Forward precession at the ball cage frequency was caused by bearing

eccentricity due to difference in ball diameters, this being similar to the case discussed in Sec.6.6. of this thesis.

The backward precession due to radial stiffness variation in the bearings occurred at the frequency $2\omega_1 - \Omega$ where ω_1 is the ball cage speed and Ω the shaft speed. This difference frequency occurred because of the presence of out of balance forces and couples, but in the absence of these the system is analogous to that dealt with in Chapter 7 of this thesis.

Whereas the previous three types of vibration were of large amplitude (0.020 in. approx. at resonance), smaller amplitude vibrations were also noted, particularly at frequencies of $3\omega_1$ and $4\omega_1 - \Omega$, and these were shown to be due to ovality of the ball races, combined with unequal ball diameters.

Yamamoto's final chapter shows the effects of bearing slackness in producing jump phenomena. The "hard spring" characteristic of the slack bearing produced the usual form of resonance curve, having a downward jump with increasing frequency.

In his 1957 paper Yamamoto[6] deals with a shaft carrying a single rotor and supported in single row radial bearings in place of the self aligning bearings used in his previous (1954) work. These bearings placed restraint on shaft deflection, converting the shaft in very approximate terms from the simply supported to the fixed end condition. Due to clearance and compliance

in the bearing the restraining moment/shaft slope characteristic is approximately bi-linear as in Fig.2. Due to misalignment of the bearing housing bores, the undeflected shaft centre line may not lie in the centre of the clearance cone and Yamamoto lists no fewer than 25 possible forms of the combined stiffness characteristics of a pair of bearings. Since the rotor was offset from mid-span, the system had four degrees of freedom corresponding to lateral deflection and tilt of the rotor, each in two planes at right angles. There were therefore four natural frequencies, speed dependent because of the gyroscopic couples.

Yamamoto describes subharmonic oscillations of order $\frac{1}{2}$ and "Summed and differential harmonic oscillations". These are parametric resonances which occur at speeds satisfying the relation $pi \pm pj = \Omega$ where pi and pj are any two of the natural frequencies and Ω is the shaft speed. The vibrations of order $\frac{1}{2}$ occur when $i = j$.

These resonances did not occur in his earlier work with self aligning bearings and were therefore due to the restraint imposed on shaft deflection by the single row radial bearings. It was found that the speeds at which the resonances occurred were different after dismantling and reassembly, indicating that misalignment was a relevant factor.

In a theoretical discussion of the vibrations Yamamoto assumes a non-linear restoring action at the bearings to be present in the x direction of

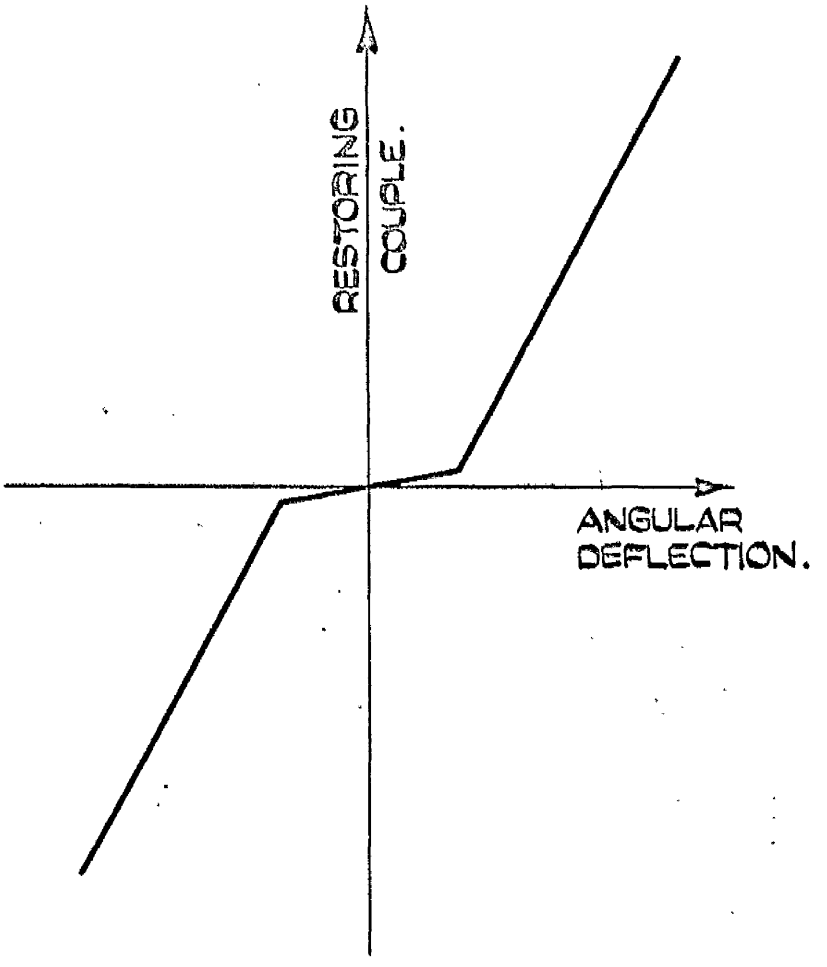

RESTORING COUPLE OF SINGLE ROW
DEEP GROOVE BALL BEARING.

FIG. 2

deflection, but not in the y direction, and later shows that the non-linear action must contain periodic terms at shaft rotation frequency in order to excite sub-harmonic resonance.

The jump phenomenon was also found to be present in the subharmonic resonances, and was again of the "hard spring" type - i.e. a downward jump in amplitude for increasing frequency.

Synchronous backward whirl was also noted at two speeds, and the amplitude was found to be influenced by

(a) type of bearing.

(b) directional non uniformity of pedestal stiffness.

(c) bearing fit.

With tightly fitted, self aligning bearings, and uniformly stiff pedestals, this type of whirl was almost entirely suppressed but was always present with single row radial bearings, irrespective of the tightness of the bearing fit or the rigidity of the pedestals.

The stiffness variation which causes the parametric resonance may arise in the bearing or in the pedestal. In the bearing, the stiffness variation may be due to variation in clearance, and this variation is reduced to zero if the fit of the outer ring in the housing is so tight that clearance is zero in all directions. Bearing stiffness variation may also be due to misalignment of the bearing housings, unless self aligning bearings are used.

To return to the literature which is more specifically related to gyroscopes, the paper by Magnus[3] takes account of inclination of the inner gimbal from the orthogonal position and in fact takes this inclination as the principal independent variable in considering stability.

Since increasing the inner gimbal inclination reduces the natural frequency of nutation, and the instability is a parametric resonance occurring when the nutation frequency is near to the spin frequency, this type of instability can only arise when the gimbals are light and the rotor is short axially in comparison with its diameter.

The papers of Quartley and Prentis are based on assumptions of spin axis bearing reactions more appropriate to hydrodynamic bearings than to ball bearings and indeed practically all of the work described by Quartley was carried out on a model in which a small gyroscope was coupled via a plain bearing to a large gimbal mounted mass representing the effect of added gimbal inertia. While Prentis shows that these assumptions result in a behaviour resembling that of the original troublesome ball bearing gyro it is not yet clear how tangential forces of the requisite magnitude and direction occur in a ball bearing.

The literature concerning ball bearings is almost exclusively devoted to questions of fatigue, lubrication and wear. With particular reference to gyroscopes Stratton[7] describes improved methods of bearing test and selection which have greatly improved bearing reliability. Holmes[8] describes

instability in cage motion which seems to be due to defective lubrication.

Kharlamov[9] develops theoretical expressions for the forces and moments acting on the inner race of an angular contact ball bearing. These expressions indicate that the radial forces are affected by the tilt of the inner race, and that the moments are affected by the radial displacement. When the equations of motion of a rotor supported in a preloaded pair of bearings are obtained, taking account of these interactions, the cross-coupling terms are found to disappear and the effect is simply equivalent to an increase of stiffness.

Theoretical approaches to the problem of parametric resonance in systems described by linear differential equations with periodic coefficients date from Floquet[13] but it is only in comparatively recent years that Malkin[14] has developed reasonably straightforward methods of obtaining the characteristic exponents which define the stability of a system close to a parametric resonance. Malkin's work is discussed more fully in Chapter 8 of this thesis, but the work of Lowis[15] quoted by Parks[16] could perhaps be mentioned here. Lowis follows the classical theory more closely in that he obtains the constant matrix C which relates the state vector of the system at time t, $X(t)$ to the state vector one period later, $X(t + T)$. The latent roots of the matrix C where $X(t + T) = C.X(t)$ must lie within the unit circle if the system is to be stable.

The matrix C is obtained by using a simple first order finite difference

approximation to the differential equations of the system and involves a number of matrix multiplications approximately equal to the chosen number of subdivisions of the period, generally about 30.

A refinement, due to Parks and James, has been described in a private communication. This refinement involves using a Runge-Kutta method of finding the transition matrix and permits the use of a smaller number of subdivisions of the period, about 10 to 20.

The advantage of this method seems to be that it can deal with cases where the amplitude of parameter fluctuation is large compared with the mean value of the parameter. Malkin's method is limited in its straightforward application to the region where μ as defined in equations (8.1.) is small.

CHAPTER 2.

THE EFFECT OF ROTOR ASYMMETRY

This analysis stems from a paper by Magnus[3]. In this paper Magnus considers the effects of rotor asymmetry on the stability of a gimbal mounted gyro and develops a stability criterion in terms of a function $F(\beta)$ where β is the inclination of the inner gimbal from the orthogonal position. The function F also contains the various moments of inertia of gimbals and rotor and if its value should lie between the two ratios

$$\frac{\text{max. or min. transverse rotor inertia}}{\text{polar inertia of rotor}}$$

the system is unstable.

2.1 Analogue solution of Magnus' equations.

In the work described here, the following equations, derived from those numbered (24) in the above paper, were chosen as being suitable for simulation on the limited analogue computer available at the time.

$$\dot{u}_{xr} - a\Omega u_{yr} = \varepsilon\left[(\dot{u}_{yr} + \Omega u_{xr}) \sin 2\varphi - (\dot{u}_{xr} - \Omega u_{yr}) \cos 2\varphi\right] \tag{2.1}$$

$$\dot{u}_{yr} + b\Omega u_{xr} = c\varepsilon\left[(\dot{u}_{xr} - \Omega u_{yr}) \sin 2\varphi + (\dot{u}_{yr} + \Omega u_{xr}) \cos 2\varphi\right]$$

where u_{xr}, u_{yr} are angular velocities of the rotor about the axes Ox_r, Oy_r. These axes are fixed to the rotor and are the axes of maximum and minimum transverse moment of inertia (See Fig. 3).

Ω is the angular velocity of spin of the rotor and a, b, c, ε are certain functions of the rotor and gimbal inertias.

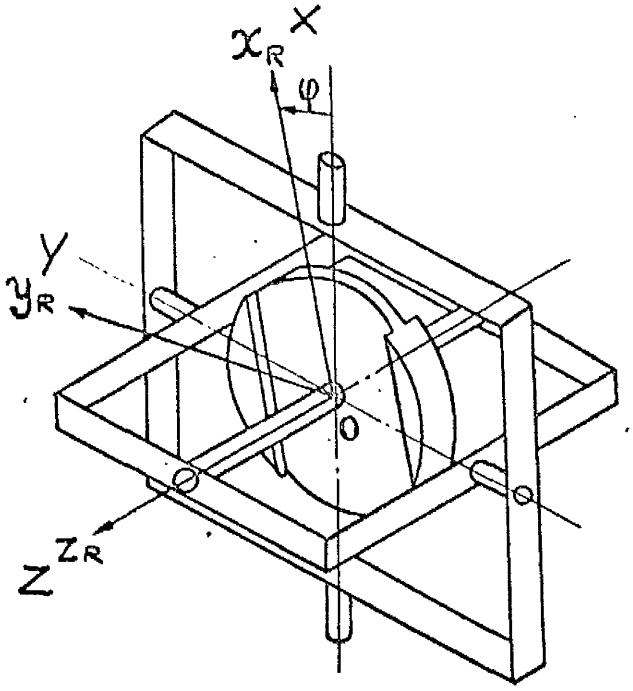

GYROSCOPE WITH UNSYMMETRICAL ROTOR
"FIXED-TO-ROTOR" AXES, USED BY MAGNUS.

FIG 3

φ is the displacement of the rotor about the z_r axis and can be taken as Ωt.

For the purpose of the computer investigation the following assumptions were made:-

$$\frac{I_{xr}}{J} = 0.6 \qquad \frac{I_{yr}}{J} = 0.5$$

$$\frac{\text{"Transverse" inertia of each gimbal}}{J} = g$$

$$\frac{\text{"Polar" inertia of inner gimbal}}{J} = 2g$$

This leads to the following values for the coefficients:-

$$a = (2g - 0.5)/(2g + 0.6)$$

$$b = (2g - 0.4)/(2g + 0.5)$$

$$\varepsilon = g/(2g + 0.6)$$

$$c\varepsilon = g/(2g + 0.5)$$

In the computer diagram Fig.4 the velocities v_{xr} and v_{yr} are abbreviated to x and y respectively. Switches are provided to allow for changes in sign and scale in a and b. Servo multipliers M_1 and M_2 are connected to a 3 amplifier oscillator loop to give the sin $2\Omega t$ and cos $2\Omega t$ terms.

2.2. Results of Simulation

A series of runs was taken for increasing values of the gimbal

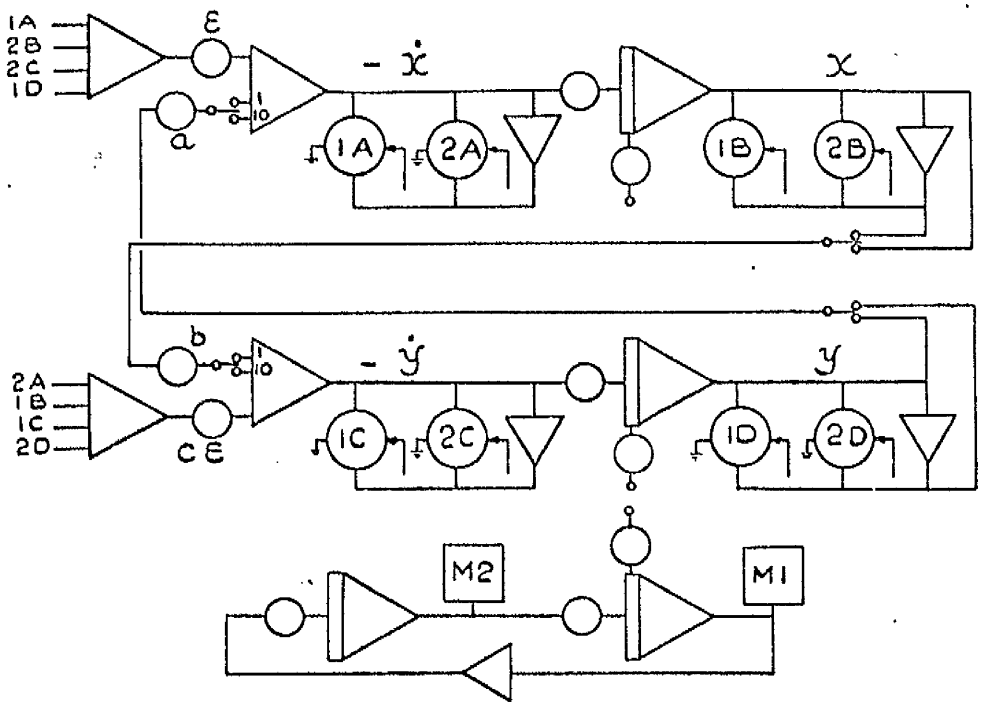

COMPUTER SET UP FOR MAGNUS'S EQUATIONS.

FIG. 4.

inertia parameter g and Figs.5a - 5c show three results in which u_{yr} is plotted against u_{xr}. For $g = 0$ a circular plot is obtained as would be expected since ϵ and $c\epsilon$ both become zero and a simple harmonic nutation of frequency $\Omega\sqrt{ab}$ is obtained.

As g is increased the plot becomes hypotrochoidal in nature, the x and y wave forms containing a main low frequency component of frequency ω^1 with a superimposed ripple of frequency $2\Omega+\omega^1$. In addition the amplitude ratio x/y of the main components becomes steadily smaller, the plot becoming more and more elongated horizontally. The ellipse is traversed in an anticlockwise direction.

For $0.21 < g < 0.28$ the plots have an unstable saddle point form, and as g increases across the unstable region the separatrices between the four possible modes of motion change from a $\asymp$ configuration to X. In the unstable region the ripple frequency is 2Ω.

For $g > 0.28$ the plots are epitrochoidal in nature, with the low frequency ellipse being traversed clockwise. The ellipse is elongated vertically at first and as g increases from 0.28 the amplitude ratio x/y of the main component increases from zero. For high values of gimbal inertia the plots lose their well defined "ellipse + ripple" shape and become a series of interlacing, non repetitive trajectories. The low frequency ω^1

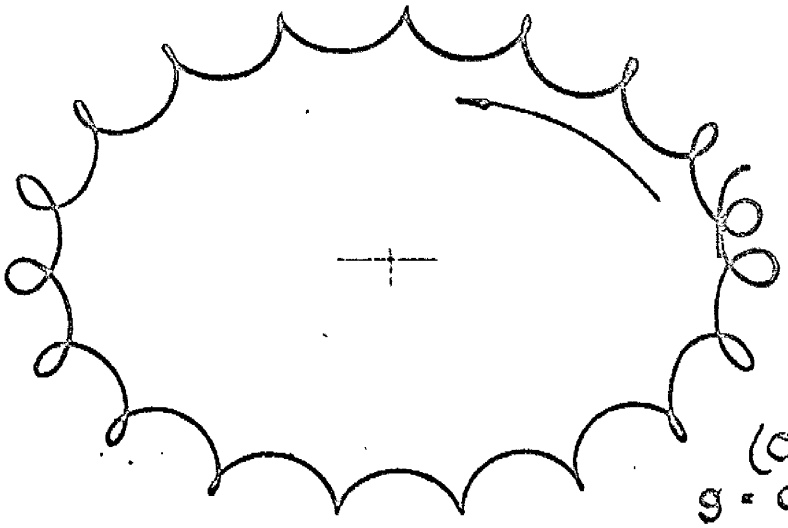

(a)
g = 0·175

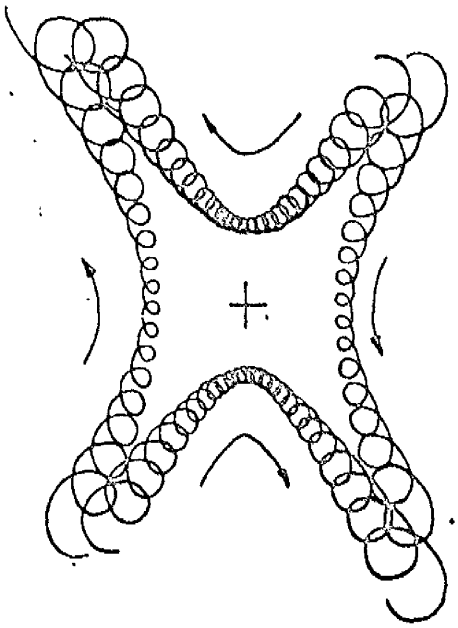

(b)
g = 0·25

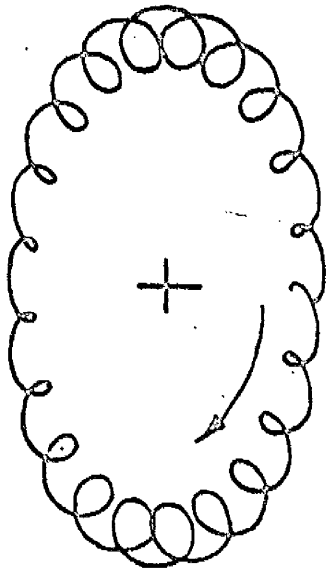

(c)
g = 0·3

FIG. 5

COMPUTER SOLUTIONS OF MAGNUS'S EQUATIONS

can be regarded as negative for $g \geq 0.28$ and the ripple frequency can then still be written as $2\Omega + \omega^1$.

2.3. Analysis of results - Stable Region.

To obtain a physical picture of the motion of the gyroscope an axis transformation is required to convert from the xr, yr axes, which are fixed to the rotor, to a fixed set of axes. In effect this superimposes an angular velocity $+\Omega$ on the radius vector of the $u_{xr} - u_{yr}$ plots. Inspection of plots in the stable region suggest solutions in the following form:-

$$\begin{aligned} u_{xr} &= X \cos \omega^1 t - x \cos (2\Omega + \omega^1)t\,(1 + a \cos 2\,\omega^1 t) \\ u_{yr} &= Y \sin \omega^1 t + y \sin (2\Omega + \omega^1)t\,(1 + a \cos 2\,\omega^1 t) \end{aligned} \qquad (2.2)$$

X, Y are the amplitudes of the main oscillation, while x, y are the mean amplitudes of the ripple. The quantity a is the amplitude of the modulation in the ripple which is noticeable only near the unstable region.

This can be rewritten:-

$$\begin{aligned} u_{xr} &= X \cos \omega^1 t - x \cos (2\Omega + \omega^1)t - \frac{ax}{2} \cos (2\Omega + 3\omega^1)t - \frac{ax}{2} \cos (2\Omega - \omega^1)t \\ u_{yr} &= Y \sin \omega^1 t + y \sin (2\Omega + \omega^1)t - \frac{ay}{2} \sin (2\Omega + 3\omega^1)t + \frac{ay}{2} \sin (2\Omega - \omega^1)t \end{aligned} \qquad (2.3)$$

or,

$$\begin{aligned} u_{xr} + j u_{xr} = {} & Ae^{j\omega^1 t} + Be^{-j\omega^1 t} + Ce^{j(2\Omega+\omega^1)t} + De^{-j(2\Omega+\omega^1)t} + Ee^{j(2\Omega+3\omega^1)t} \\ & + Fe^{-j(2\Omega+3\omega^1)t} + Ge^{j(2\Omega-\omega^1)t} + He^{-j(2\Omega-\omega^1)t} \end{aligned}$$

where $A + B = X$ $\quad A - B = Y$ $\quad A = \frac{X+Y}{2}$ $\quad B = \frac{X-Y}{2}$

$C + D = -x$ $\quad C - D = y$ $\quad C = \frac{-x+y}{2}$ $\quad D = \frac{-x-y}{2}$

$E + F = \frac{-ax}{2}$ $\quad E - F = ay/2$ $\quad E = \frac{a(-x+y)}{2}$ $\quad F = \frac{-a(x+y)}{2}$

$G = E$ $\quad H = F$

The axis transformation can be expressed as follows,

$$u_x + j u_y = (u_{xr} + j u_{yr}) e^{j\Omega t} \tag{2.4}$$

where u_x and u_y are the angular velocity components of the rotor relative to fixed axes.

i.e. $u_x + j u_y = Ae^{j(\Omega + \omega^1)t} + Be^{j(\Omega - \omega^1)t} + Ce^{j(3\Omega + \omega^1)t} + De^{-j(\Omega + \omega^1)t}$

$$+ Ee^{j(3\Omega + \omega^1)t} + Fe^{-j(\Omega + 3\omega^1)} + Ge^{j(3\Omega - \omega^1)t} + He^{-j(\Omega - \omega^1)t} \tag{2.5}$$

Since the ripple amplitudes are about 5 - 10% of the main amplitudes, C, E and G will be negligible, leaving

$$u_x + j u_y = Ae^{j(\Omega + \omega^1)t} + De^{-j(\Omega + \omega^1)t} + Be^{j(\Omega - \omega^1)t} + He^{-j(\Omega - \omega^1)t}$$

$$+ Fe^{-j(\Omega + 3\omega^1)t} \tag{2.6}$$

i.e.

$$u_x = (A + D)\cos \omega_n t + (B + H)\cos(\omega_n - 2\omega^1)t + F\cos(\omega_n + 2\omega^1)t$$

$$u_y = (A - D)\sin \omega_n t + (B - H)\sin(\omega_n - 2\omega^1)t - F\sin(\omega_n + 2\omega^1)t \tag{2.7}$$

where ω_n is the nutation frequency, $\Omega + \omega^1$

or, since $H = F$

$$u_x = (A + D + F\cos 2\omega' t)\cos\omega_n t + B\cos(\omega_n - 2\omega')t$$
$$u_y = (A - D - F\cos 2\omega' t)\cos\omega_n t + B\sin(\omega_n - 2\omega')t \qquad (2.7)$$

In terms of the nutation frequency ω_n and rotor spin frequency Ω these become

$$u_x = \tfrac{1}{2}\left[X + Y - (x+y)(1+a\cos 2(\omega_n - \Omega)t)\right]\cos\omega_n t + \tfrac{1}{2}(X-Y)\cos(2\Omega - \omega_n)t$$
$$u_y = \tfrac{1}{2}\left[X + Y + (x+y)(1+a\cos 2(\omega_n - \Omega)t)\right]\sin\omega_n t + \tfrac{1}{2}(X-Y)\sin(2\Omega - \omega_n)t \qquad (2.9)$$

The major component of this motion is the oscillation with frequency ω_n, with unequal amplitudes in x and y directions, and modulated at a frequency $2(\omega_n - \Omega)$. In addition a component at frequency $2\Omega - \omega_n$ is present but with a smaller amplitude $(X - Y)/2$.

2.4. Analysis of solutions of Magnus' equations by curve-fitting.

Earlier in this work, before the pattern of the solution had become apparent an attempt was made to analyse the results by a curve fitting procedure, using a digital computer. First a Deuce Alphacode programme was written to solve Magnus' equations, and obtain the solutions in a form suitable for further processing. Since the various frequency components are non-commensurate, normal Fourier harmonic analysis is not possible and a 'least squares' method due to Prony[10] was utilised. The sum of the squares of the errors between actual and 'fitted' values of the ordinates is minimised and the smallness of the minimum is a measure of the success of the procedure.

The results of this analysis were not completely satisfactory, probably due to a non-optimum choice of step length in the solution of the equations, but were sufficient to show good agreement between the frequencies obtained by this method and those shown in equations 2.3.

For example the equation obtained by curve fitting for g = 0.1 was as follows:-

$$u_{xr} = e^{-0.0066t}(1.0595 \cos 3.386t - 0.0644 \sin 3.386t)$$
$$+ e^{-0.2170t}(0.0007 \cos 16.46t - 0.0008 \sin 16.46t)$$
$$+ e^{-0.0120t}(0.0005 \cos 23.39t + 0.0052 \sin 23.39t)$$
$$+ e^{-1.4611t}(-0.0003 \cos 31.42t - 0.0004 \sin 31.42t)$$

where Ω has the arbitrary value 10. Taking ω^1 as 3.386, frequencies of approximately $2\Omega + \omega^1$, $2\Omega - \omega^1$ and $2\Omega + 3\omega^1$ are seen to be present.

2.5. Analysis of results - unstable region.

The empirical solutions obtained in Sec.2.3 are concerned with the stable region of the problem.

The unstable region occurred where the value of the low frequency ω^1 in the u_{xr}, u_{yr} waveforms passed through zero. This corresponds in fixed axes to the condition that the nutation frequency is equal to the spin frequency of the rotor, i.e. $\omega_n = \Omega$. Fig.6. shows the nutation frequency

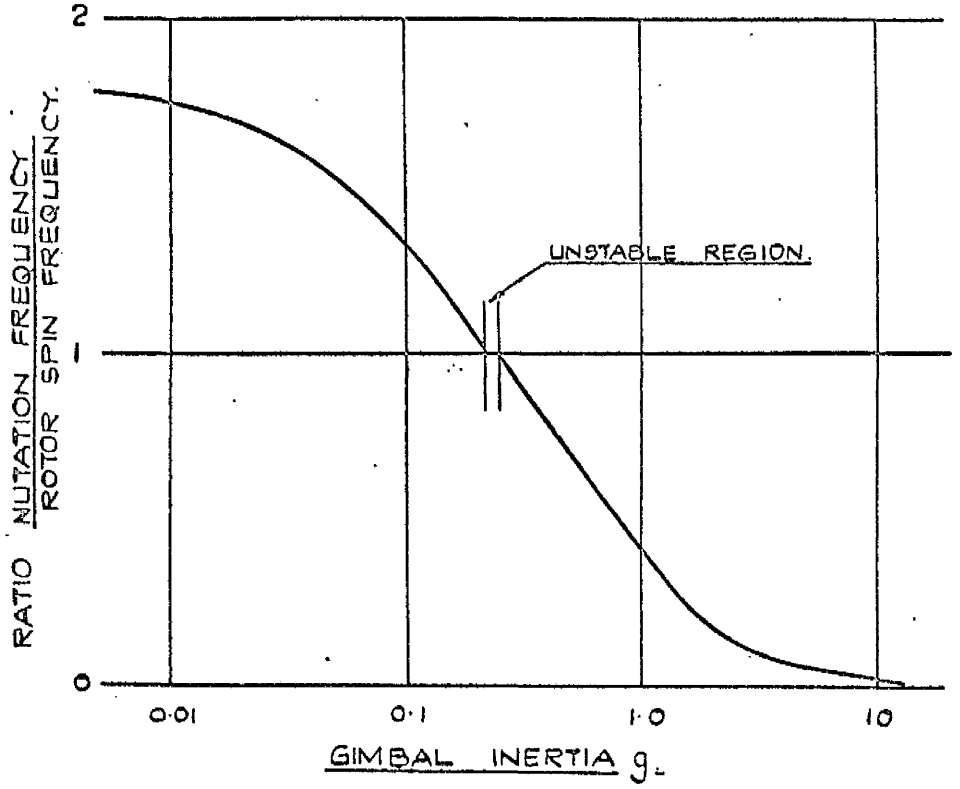

NUTATION FREQUENCY OF AN UNSYMMETRICAL GYRO.

FIG. 6

ω_n plotted to a base of gimbal inertia g and indicates a step at the unstable region.

The saddle point form of the u_{xr}, u_{yr} plots in the unstable region indicates the presence of two exponentials, one with a positive index and one with a negative index. In addition there is a ripple at frequency 2Ω

The solutions would therefore appear to be of the form:-

$$u_{xr} = A_x e^{at}(1 + \frac{ax}{Ax} \cos 2\Omega t) + B_x e^{-bt}(1 + \frac{bx}{Bx} \cos 2\Omega t)$$

$$u_{yr} = A_y e^{at}(a - \frac{ay}{Ay} \sin 2\Omega t) + B_y e^{-bt}(1 - \frac{by}{By} \sin 2\Omega t) \qquad (2.11)$$

giving $u_r = u_{xr} + j u_{yr}$

$$= e^{at}\left[(A_x + j A_y) + a_1 e^{j 2\Omega t} + a_2 e^{-j 2\Omega t}\right]$$

$$+ e^{-bt}\left[(B_x + j B_y) + b_1 e^{j 2\Omega t} + b_2 e^{-j 2\Omega t}\right] \qquad (2.12)$$

where $a_1 + a_2 = a_x \qquad a_1 - a_2 = -a_y$

$b_1 + b_2 = b_x \qquad b_1 - b_2 = -b_y$

Relative to fixed axes,

$$u = u_x + j u_y = e^{j\Omega t} . u_r$$

i.e. $$u = e^{(a + j\Omega)t}(A_x + j A_y) + a_1 e^{j 3\Omega t} + a_2 e^{-j\Omega t}$$

$$+ e^{(-b + j\Omega)t}(B_x + j B_y) + b_1 e^{j 3\Omega t} + b_2 e^{-j\Omega t} \qquad (2.13)$$

i.e.

$$u_x = e^{at}\left[A_x \cos\Omega t + j A_x \sin\Omega t - A_y \sin\Omega t + j A_y \cos\Omega t\right] + a_1 e^{j3\Omega t} + a_2 e^{-j\Omega t}$$
$$+ e^{-bt}\left[B_x \cos\Omega t + j B_y \sin\Omega t - B_y \sin\Omega t + j B_y \cos\Omega t\right] + b_1 e^{j3\Omega t} + b_2 e^{-j\Omega t} \quad (2.14)$$

i.e.

$$u_x = e^{at}(A_x \cos\Omega t - A_y \sin\Omega t) + e^{-bt}(B_x \cos\Omega t - B_y \sin\Omega t) + (a_2+b_2)\cos\Omega t$$
$$+ (a_1 + b_1)\cos 3\Omega t$$
$$u_y = e^{at}(A_x \sin\Omega t + A_y \cos\Omega t) + e^{-bt}(B_x \sin\Omega t + B_y \cos\Omega t) \quad (2.15)$$
$$+ (a_2 + b_2)\sin\Omega t + (a_1 + b_1)\sin 3\Omega t$$

but $a_1 = \frac{a_x - a_y}{2}$ $\qquad a_2 = \frac{a_x + a_y}{2}$

$b_1 = \frac{b_x - b_y}{2}$ $\qquad b_2 = \frac{b_x + b_y}{2}$

$a_{x,y}$ and $b_{x,y}$ are small compared with $A_{x,y}$ and $B_{x,y}$ and hence $a_1 + b_1$ will be negligible, i.e. the 3rd harmonic will have a very small amplitude.

Hence

$$x \doteq e^{at}(A_x \cos\Omega t - A_y \sin\Omega t) + e^{-bt}(B_x \cos\Omega t - B_y \sin\Omega t)$$
$$+ \tfrac{1}{2}(a_x + a_y + b_x + b_y)\cos\Omega t \quad (2.16)$$

$$y \doteq e^{at}(A_x \sin\Omega t + A_y \cos\Omega t) + e^{-bt}(B_x \sin\Omega t + B_y \cos\Omega t)$$

$$- \tfrac{1}{2}(a_x + a_y + b_x + b_y)\sin\Omega t$$

Depending on the initial conditions, it will be possible to have transient oscillations which diverge immediately due to the e^{at} term, or transients which converge at first due to the e^{-bt} term being dominant but which finally diverge as the e^{at} term becomes large.

2.6. Values of the exponents a and b

These were obtained from the analogue computer by feeding either the u_{xr} or the u_{yr} signal into a logarithmic amplifier and recording the output, $\log u_r$, on a strip chart recorder. The mean slope of the trace gave the exponents a and b. The initial condition of the computer run was taken near the extremity of one of the separatrices of the 'saddle-point' diagram (Fig.5b) so that a long run was available with a decreasing signal, giving the negative exponent, followed after an intermediate stage by a portion where the positive exponent was dominant. A typical output from the logarithmic amplifier is shown in Fig.7.

The values obtained for the exponents are shown in Table 1 for various values of the gimbal inertia parameter g.

Table 1/

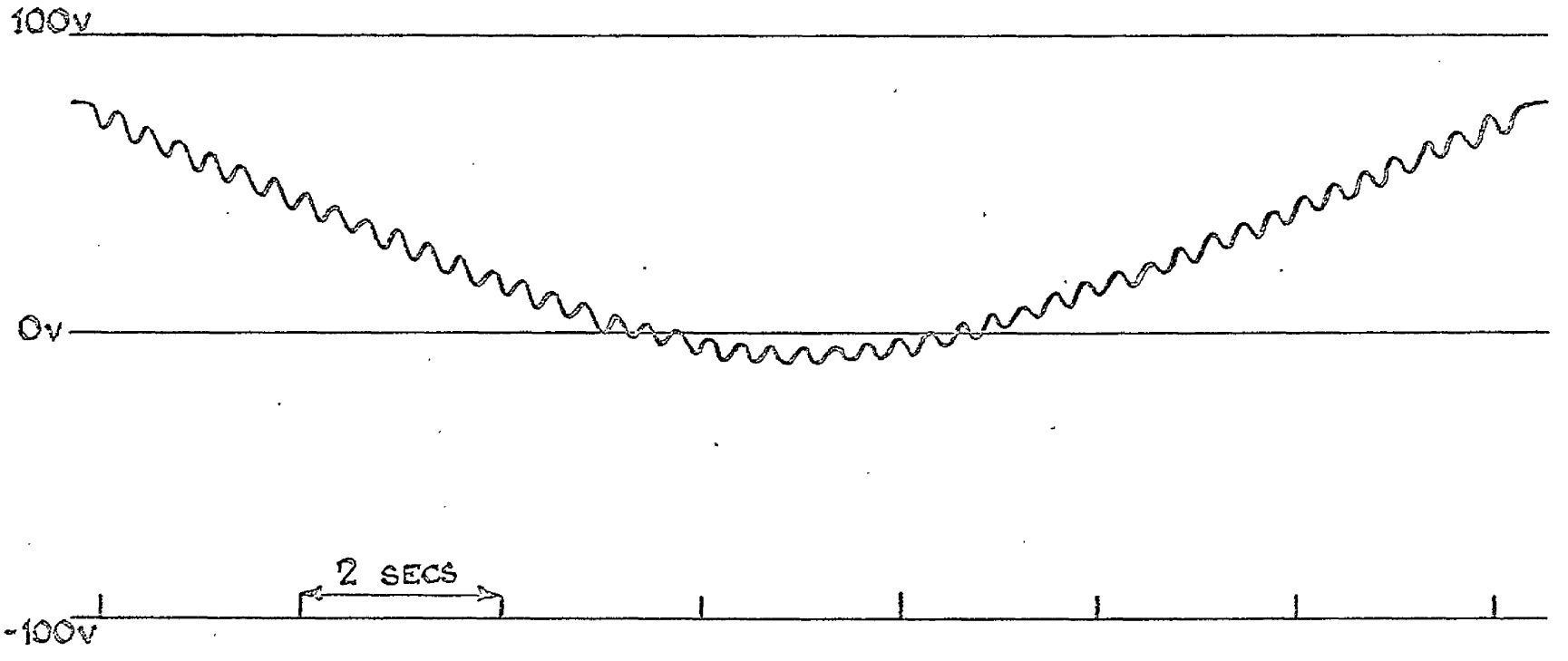

RECORDING FROM LOGARITHMIC AMPLIFIER FOR $g = 0.24$.

FIG. 1

Table 1

g	Exponents (sec^{-1})	
	negative	positive
0.22	0.363	0.380
0.24	0.504	0.475
0.25	0.475	0.445
0.26	0.276	0.317

2.7 Frequency Response Analysis

Consideration of the form of the transient response (Eqn. 2.9) suggests that the response of the unsymmetrical gyro to sinusoidal forcing torques on the gimbals will exhibit beating corresponding to the modulation of the transient and may also show a subsidiary resonance at the frequency $2\Omega - \omega_n$.

In order to obtain the frequency response from a simulation of the unsymmetrical gyro it is necessary to rewrite Magnus' equations in terms of fixed axes. This can either be done by substituting the axis transformation:-

$$u_{xr} = \dot{\theta}_x \cos\Omega t + \theta_y \sin\Omega t$$
$$u_{yr} = -\dot{\theta}_x \sin\Omega t + \dot{\theta}_y \cos\Omega t$$

in Magnus' equations, or by derivation from first principles as follows. Referring to fig. 3, in which the xr, yr, zr, axes are fixed to the rotor, the angular momenta of the rotor about these axes are:-

$$h_{xr} = I_x (\dot{\theta}_x \cos\Omega t + \dot{\theta}_y \sin\Omega t)$$
$$h_{yr} = I_y (-\dot{\theta}_x \sin\Omega t + \dot{\theta}_y \cos\Omega t)$$
$$h_{zr} = J\Omega$$

where I_x and I_y are the moments of inertia of the rotor about the x_r and y_r axes respectively.

About the fixed axes OXYZ (fig. 1) the momenta are:-

$$h_x = h_{xr} \cos\Omega t - h_{yr} \sin\Omega t$$
$$h_y = h_{xr} \sin\Omega t + h_{yr} \cos\Omega t$$
$$h_z = h_{zr} = J\Omega$$

i.e. $$h_x = I_x (\dot{\theta}_x \cos^2 \Omega t + \dot{\theta}_y \sin \Omega t \cos \Omega t) - I_y (-\dot{\theta}_x \sin^2 \Omega t + \dot{\theta}_y \sin \Omega t \cos \Omega t)$$

$$= \frac{I_x + I_y}{2} \dot{\theta}_x + \frac{I_x - I_y}{2} (\dot{\theta}_x \cos 2\Omega t + \dot{\theta}_y \sin 2\Omega t)$$

If we let

$$\frac{I_x + I_y}{2} = I \text{ and } \frac{I_x - I_y}{2} = rI$$

I is the mean transverse inertia of the rotor and r is a measure of the asymmetry. Hence

$$h_x = I\dot{\theta}_x + rI (\dot{\theta}_x \cos 2\Omega t + \dot{\theta}_y \sin 2\Omega t)$$

similarly $$h_y = I\dot{\theta}_y + rI (\dot{\theta}_x \sin 2\Omega t - \dot{\theta}_y \cos 2\Omega t)$$

The rates of change of momentum are:-

$$\dot{h}_x = I\ddot{\theta}_x + rI (\ddot{\theta}_x \cos 2\Omega t + \ddot{\theta}_y \sin 2\Omega t) + 2rI\Omega(-\dot{\theta}_x \sin 2\Omega t + \dot{\theta}_y \cos 2\Omega t)$$

$$\dot{h}_y = I\ddot{\theta}_y + rI (\ddot{\theta}_x \sin 2\Omega t - \ddot{\theta}_y \cos 2\Omega t) + 2rI\Omega (\dot{\theta}_x \cos 2\Omega t + \dot{\theta}_y \sin 2\Omega t)$$

$$\dot{h}_z = 0$$

Hence the torques on the rotor are

$$T_x = \dot{h}_x - h_y \dot{\theta}_z + h_z \dot{\theta}_y$$

$$T_y = \dot{h}_y - h_z \dot{\theta}_x + h_x \dot{\theta}_z$$

$$T_z = \dot{h}_z - h_x \dot{\theta}_y + h_y \dot{\theta}_x$$

where $\dot{\theta}_z$ is the z component of the angular velocity of the axes = 0.

i.e.
$$T_x = \dot{h}_x + J\Omega\dot{\theta}_y$$
$$T_y = \dot{h}_y - J\Omega\dot{\theta}_x$$
$$T_z = 0$$

T_x and T_y are provided by inertia couples from the gimbals and damping torques at the gimbal bearings so that the equations of motion of the system become:-

$$(I + M_x)\ddot{\theta}_x + J\Omega\dot{\theta}_y + R_g\dot{\theta}_x + rl(\ddot{\theta}_x \cos 2\Omega t + \ddot{\theta}_y \sin 2\Omega t) \quad (2.17)$$
$$+ 2rl\Omega(-\dot{\theta}_x \sin 2\Omega t + \dot{\theta}_y \cos 2\Omega t) = 0$$
$$(I + M_y)\ddot{\theta}_y - J\Omega\dot{\theta}_x + R_g\dot{\theta}_y + rl(\ddot{\theta}_x \sin 2\Omega t - \ddot{\theta}_y \cos 2\Omega t)$$
$$+ 2rl\Omega(\dot{\theta}_x \cos 2\Omega t + \dot{\theta}_y \sin 2\Omega t) = 0$$

For the purpose of frequency response analysis, forcing torques T_x and T_y can be included on the right hand sides of these equations.

In fig. 8, which shows the arrangement of the analogue computer to simulate these equations, the three amplifier oscillator loop A8, A9, A10 generates the signals cos 2Ω t and sin 2Ω t and these drive the servo multiplier shafts M1 and M2. A small amount of feedback, (through two potentiometers in series to give fine control) was applied across amplifier A9 to give constant amplitude signals, although this is not shown in the diagram.

Since Ω was taken as 10 rad/sec, scaling the velocities $\dot{\theta}_x$, $\dot{\theta}_y$, as (20 $\dot{\theta}_x$) volts and (20 $\dot{\theta}_y$) volts allowed the periodic terms, derived from the multiplier cups 1A - 1D and 2A - 2D, to be summed at unity gain in the amplifiers A11 and A12.

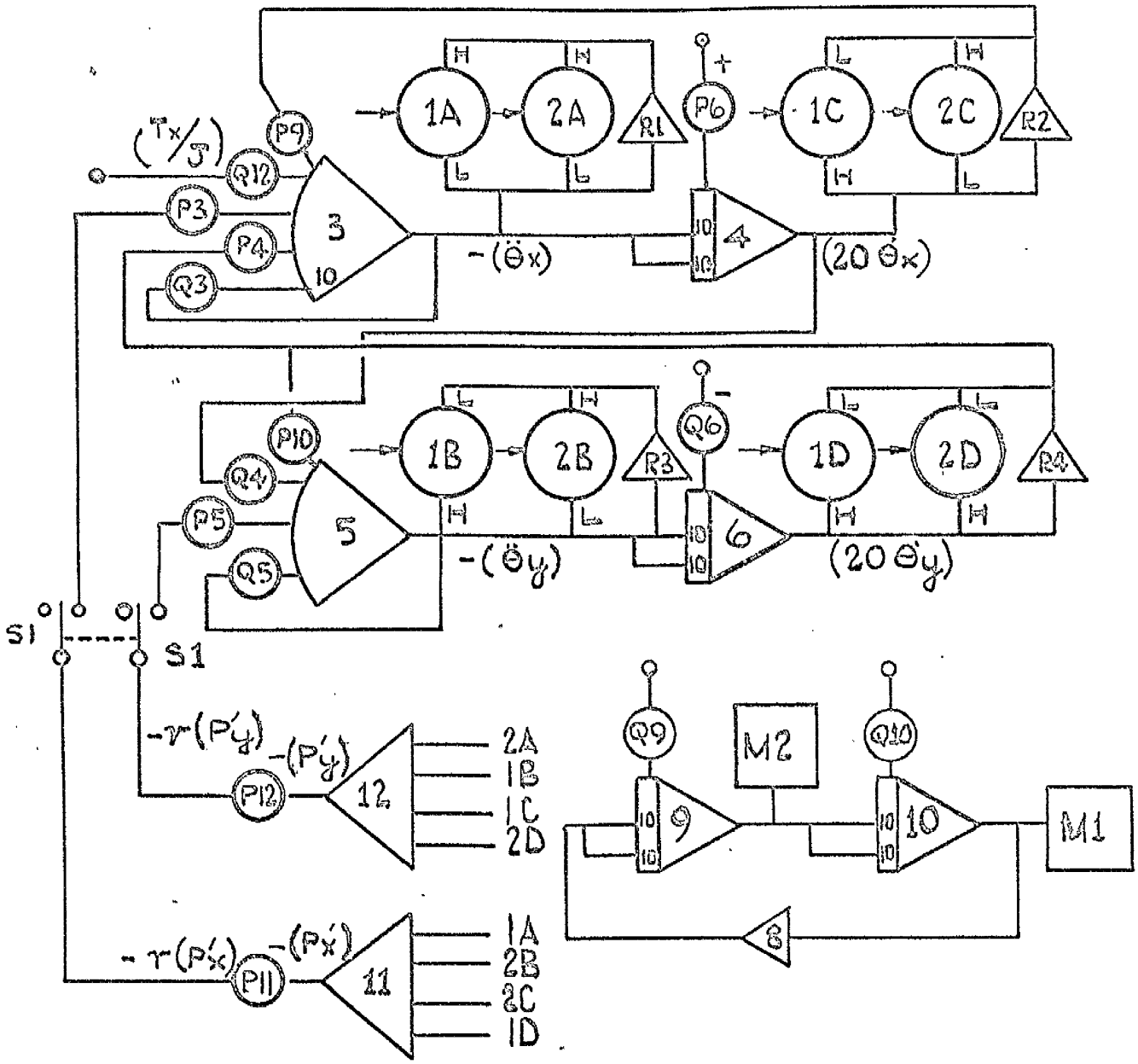

SIMULATION OF UNSYMMETRICAL GYRO. FIG. 8.

The asymmetry coefficient r could be then set using only the two potentiometers P11 and P12, and the system could be rapidly switched from the symmetrical to the unsymmetrical condition by the switch S1.

The forcing "torque" T_x was applied to the simulation by a Solartron transfer function analyser, via the potentiometer Q12 at the input to amplifier 3.

Frequency response curves of $\dot{\theta}_y$ to T_x are shown in figures 9 and 10, both responses being for g = 0.15.

Fig. 9 shows the effect of an asymmetry coefficient r = 0.0909, while fig. 10 shows the response for a larger value, r = 0.2.

The full lines give the average response of the unsymmetrical gyro, while the dotted lines give the response in the symmetrical case.

The chain dotted lines show the extent of the beating indicated by the "in-phase" meter of the transfer function analyser, the quadrature meter being nulled at the centre of its swing using the reference resolver of the T.F.A. The reading of the reference resolver was taken as the average phase shift between the torque T_x and velocity $\dot{\theta}_y$.

As the forcing frequency recedes from the spin frequency the indicated beat amplitude is attenuated by the meters of the T.F.A., so that the beating is actually more extensive than indicated in figs. 9 and 10.

The main effect of rotor asymmetry is seen to be an increase in the height of the main resonance peak, coupled with a displacement of the peak towards

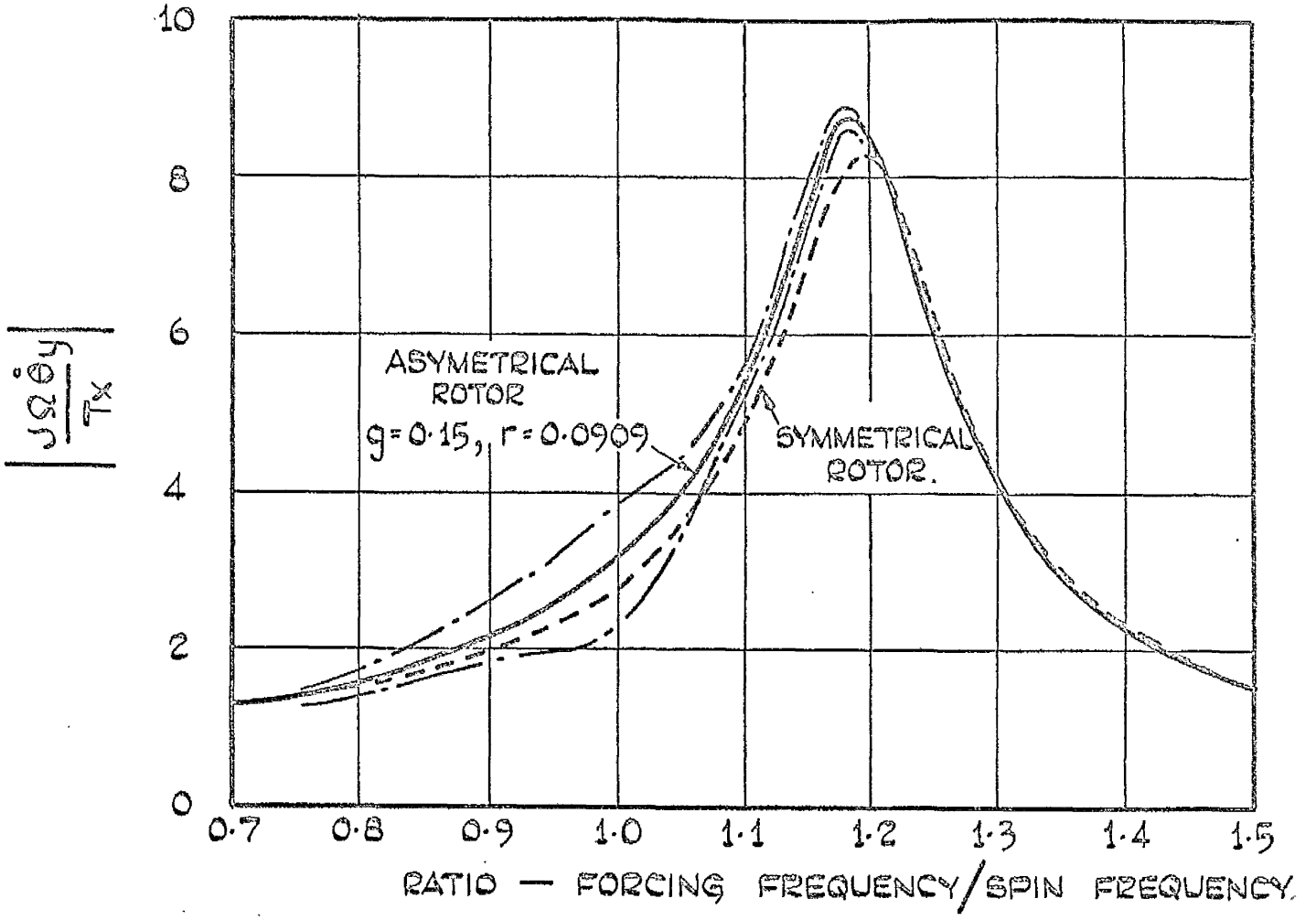

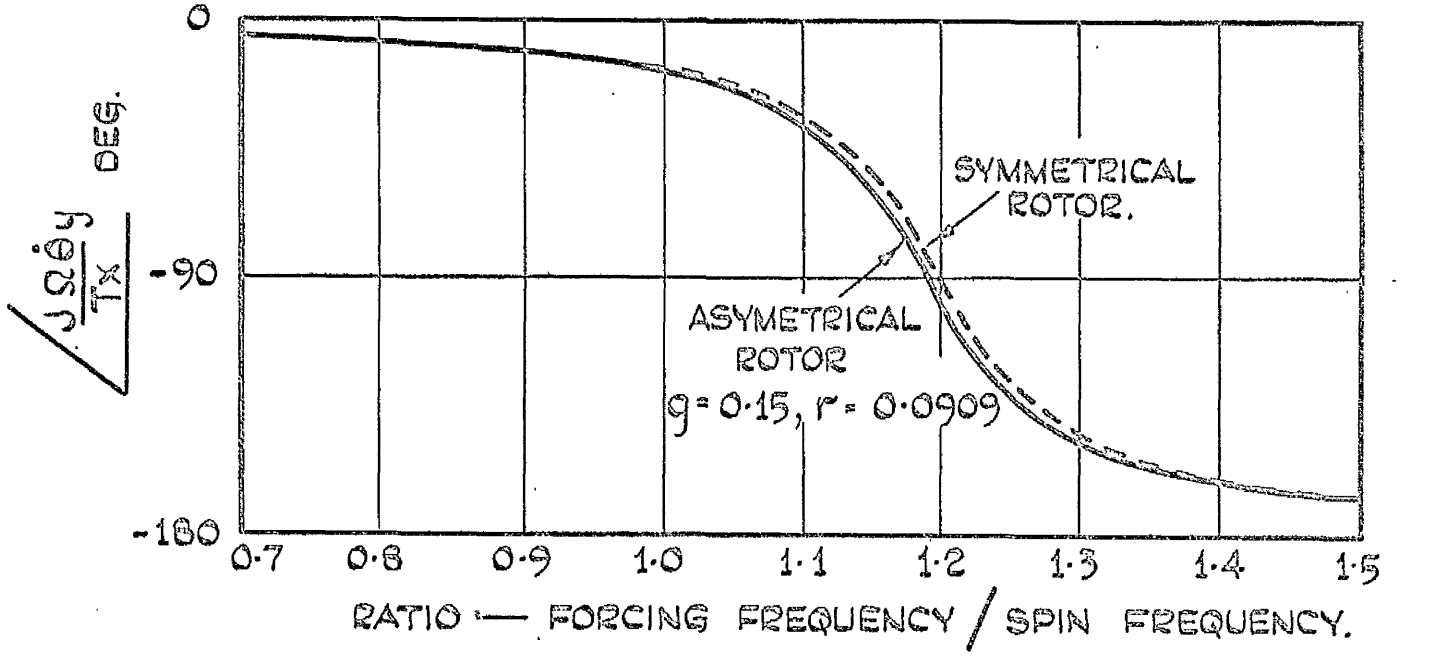

PARAMETERS $g = 0.15$, $I_{max}/J = 0.6$, $I_{min}/J = 0.5$, $R_g/J = 0.6$.

EFFECT OF ROTOR ASYMMETRY ON FREQUENCY RESPONSE.

Fig. 9.

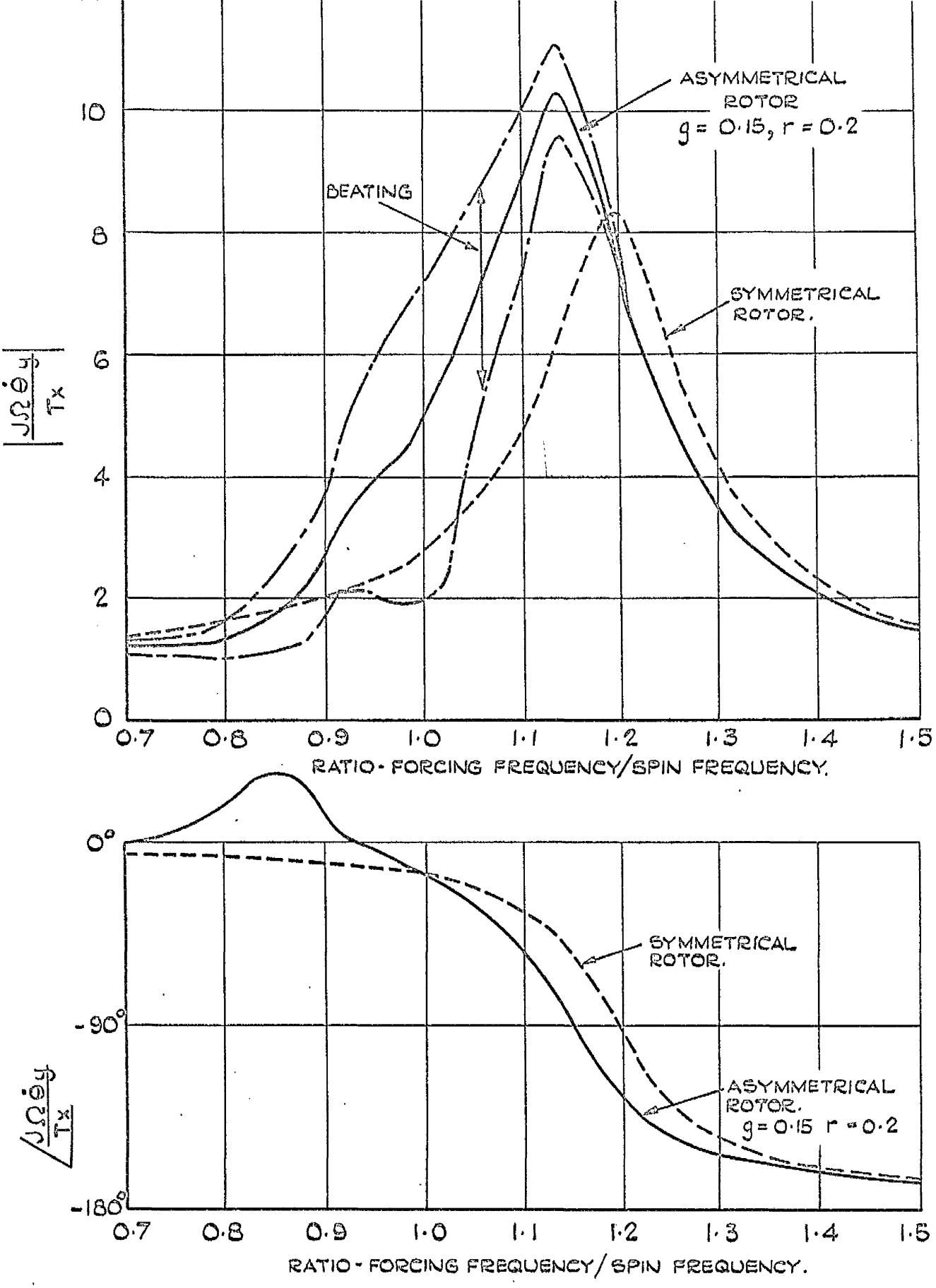

PARAMETERS $g = 0.15$, $I_{max}/J = 0.66$, $I_{min.}/J = 0.44$, $R_g/J = 0.6$

EFFECT OF ROTOR ASYMMETRY ON FREQUENCY RESPONSE.

FIG 10

the spin frequency Ω. At the frequency $2\Omega - \omega_n$, where ω_n is the natural frequency of the symmetrical gyro, the amplitude response is reduced by asymmetry. A "hump" appears in the amplitude response at a frequency just less than Ω but this effect is obscured by the large beat amplitudes.

In the phase response (Fig. 10) the main effect, apart from the shift towards Ω, is the large positive phase shift produced at about $\omega/\Omega = 0.85$. Since the resonance peak occurs at about $\omega/\Omega = 1.15$, the peak positive phase shift seems to occur at $2\Omega - \omega_n'$ where ω_n' is the resonant frequency of the unsymmetrical gyro.

2.8 Response to a constant torque T_x

For a symmetrical gyro, without damping, a constant torque T_x simply produces a constant angular velocity $\dot{\theta}_y = T_x / J\Omega$ and $\dot{\theta}_x = 0$.

As is shown later, in section 6.3.1, the introduction of damping torques $R_g\dot{\theta}_x$ and $R_g\dot{\theta}_y$ gives $\dfrac{\dot{\theta}_x}{T_x} = \dfrac{R_g}{(J\Omega)^2 + R_g^2}$ and $\dfrac{\dot{\theta}_y}{T_x} = \dfrac{J\Omega}{(J\Omega)^2 + R_g^2}$

Since R_g will generally be small compared with $J\Omega$, the effect of damping is to give a small velocity in the x direction, and a small reduction in the velocity $\dot{\theta}_y$.

When the effect of asymmetry is taken into account, it is found that $\dot{\theta}_x$ and $\dot{\theta}_y$ have oscillations at frequency 2Ω superimposed on their steady values. Fig. 11 shows transients obtained from the computer by applying a constant

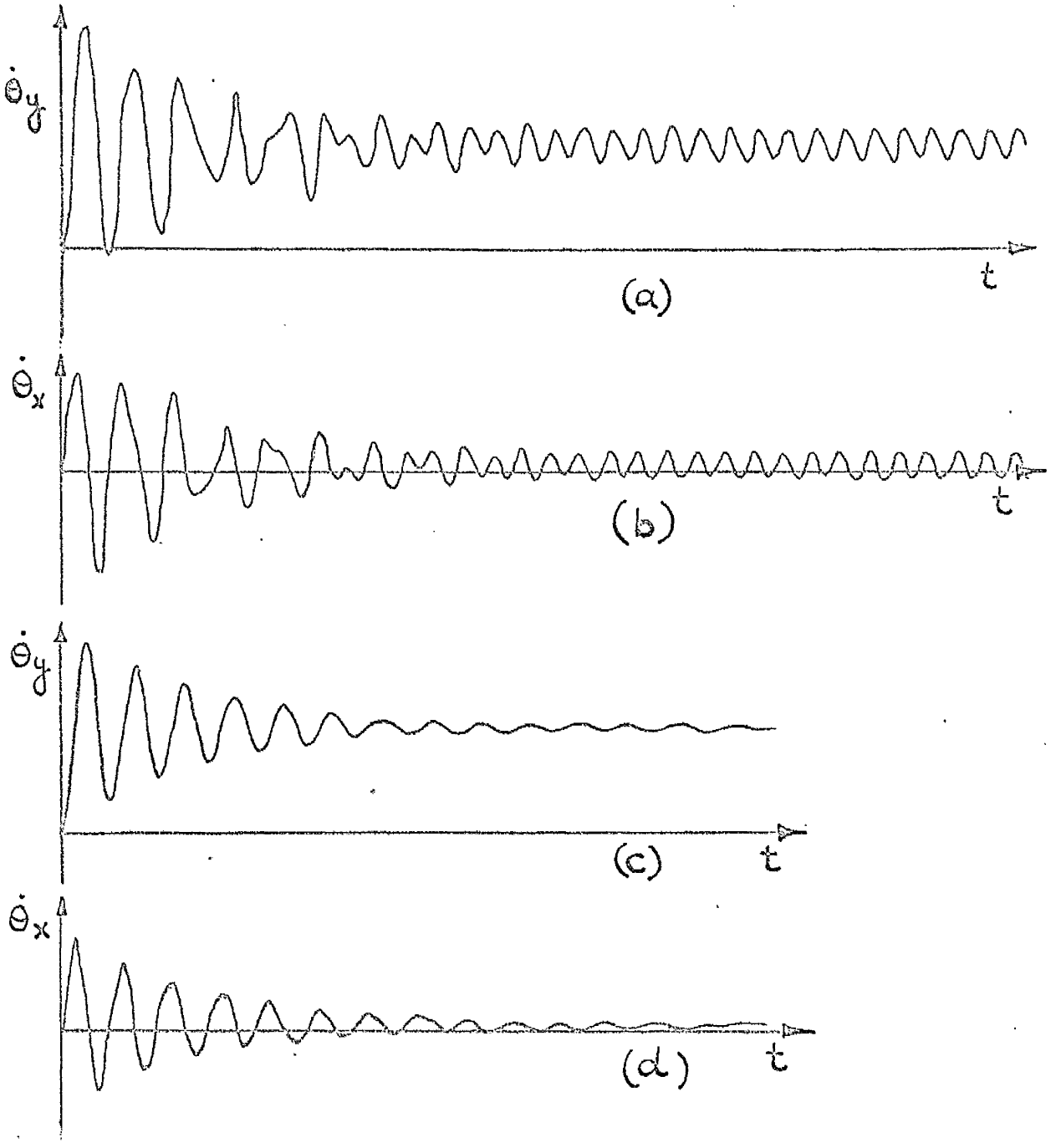

(a) AND (b) - UNSYMMETRICAL ROTOR

(c) AND (d) - SYMMETRICAL ROTOR

PARAMETERS $I/J = 0.55$, $r = 0.0909$, $g = 0.15$, $R_g/J = 0.6$

EFFECT OF ROTOR ASYMMETRY ON TRANSIENT RESPONSE

FIG. 11.

voltage at the input to amplifier 3, to represent a constant torque T_x.

It is possible to calculate the amplitude of the steady state oscillation by substituting the following expressions in equations 2.17:-

$$\dot{\theta}_x = X + x \cos 2\Omega t, \quad \ddot{\theta}_x = -2\Omega x \sin 2\Omega t$$

$$\dot{\theta}_y = Y + y \sin 2\Omega t, \quad \ddot{\theta}_y = 2\Omega y \cos 2\Omega t$$

X and Y can be taken as the response of the symmetrical gyro to constant T_x. The expressions obtained for x and y are rather cumbersome, but the following expression:-

$$x = \frac{2 I r T_x}{J\Omega \sqrt{J^2 + 4 (I + M)(I + M - J)}}$$

is obtained when it is assumed that $M_x = M_y = M$, $y = x$, $R_g = 0$.

2.9 Energy Analysis

Assessment of the relative stability of the simulated gyro under various conditions is not always easy, particularly if the transient waveforms are distorted by beating, as in Fig. 12. In addition, the analysis of pen recordings is time consuming and tedious.

In order to study the effect of varying gimbal inertia on the stability of the unsymmetrical gyro, the circuits shown in Fig. 13 were added to the simulation in order to show the time variation of the kinetic energy E of the nutational oscillation, and the energy dissipated by damping, W.

The kinetic energy E is obtained from the expression:-

$$E = \tfrac{1}{2}\left(M_x \dot{\theta}_x^2 + M_y \dot{\theta}_y^2 + I_x u_{xR}^2 + I_y u_{yR}^2\right)$$

and when the velocities u_{xR}, u_{yR} are expressed in terms of $\dot{\theta}_x$, $\dot{\theta}_y$ this becomes, for small displacements θ_x, θ_y,

$$E = \tfrac{1}{2}\left[(M_x + I)\dot{\theta}_x^2 + (M_y + I)\dot{\theta}_y^2 + r I\left\{(\dot{\theta}_x^2 - \dot{\theta}_y^2)\cos 2\Omega t + 2\dot{\theta}_x \dot{\theta}_y \sin 2\Omega t\right\}\right]$$

The kinetic energy of spin, $\frac{1}{2}J\Omega^2$ is assumed constant and is not included in E. The energy W dissipated by damping is given by

$$\frac{dW}{dt} = R_g\left(\dot{\theta}_x^2 + \dot{\theta}_y^2\right)$$

When the symmetrical gyro oscillates in the presence of damping the energy E falls exponentially to zero, while the energy dissipated in damping, W, rises exponentially to a final value W_f equal to the initial kinetic energy, I. E.

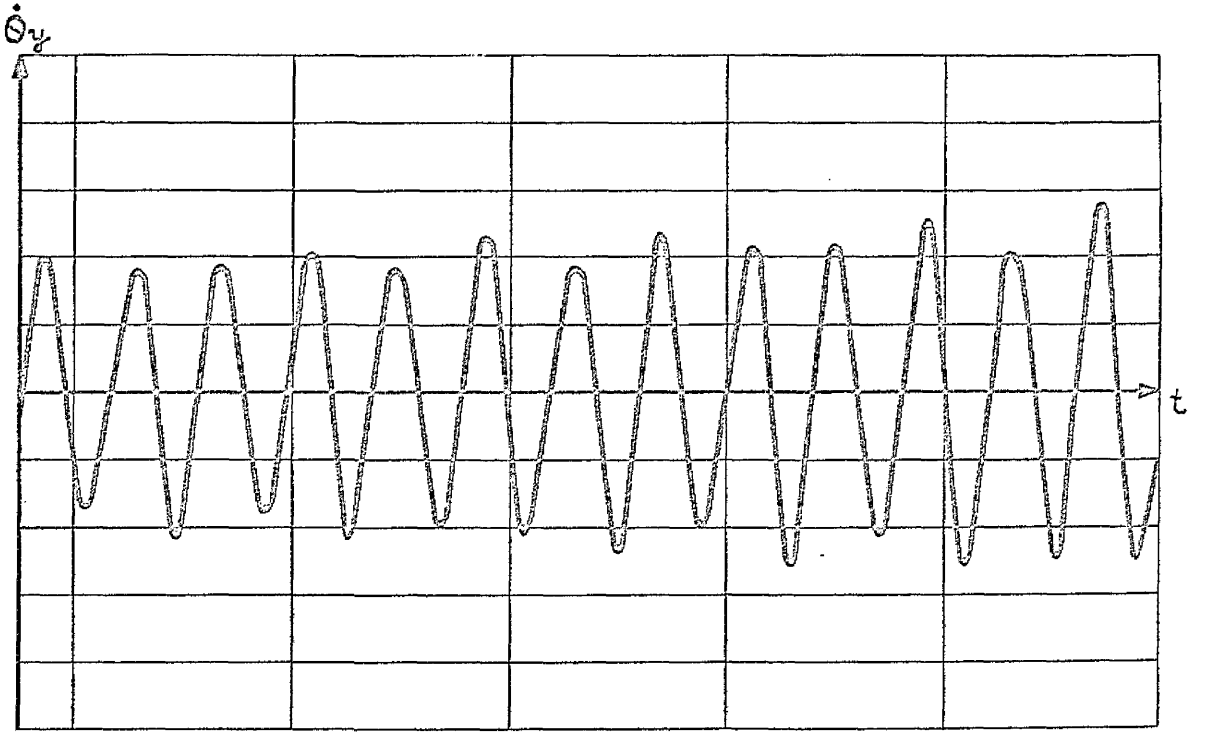

$r = 0.0909,\ q = 0.4$

WAVE FORM HAVING ENVELOPE OBSCURED BY BEATING.

FIG. 12.

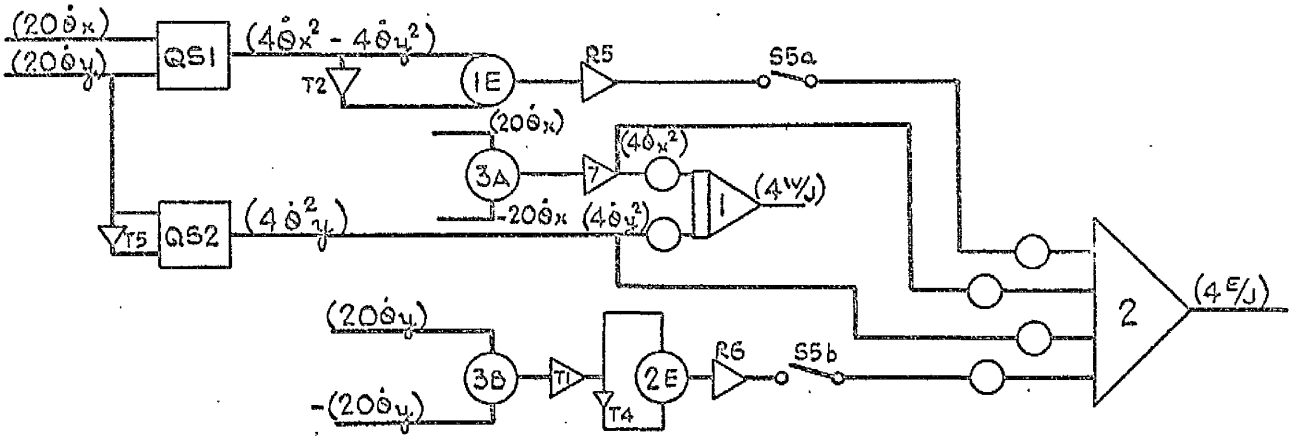

UNSYMMETRICAL GYRO.

WORK & ENERGY CIRCUITS.

FIG. 13.

When the gyro is unsymmetrical, however, energy may be fed into the nutation or removed from it, and in the real gyro, as distinct from the simulation, this energy would reduce or increase the spin kinetic energy of the rotor. Ultimately this energy would be replaced by the driving motor, or dissipated by the various resistances to spin. In the simulation this would be indicated by a value of W_f/IE different from unity. If $W_f/IE > 1$, then more energy has been absorbed by damping than was originally present in the oscillation and the rotor asymmetry has reduced the stability of the gyro by feeding energy into the nutation.

The main advantage of this approach is that all the information from a computer run is contained in a single reading of W_f at the end of the run and no pen recordings are necessary. Also, the simulation may be damped sufficiently to obtain stable transients throughout.

2.9.1 Effect of gimbal inertia

Fig. 14 shows curves of W_f/IE plotted to a base of gimbal inertia g. It appears that the destabilising effect of rotor asymmetry extends beyond the unstable zone into the region of higher gimbal inertia for the case of zero initial condition on $\dot{\theta}_y$. Conversely if there is a zero initial condition on $\dot{\theta}_x$, the destabilising effect extends into the region of lower gimbal inertias, being balanced by a stabilising effect at high gimbal inertias.

These curves are unaltered by changing the sign of the initial conditions, or by interchanging gimbal inertias.

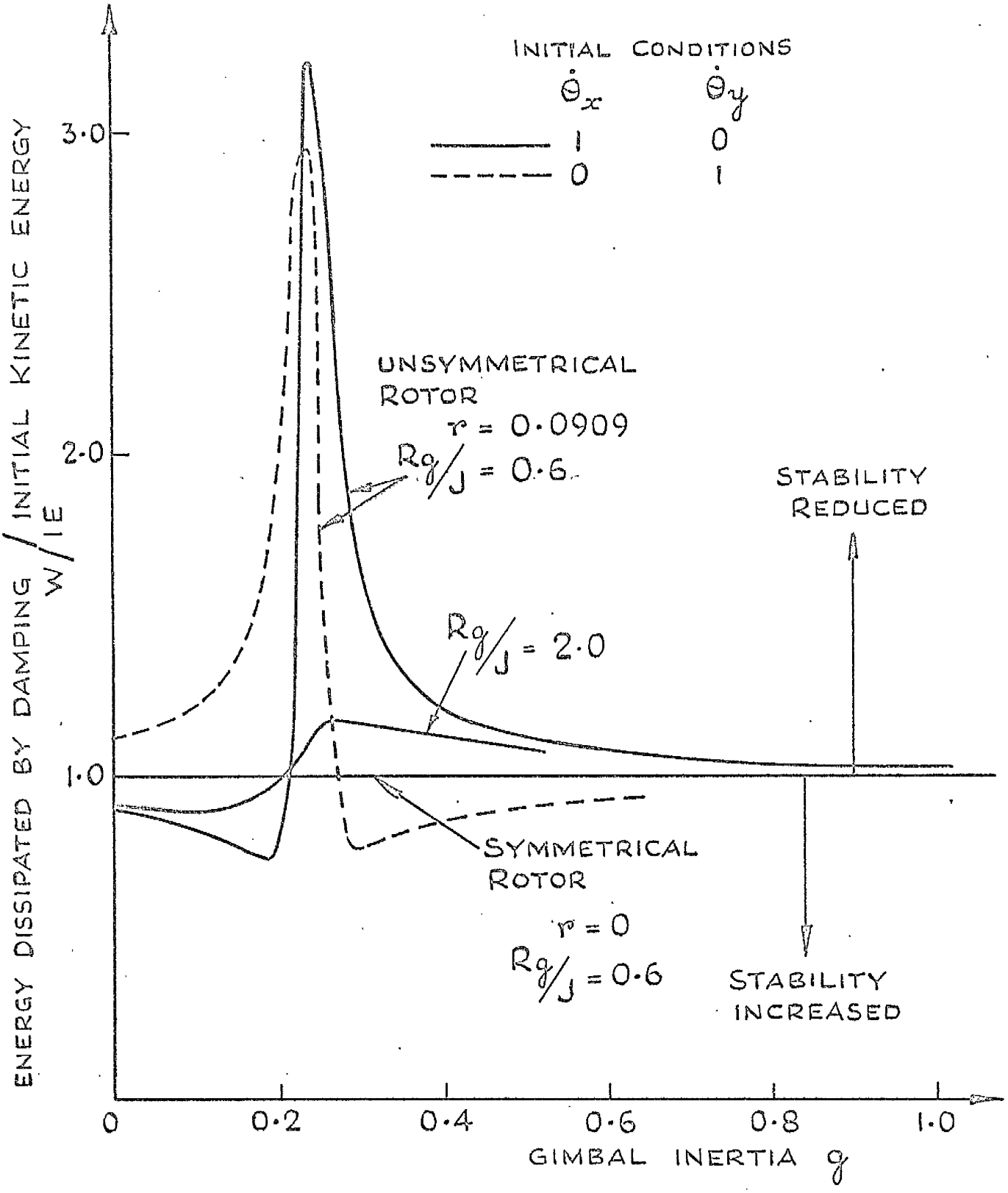

EFFECT OF ROTOR ASYMMETRY ON STABILITY

FIG. 14.

2.9.2 Effect of initial rotor position

The curves of fig. 14 are obtained by assuming that the transient starts when the rotor is lying with its axis of maximum transverse inertia in the OX direction. Fig. 15 shows the effect of varying this initial rotor position, for the two cases of initial gimbal velocity, at a particular value of gimbal inertia. This shows that the effect of rotor asymmetry can be stabilising or destabilising according to the initial rotor position, but for this value of gimbal inertia, the average effect over a large number of transients starting at random rotor positions would be destabilising.

2.9.3 Variation of energy of vibration

Another convenient measure of the relative stability of a vibrating system under various conditions is the rate of change of vibration energy, which comprises both kinetic and strain energy.

The energy function is a particular case of the Lyapunov V function since it is positive definite for all values of the state variables but has the advantage over an arbitrary V function that negative dE/dt is a sufficient and a necessary condition of stability whereas negative dV/dt is only a sufficient condition, in general. The quantity E also has the virtue of possessing physical significance but on the other hand may not lend itself to analytical treatment. Indeed, it may not always be possible to express the energy quantities analytically.

The variation of E is used more extensively in later chapters of this thesis.

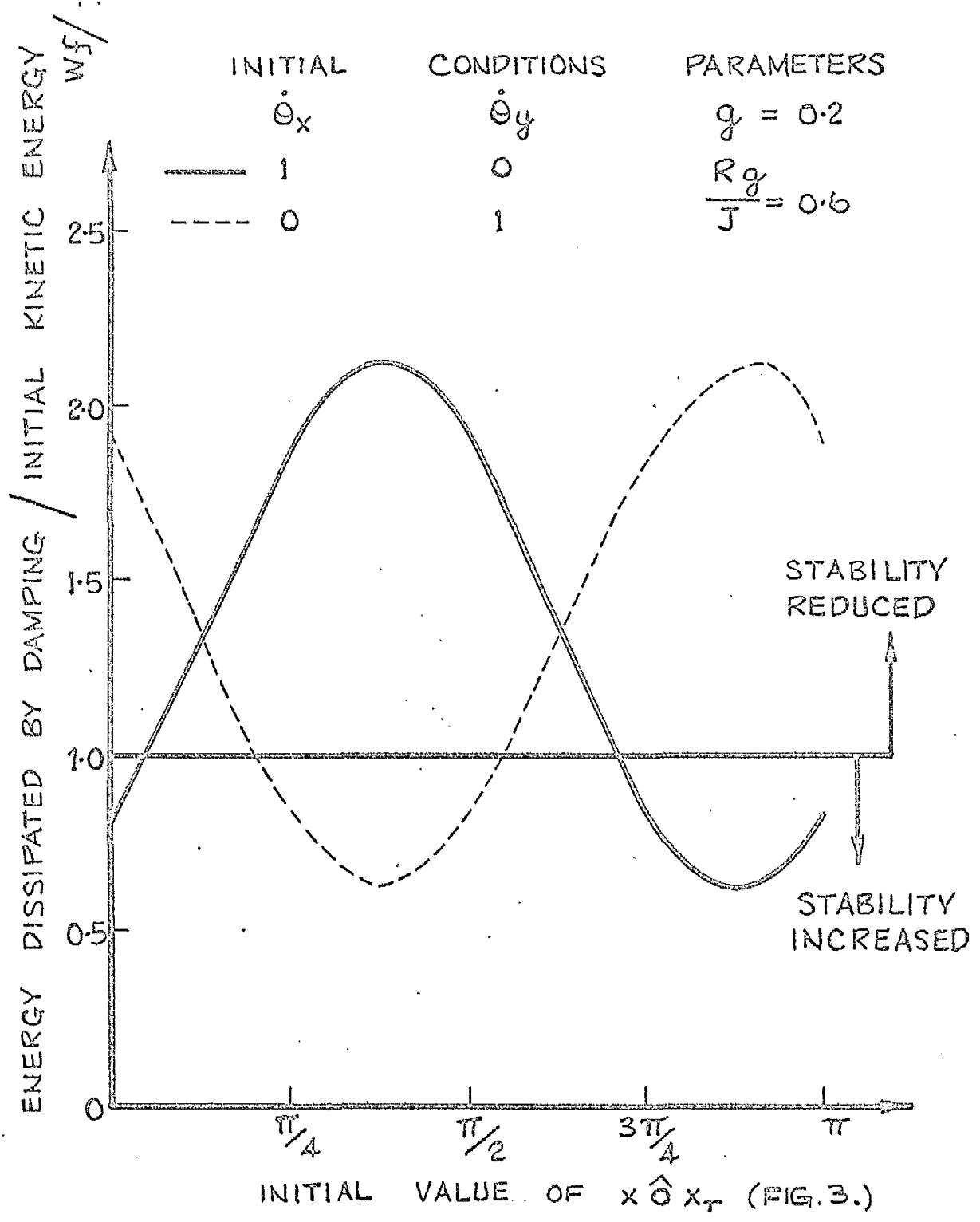

EFFECT OF INITIAL ROTOR POSITION ON STABILITY

FIG. 15.

2.10 Characteristic exponent

The question of characteristic exponents is dealt with fully in Chapter 8 of this thesis, but as a check on the results obtained in Sec. 2.6 and summarised in Table 1, computer runs were taken using the set up shown in Figs. 8 and 12b. The damping was set to zero, and for $g = 0.24$, $r = 0.0909$ it was found that the positive exponent had the value 0.506. This was obtained by logarithmic plotting of the peak amplitudes in the $\dot{\theta}_x$, $\dot{\theta}_y$ waveforms, and checked by logarithmic plotting of the energy quantity E. Since E is a quadratic function of the angular velocities $\dot{\theta}_x$, $\dot{\theta}_y$, the slope of the log E/t graph is double the value of the characteristic exponent.

2.11 Damping required to stabilise the system

With the same settings as in the previous section the damping was adjusted using potentiometers P 9 and P 10 (Fig. 8) until the transient was a constant amplitude sine wave. At this limit of stability R_g / J was found to be 0.5.

CHAPTER 3.

THE EFFECT OF SLACKNESS AND TANGENTIAL FORCES IN THE ROTOR BEARINGS

The paper by Quartley [1] indicates that rotor bearing slackness was a contributory cause of the instability he described. Also he suggests the existence of tangential forces of the type which are known to cause "oil whip" in hydrodynamic bearings.

3.1. Assumptions and equations of motion

It was decided in the present work to investigate the effect of rotor bearings slackness assuming a rather different set of bearing reaction forces. In the radial direction the bearings are assumed to be elastic outside the clearance with the result that the restoring couple applied by the bearings to the rotor is as shown in Fig. 16.

In addition a tangential force equal to μ times the radial force is included in the analysis and in the following equations the signs are such that positive μ corresponds to the action of dry friction while negative μ corresponds to the direction of an "oil whip" force.

The equations of motion of the system are then:-

$$I(\ddot{\theta}_x + \ddot{\varphi}_x) + J\Omega(\dot{\theta}_y + \dot{\varphi}_y) + R_b\dot{\varphi}_x + \frac{kF\varphi_x}{\varphi} - \frac{\mu kF\varphi_y}{\varphi} = 0$$

$$I(\ddot{\theta}_y + \ddot{\varphi}_y) - J\Omega(\dot{\theta}_x + \dot{\varphi}_x) + R_b\dot{\varphi}_y + \frac{kF\varphi_y}{\varphi} + \frac{\mu kF\varphi_x}{\varphi} = 0 \qquad (3.1)$$

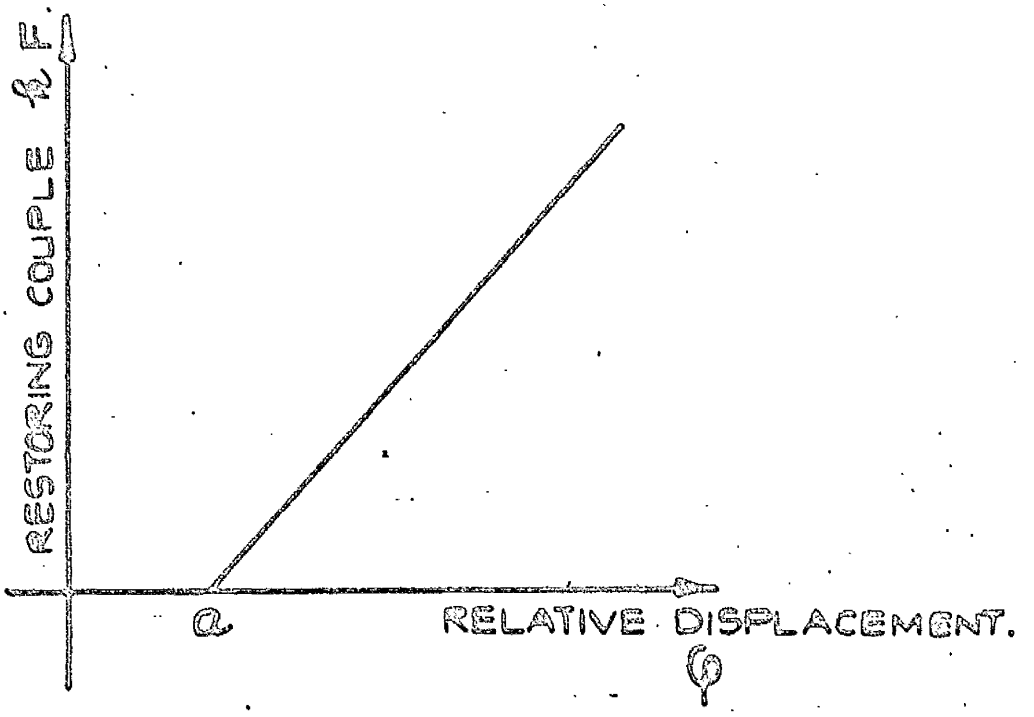

ASSUMED EFFECT OF BEARING SLACKNESS.

FIG. 16

$$M_x \ddot{\Theta}_x + R_g \dot{\Theta}_x - R_b \dot{\varphi}_x - \frac{kF\varphi_x}{\varphi} + \frac{\mu kF\varphi_y}{\varphi} = 0$$

$$M_y \ddot{\Theta}_y + R_g \dot{\Theta}_y - R_b \dot{\varphi}_y - \frac{kF\varphi_y}{\varphi} + \frac{\mu kF\varphi_x}{\varphi} = 0$$

3.2. Analogue Simulation

Initially, when these equations were simulated on an analogue computer, the tangential force μkF was not taken into consideration and the computer set up shown in Fig. 17 was used to simulate bearing slackness.

At first the analogue results indicated that bearing slackness gave rise to instability in the system but the instability was eventually traced to dynamic errors in the servo multipliers. With the "clearance" or dead space adjusted to zero, the voltage representing the restoring couple $\frac{k\varphi_x F}{\varphi}$ was plotted against φ_x on an oscilloscope as the transient took place. An elliptical trace resulted, indicating a phase shift where none should have occurred, since when the dead space a is zero $F = \varphi$. This could perhaps have been overcome by slowing down the solution time, or adding a proportion of $\dot{\varphi}_x$ and $\dot{\varphi}_y$ to φ_x and φ_y respectively to provide phase-advanced signals to drive the multipliers M 1 and M 2. "Quarter squares" or time division multipliers with a higher frequency response were not available. At this stage, however, it was decided to discontinue the analogue investigation of this case.

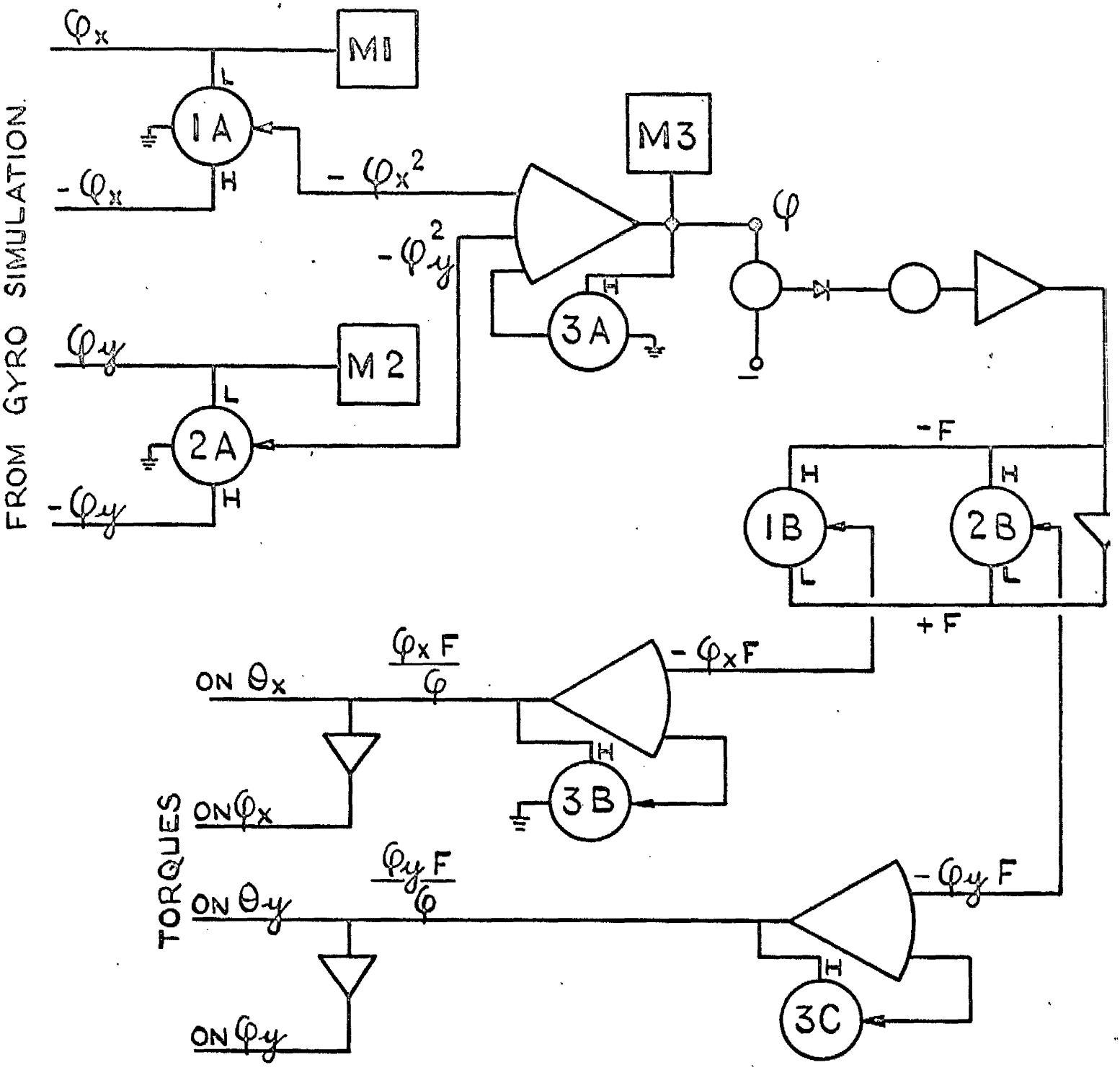

SIMULATION OF BEARING SLACKNESS.

FIG. 17.

3.3. Digital solution of "dead space" equations.

The equations were then programmed for solution on a Sirius digital machine, using Sirius autocode. The programme uses a library sub-routine based on a 4th order Runge-Kutta method. As with all step-by-step numerical integration procedures, the accuracy increases as the step length is reduced, and some experiment with the step length was required to obtain sufficient resolution of the high frequency components in the relative displacements φ_x, φ_y, without making the computation unduly long. In order to ascertain the effect of the dead space on the stability of the system the total energy at each step was calculated. This energy is equal to the sum of the kinetic energies of the moving masses and the strain energy due to deformation of the elastic bearings, i.e.:-

$$E = \tfrac{1}{2}\left[M_x \dot{\Theta}_x^2 + M_y \dot{\Theta}_y^2 + I(\dot{\theta}_x + \dot{\varphi}_x)^2 + I(\dot{\Theta}_y + \dot{\varphi}_y)^2 + kF^2 \right] \quad (3.2)$$

Also, at each step the rate of dissipation of energy by damping in the bearings was calculated from the expression:-

$$\frac{dW}{dt} = R_b(\dot{\varphi}_x^2 + \dot{\varphi}_y^2) + Rg(\dot{\Theta}_x^2 + \dot{\Theta}_y^2) \quad (3.3)$$

This rate was integrated along with the other derivatives by the Runge-Kutta process, to give the quantity W representing the total energy dissipated by damping since the beginning of the transient. The quantity W + E was then compared with the initial energy in the system at the start

of the transient. The quantities E/IE and $(W + E)/IE$ appear in the tables of computer results, of which a sample is shown in table 2. It can be seen that $(W + E)/IE$ does not depart significantly from unity, and it did not do so under any of the conditions of dead space or gimbal inertia. This is taken to mean that all the energy quantities have been accounted for, both in storage and dissipation, and the quantity $(W + E)/IE$ therefore acts as a valuable check on the accuracy of the computation.

The rate of change of E/IE is used as a measure of the relative stability of the system under varying conditions of gimbal inertia, dead space, etc.

Since the Sirius was extremely slow, and was a "self-drive" machine, the process of experimenting with step length to maintain accuracy became very time consuming. A computing service became available in Manchester, using a much larger and faster Atlas machine, so the problem was re-programmed for solution on Atlas, using the Kutta-Merson method for integrating the equations. At the same time the programme was extended to take account of the tangential forces in the bearings, described in section 3.1.

The Kutta-Merson method automatically adjusts the step length to maintain the truncation error within a value e chosen by the programmer. If the error exceeds this value the machine halves the step length chosen by the programmer and repeats the integration. If after three successive

27 - 14 1900
RO NUTATION -DEAD SPACE MK. VI EJJ

RAMETERS J I OMEGA MX MY K RB RG A

5250	0	J
1500	0	I
5140	3	Ω
0000	0	M_x
0000	0	M_y
0000	7	A
1500	3	R_b
0000	3	R_g
0000	-4	a

TIAL CONDITIONS DELTA T ,T, PHI X D PHI X
Y, D PHI Y ,THETA X ,D THETA X,THETA Y
HETA Y, W

0000	-5	Δt
0000	-52	t
0000	-4	ϕ_x
0000	-1	$\dot{\phi}_x$
0000	-52	ϕ_y
0000	-52	$\dot{\phi}_y$
0000	-52	θ_x
0000	-1	$\dot{\theta}_x$
0000	-52	θ_y
0000	-52	$\dot{\theta}_y$
0000	-52	W

ITIAL ENERGY

7500 -1
E, W+E/IE

0000 0 1.0000 0
RIABLES

0000	-4	t
6820	-5	ϕ_x
8657	-1	
1392	-5	
6810	-2	as above
9944	-4	
2113	-1	
0927	-6	
8000	-3	$\dot{\theta}_y$
9627	-1	W

TOR DISPLACEMENT
XR YR

4262 -4 1.2485 -5
E, W+E/IE

7662 -1 1.0000 0

VARIABLES

1.0000	-3
-1.2657	-4
-1.1589	-1
5.3993	-5
1.0367	-1
3.3458	-4
2.2610	-1
1.1261	-5
3.4941	-2
2.6278	-1

ROTOR DISPLACEMENT
XR YR

2.0801 -4 6.5254 -
E/IE, W+E/IE

2.9926 -1 1.0000
VARIABLES

1.5000	-3
-1.8437	-4
-1.1292	-1
1.0449	-4
8.6530	-2
4.2887	-4
1.5041	-1
3.6174	-5
6.4421	-2
3.0742	-1

ROTOR DISPLACEMENT
XR YR

2.4450 -4 1.4066 -
E/IE, W+E/IE

1.8024 -1 1.0000 (
VARIABLES

2.0000	-3
-2.0275	-4
4.6608	-2
1.2137	-4
-1.2592	-2
4.7313	-4
2.8892	-2
8.1523	-5
1.1627	-1
3.2262	-1

ROTOR DISPLACEMENT
XR YR

2.7038 -4 2.0289 -4
E/IE, W+E/IE

1.3971 -1 1.0000 0

TABLE 2

reductions of the step length the accuracy is not achieved, e is replaced by twice the smallest error in the foregoing trials. On the other hand, if the error is less than e/100 the step length is doubled. A print of the programme and some typical results are shown in Appendix 1.

3.4. Results of digital solution.

Fig.18. shows a typical plot of log E/IE against time for $M_x = M_y = 1.5$ gm.cm.sec^2 curves being drawn for μ positive, negative and zero, both with and without dead space. Similar plots were obtained for a range of values of gimbal inertia.

Throughout this series of computations the damping was held constant, the initial velocity of the gimbals was 0.5 rad/sec in the $\dot{\theta}_x$ direction and the initial relative displacement or rotor and gimbals was 10^{-4} radians, i.e. half the dead space radius. The rotor was assumed to be at rest initially so that the initial relative velocity $\dot{\varphi}_x$ was - 0.5 rad/sec.

These plots show that for the parameters chosen the introduction of dead space makes the system more stable or less unstable, irrespective of the value of μ.

3.5. Effect of tangential forces

In Fig.19. the value of log (E/IE) at 20 millisec. from the start or the transient is plotted against gimbal inertia M for μ positive, negative and zero, both with and without dead space. Damping is held constant

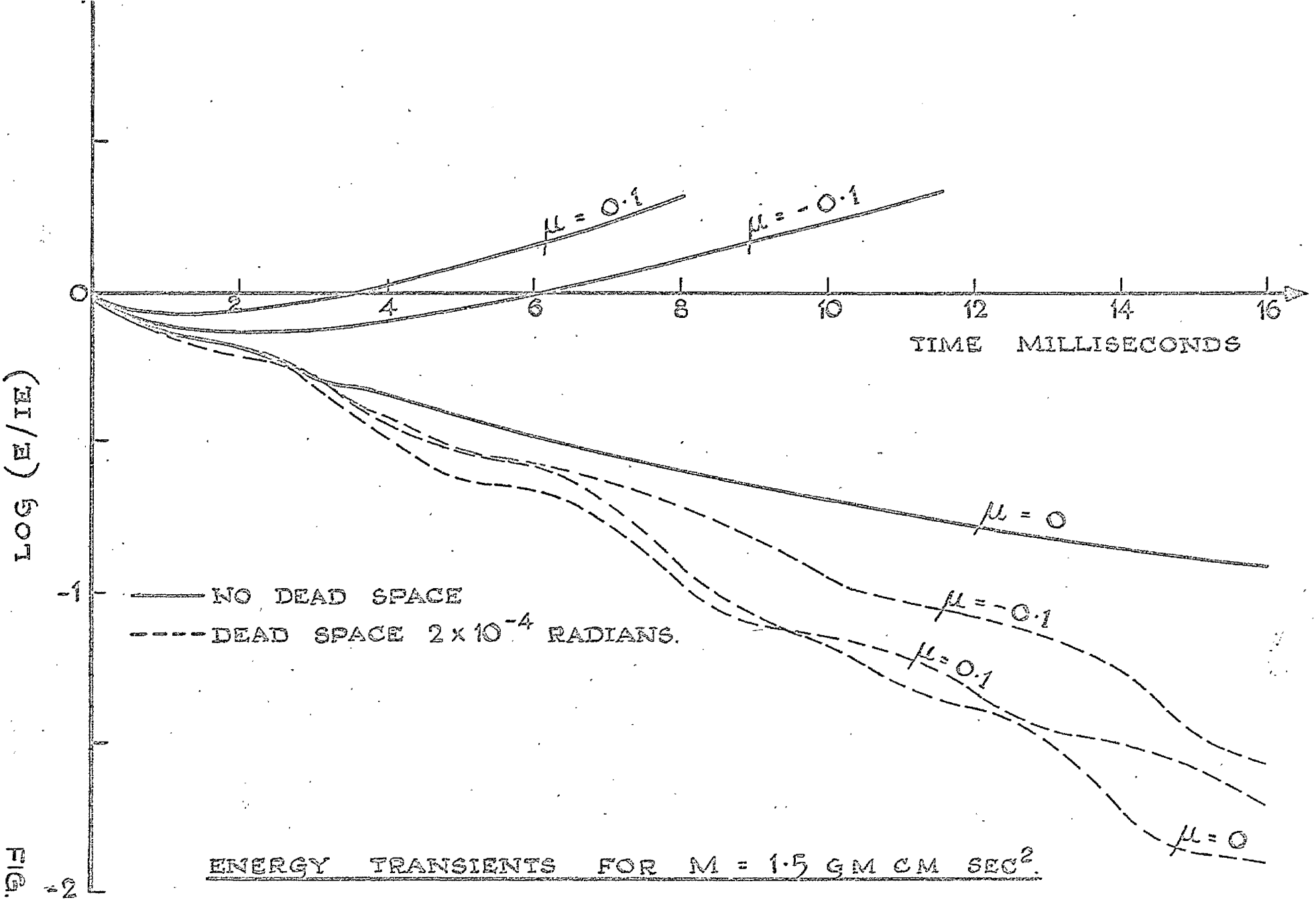

ENERGY TRANSIENTS FOR M = 1·5 GM CM SEC^2.

FIG. 18

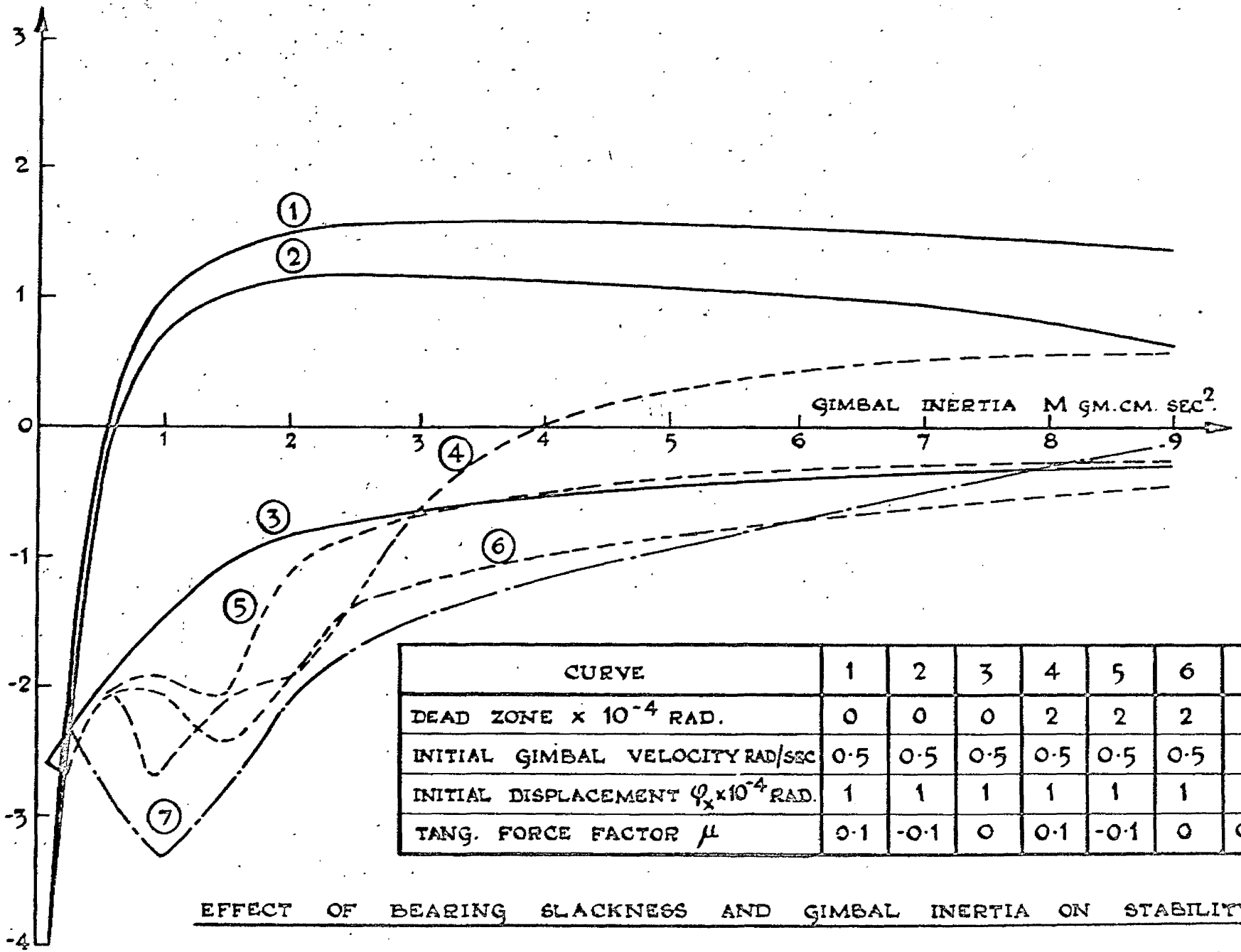

CURVE	1	2	3	4	5	6	7
DEAD ZONE x 10^{-4} RAD.	0	0	0	2	2	2	2
INITIAL GIMBAL VELOCITY RAD/SEC	0·5	0·5	0·5	0·5	0·5	0·5	0
INITIAL DISPLACEMENT $\varphi_x \times 10^{-4}$ RAD.	1	1	1	1	1	1	3
TANG. FORCE FACTOR μ	0·1	-0·1	0	0·1	-0·1	0	0·1

EFFECT OF BEARING SLACKNESS AND GIMBAL INERTIA ON STABILITY.

FIG. 19.

throughout.

Where no dead space is present, the introduction of tangential forces in either direction makes the system less stable than before.

This is also true in the case where dead space is present provided $M>2.5$. For $M<2.5$ and μ negative, the system is less stable than for zero tangential force, but the curve for μ positive crosses the curve for μ zero several times in the range $0.2<M<2.5$.

All the curves appear to show a reduction in stability with increasing M but as indicated in the next section some reduction is to be expected.

3.6. Effect of gimbal inertia

Consideration of a simple one degree of freedom system of mass M, elasticity K and viscous damping R, executing a transient vibration $x = Ae^{-\Delta t}\cos(mt + \varphi)$, indicates that the total energy (strain + kinetic) is given by the expression:-

$$E = \tfrac{1}{2} KA^2 e^{-2\Delta t}\left[1 + d^2\cos 2(mt+\varphi) + d\sqrt{1-d^2}\sin 2(mt+\varphi)\right] \qquad (3.4)$$

where

$$\Delta = R/2M,\quad m = \sqrt{\frac{K}{M} - \frac{R^2}{4M^2}}\quad d = \frac{R}{2\sqrt{KM}}$$

Hence, omitting the sinusoidal terms

$$\log (E/IE) = -2\Delta t \qquad (3.5)$$

A plot of log (E/IE) against time would therefore be a straight line of slope -2Δ with a sinusoidal variation of frequency 2m superimposed. Since $\Delta = R/2M$, if R is kept constant and M increased the log (E/IE) plots will become less steep.

By analogy in Fig.19 the value of log E/IE at 20 ms. will approach zero as M becomes large.

3.7. Effect of initial conditions

Since curves 1 - 6 in Fig.19. are drawn with constant initial velocity in the transient, as M increases the initial kinetic energy in the vibration increases. The amplitude of the resulting transient is therefore increased and the dead space becomes smaller in relation to the total excursion of the rotor shaft across the bearing. Hence, each curve in the set for "slack" bearings (4 - 6) approaches the corresponding curve in the set for "tight" bearings (1 - 3) as M is increased.

Also shown on Fig.19. is curve 7 which shows the variation of log (E/IE) at 20 ms. with M for μ positive, zero initial velocity, but an initial value of $\varphi_x = 3 \times 10^{-4}$ radians, i.e. 10^{-4} radians outside the dead space. All the vibrations therefore start with the same energy $E_o = \frac{1}{2} \times 2 \times 10^{7} \times (10^{-4})^2 = 0.1$ gm.cm. This curve lies below curve 4 for all values of $M > 0.35$. For curve 4 the initial energy is $\frac{1}{2} M \times (0.5)^2 = \frac{M}{8}$ and points on curves 4 and 7 will represent the same initial energy when $M = 0.8$.

A further series of runs was contemplated, in which the initial impulse or momentum $M\dot{\Theta}_x$ would have been held constant, but it was felt to be of doubtful value.

The effect of varying the initial gimbal velocity was also studied, the results for a constant gimbal inertia $M_x = M_y = 1$ gm.cm.sec^2 being shown in Fig. 20. This shows again that the system with dead space is always more stable than that without dead space and shows also that as the initial velocity increases the effect of dead space decreases, since the dead space then becomes small in comparison with the amplitude of the relative motion between shaft and bearing.

3.8. Modes of vibration

Figs. 21 - 25 show some sample plots of the relative displacement between rotor and gimbal, obtained by digital computation. The various motions can be regarded as lying between the following limiting cases.

(a) Rotor "free" This mode appears in Fig. 21. where the transient has decayed inside the clearance circle or dead zone. In the absence of damping the motion would be a forward precession at frequency $J\Omega/I = 284$ c/s for the parameters used.

(b) Gimbals fixed - no dead zone

Putting $\dot{\Theta}_x = \dot{\Theta}_y = 0$ the equations of motion become:-

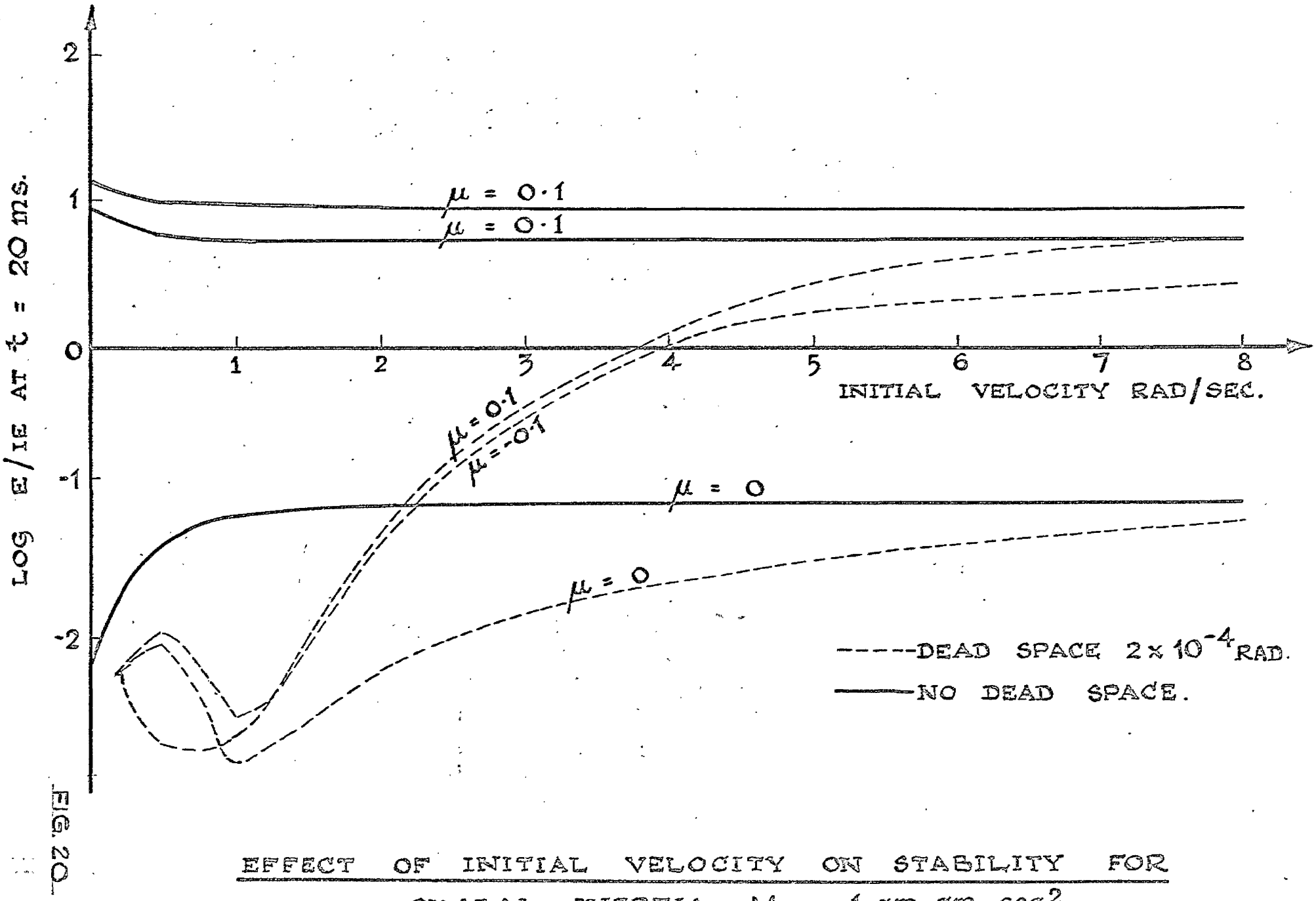

EFFECT OF INITIAL VELOCITY ON STABILITY FOR GIMBAL INERTIA M = 1 gm cm sec^2

RELATIVE DISPLACEMENT BETWEEN ROTOR AND GIMBAL.

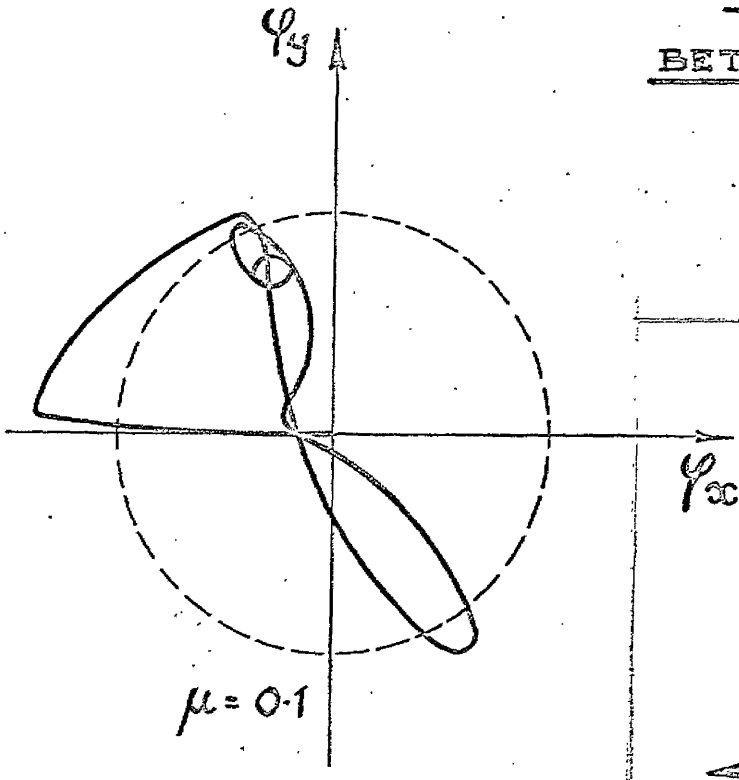

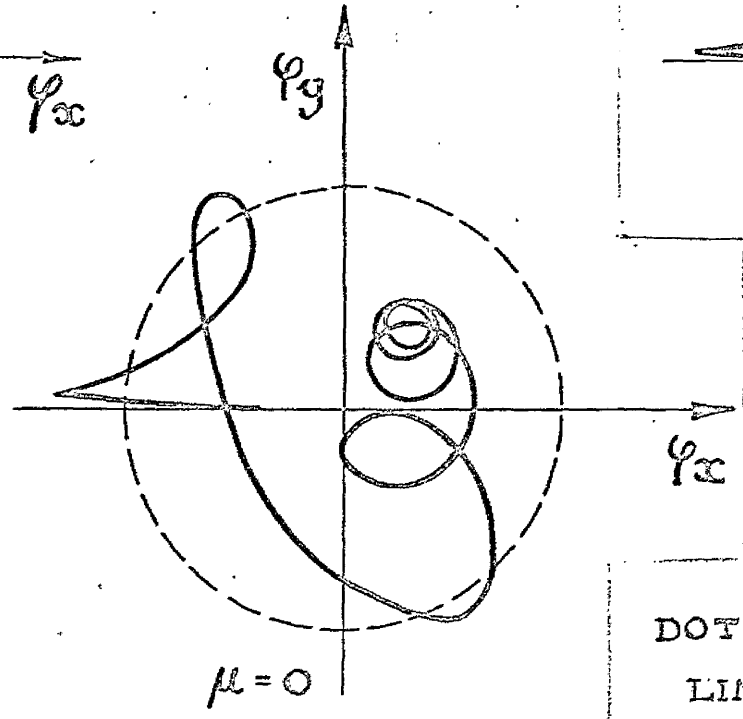

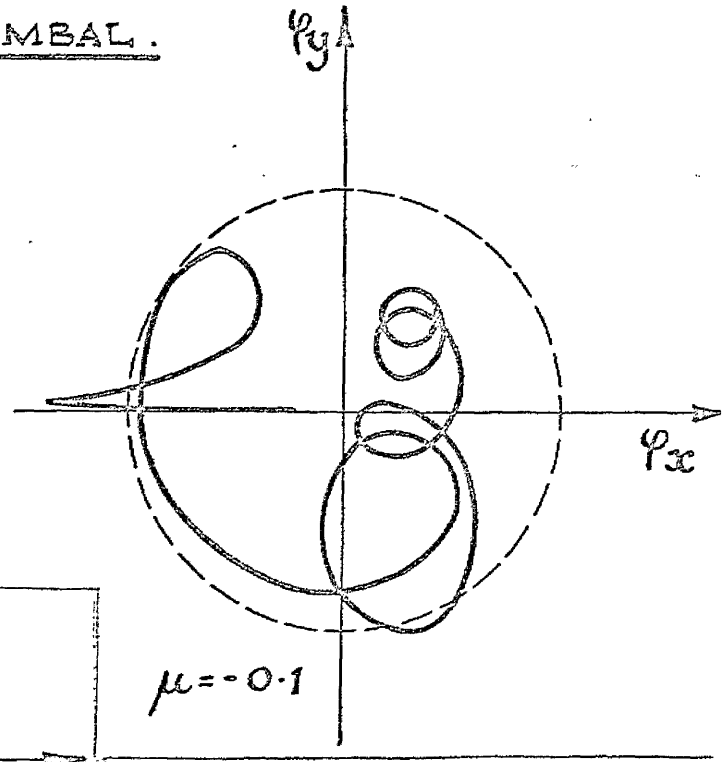

DOTTED CIRCLES INDICATE LIMIT OF DEAD ZONE, $\pm$ 0·0002 RADIANS

M = 1 gm. cm. sec^2.

$\dot{\theta}_{xo}$ = 0·5 RAD/sec.

FIG. 21.

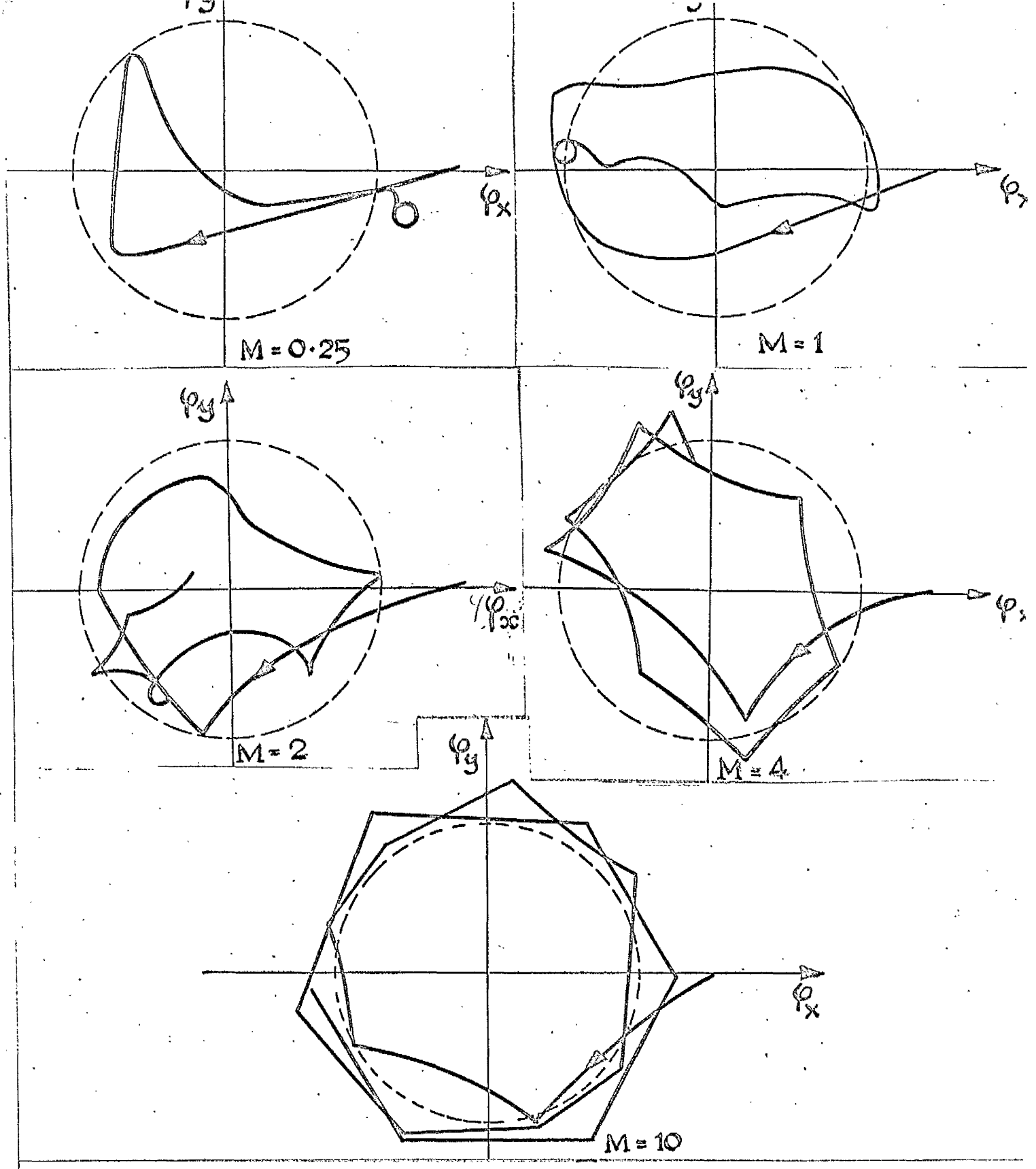

RELATIVE DISPLACEMENT OF ROTOR AND GIMBALS FOR $\mu = 0{\cdot}1$

INITIAL CONDITIONS $\dot{\varphi}_{x0} = \dot{\theta}_{x0} = 0$ $\varphi_{x0} = 3 \times 10^{-4}$ RADIANS.

DOTTED CIRCLES INDICATE LIMIT OF DEAD ZONE ($\pm 2 \times 10^{-4}$ RADIAN

FIG. 22.

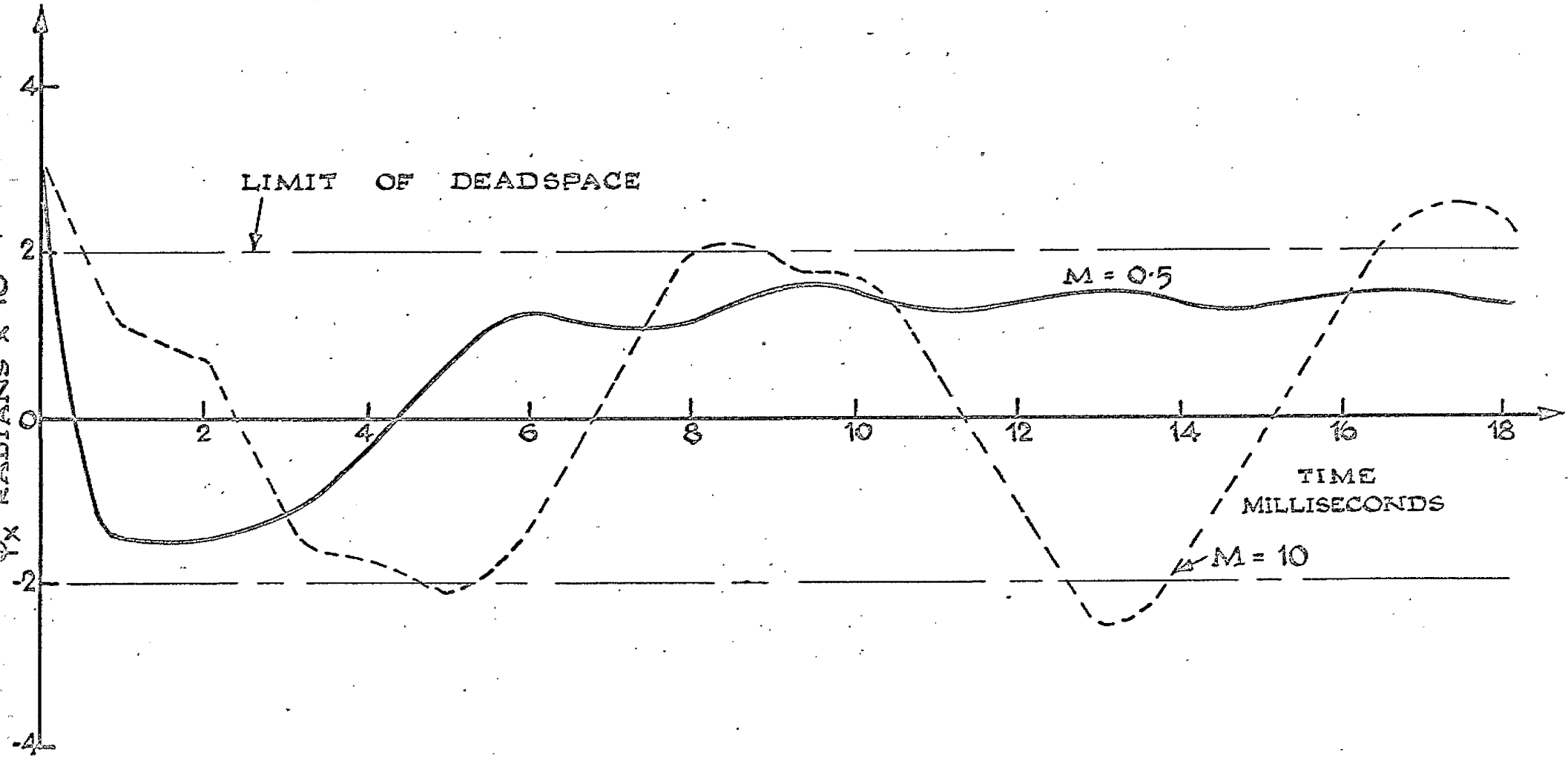

RELATIVE DISPLACEMENT TRANSIENTS FOR $\mu = 0{\cdot}1$.

INITIAL CONDITIONS $\varphi_{x0} = 3 \times 10^{-4}$ RADIANS $\dot{\varphi}_{x0} = \dot{\theta}_{x0} = 0$.

FIG. 2.

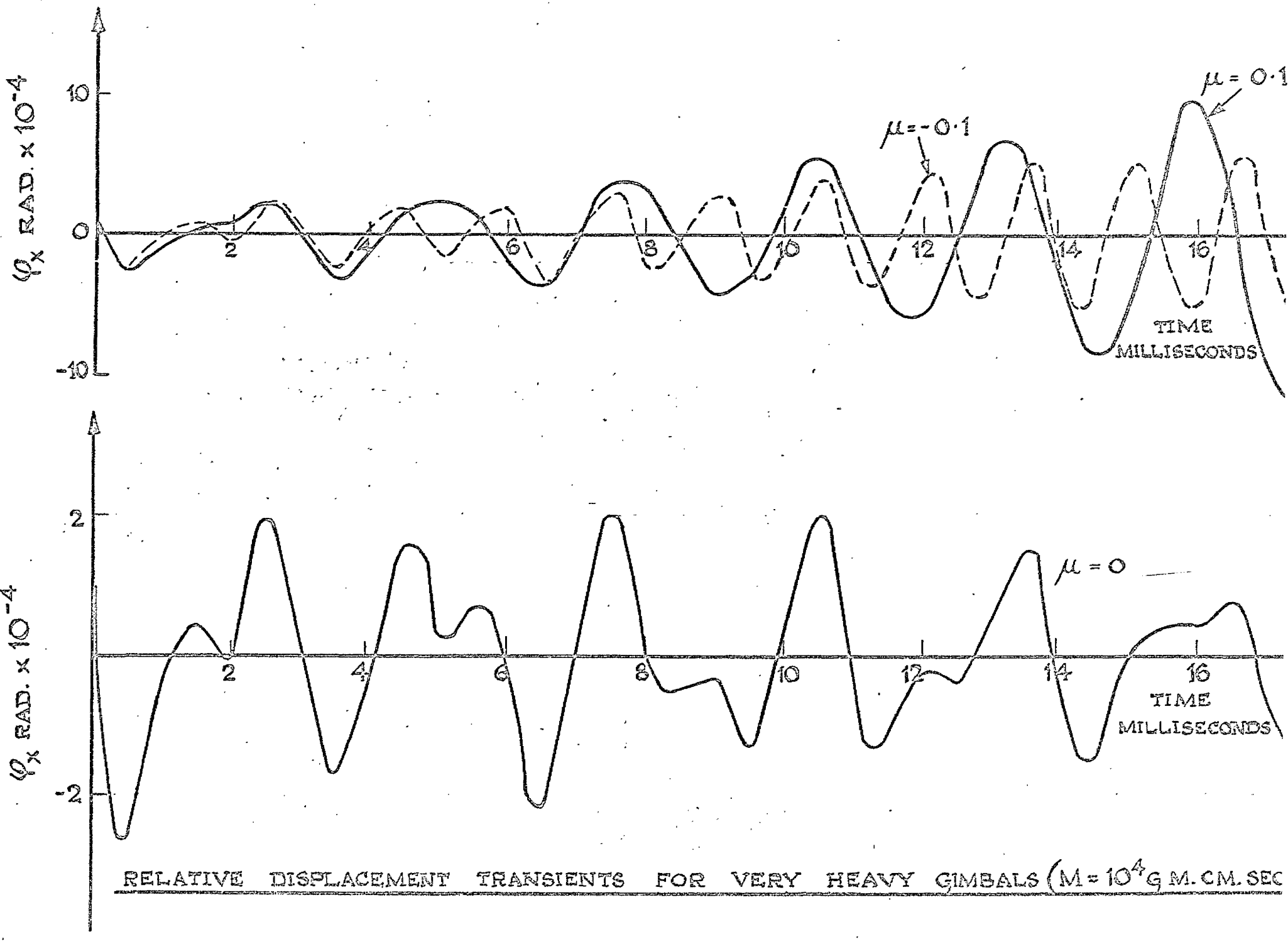

RELATIVE DISPLACEMENT TRANSIENTS FOR VERY HEAVY GIMBALS ($M = 10^4$ G M. CM. SEC

Fig. 24.

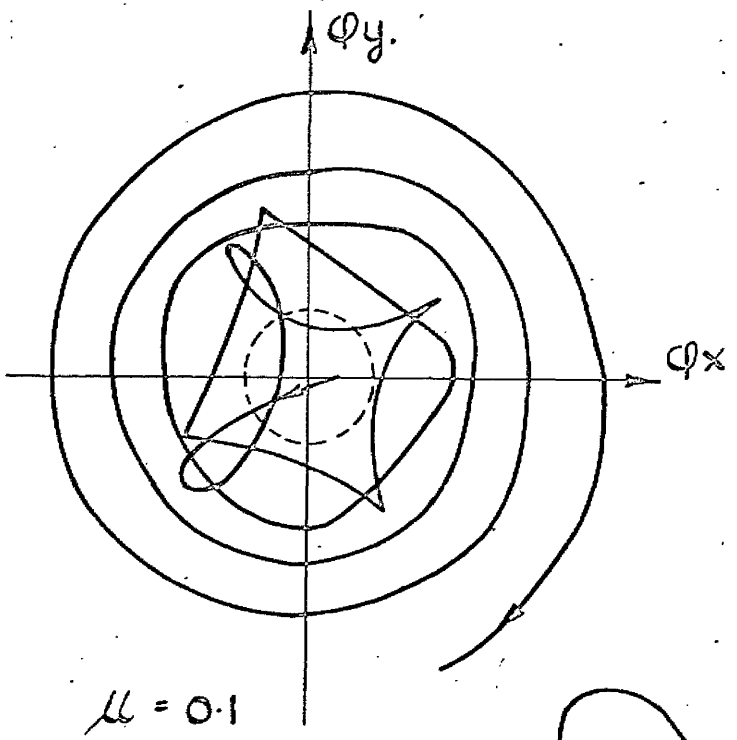

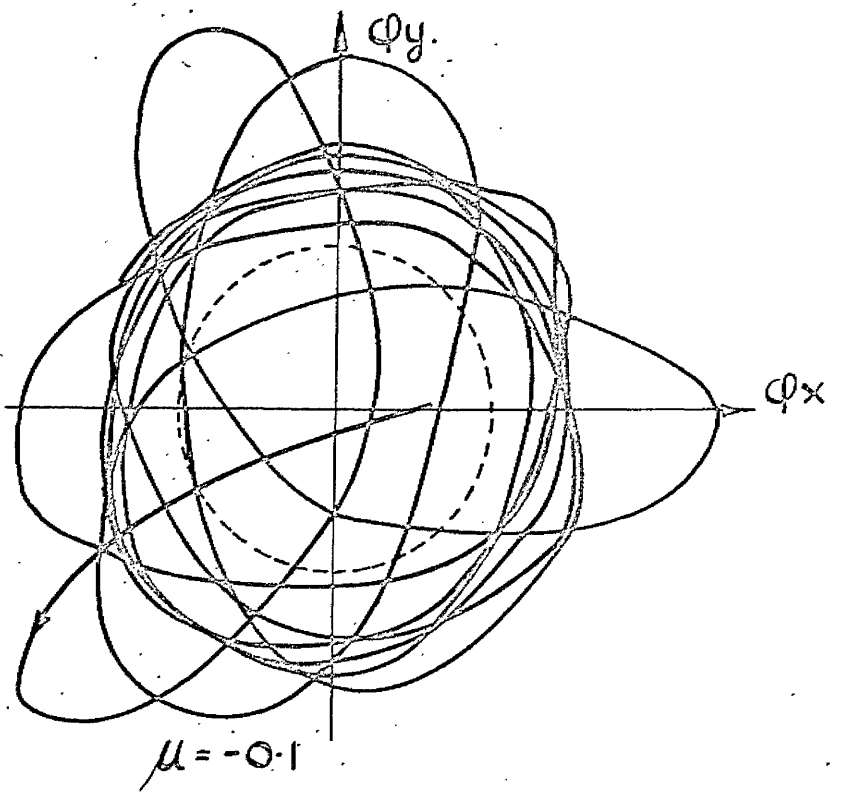

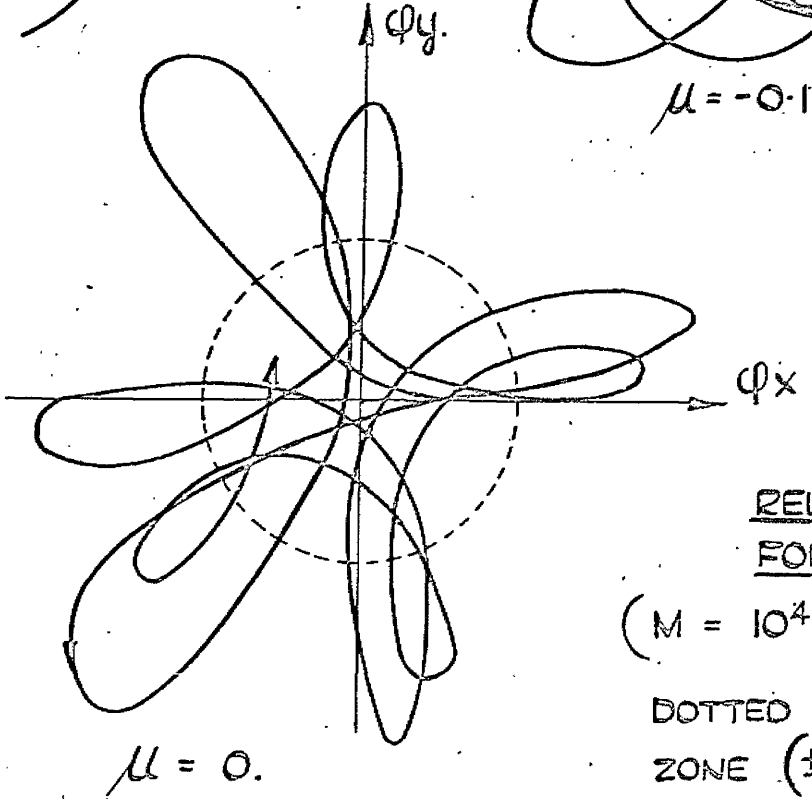

RELATIVE DISPLACEMENT FOR VERY HEAVY GIMBALS.

$(M = 10^4$ gm. cm. $s^2)$

DOTTED CIRCLES SHOW LIMIT OF DEAD ZONE $(\pm 2 \times 10^{-4}$ RADIANS.)

FIG. 25.

$$I\ddot{\varphi}_x + J\Omega\dot{\varphi}_y + k\varphi_x = 0$$
$$I\ddot{\varphi}_y - J\Omega\dot{\varphi}_x + k\varphi_y = 0 \qquad (3.6)$$

By assuming $\varphi_x = x \cos pt$, $\varphi_y = y \sin pt$ it can be shown that the two natural frequencies are 364 c/s and 649 c/s, the higher frequency giving a forward precession and the lower frequency a backward precession. Fig.24 shows transients for this case with values of μ of 0.1, - 0.1 and zero.

For $\mu = 0.1$ the lower frequency mode with backward precession is excited and the other mode inhibited while the reverse is the case for $\mu = -0.1$. For $\mu = 0$ both frequencies are present in the waveform.

Fig.25 shows the effect of introducing dead zone which lowers the frequencies because of the reduction in effective stiffness but the inhibition of one mode and accentuation of the other is still evident for $\mu = \pm 0.1$.

CHAPTER 4.

THE EFFECT OF "OIL-WHIP" FORCES

4.1. Assumptions and equations of motion

Fig. 26 shows the bearing reaction forces assumed by Prentis[2] in his work on the problem put forward by Quartley[1]. These forces are of a type appropriate to a hydrodynamic bearing, and are known to cause "oil-whip" vibration in certain circumstances.

With these assumptions regarding the forces in the spin axis bearings, the equations of motion of the gyroscope become:-

$$I(\ddot{\varphi}_x + \ddot{\Theta}_x) + 2\nu l^2 \dot{\varphi}_x - J\Omega(\dot{\varphi}_y + \dot{\Theta}_y) - \nu l^2 \Omega \varphi_y = 0$$

$$I(\ddot{\varphi}_y + \ddot{\Theta}_y) + 2\nu l^2 \dot{\varphi}_y + J\Omega(\dot{\varphi}_x + \dot{\Theta}_x) + \nu l^2 \Omega \varphi_x = 0$$

$$M\ddot{\Theta}_x + f\dot{\Theta}_x - 2\nu l^2 \dot{\varphi}_x + \nu l^2 \Omega \varphi_y = 0 \qquad (4.1)$$

$$M\ddot{\Theta}_y + f\dot{\Theta}_y - 2\nu l^2 \dot{\varphi}_y - \nu l^2 \Omega \varphi_x = 0$$

where ν is a spin axis bearing parameter,

l is half the axial pitch of the spin axis bearings,

f is a damping coefficient representing friction at the gimbal bearings.

These are the equations given by Prentis in his paper except that the signs of the $\nu l^2 \Omega \varphi$ terms in the 3rd and 4th equations have been corrected. It should also be noted that Prentis has used a left handed set of axes, which affects the signs of the gyroscopic couples.

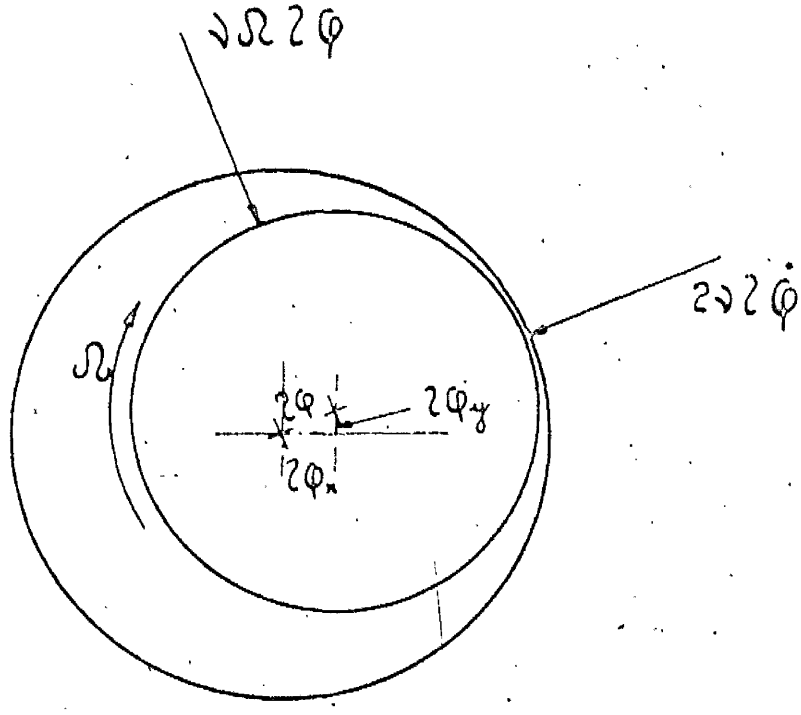

SPIN AXIS BEARING REACTIONS
ASSUMED BY PRENTIS.

FIG 26.

4.2. Analogue simulation

Fig.27 shows the computer set up used to solve the above equations.

In addition to checking a few sample points in Prentis' stability chart, the computer was used to simulate a gyro with parameters similar to those used in other sections of this thesis viz. $J = 1.525$ gm.cm.sec^2 ; $I = 2.15$ gm.cm.sec^2 ; $M_x = 1.4$ gm.cm.sec^2 ; $M_y = 5.6$ gm.cm.sec^2 ; $\Omega = 2514$ rad/sec.

The stability limit was obtained from the computer and the results are shown in Fig.28 . This shows the amount of gimbal damping required to give a simple harmonic transient for a given value of the spin axis bearing parameter μ where $\mu = \gamma l^2/J\Omega$. The gimbal damping is also non dimensional, i.e. $\xi = f/J\Omega$.

Since the parameter μ varies inversely with clearance, it can be seen that the gyro is least stable when the bearings are slack, at least for $\mu \geq 0.1$.

Also shown in Fig.28 is a curve of nutation frequency, showing a considerable reduction in frequency as the bearings become slacker.

Fig.29 shows a set of transients for the conditions $\mu = 0.1$ $\xi = 0.5$. The shaft trajectory in the bearing, represented by the φ_x, φ_y plot shows a high frequency oscillation superimposed on the main trajectory, and this frequency was found to be the nutation frequency of the free rotor, viz. $J\Omega/I$.

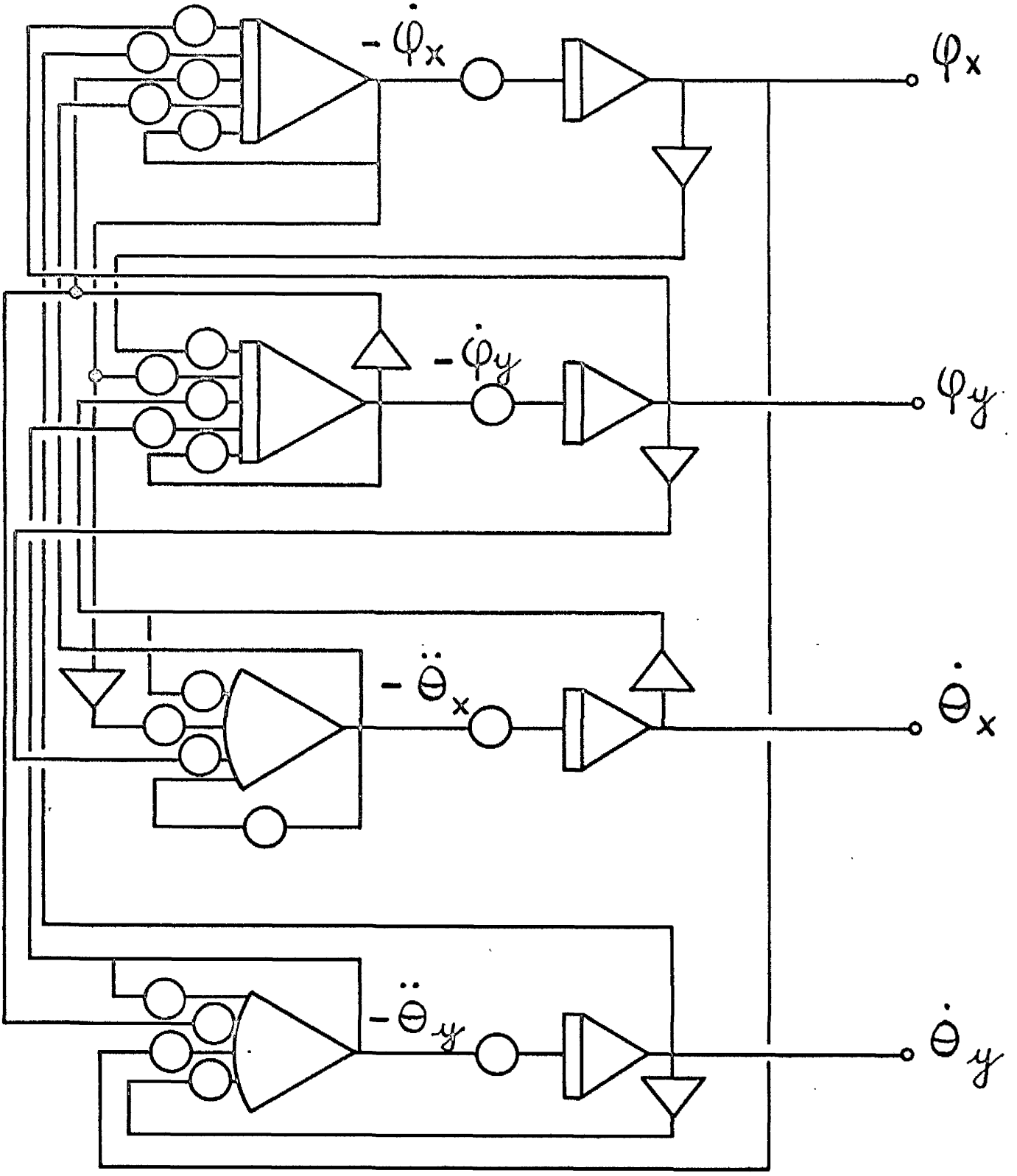

COMPUTER SET UP FOR PRENTIS'S EQUATIONS

FIG. 2?

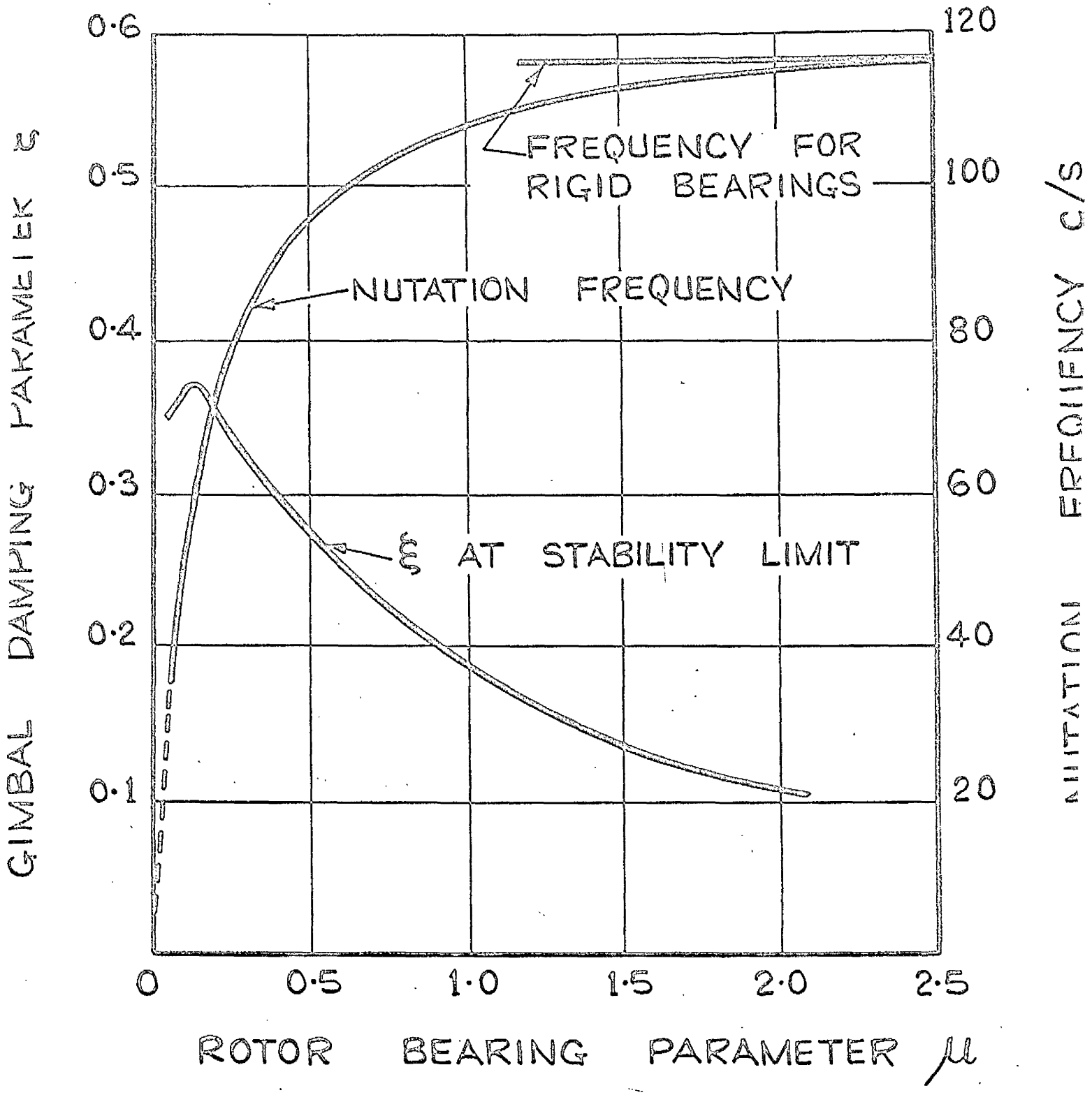

EFFECT OF BEARING CLEARANCE ON FREQUENCY AND STABILITY.

FIG. 21

MOTION OF GIMBAL

θ

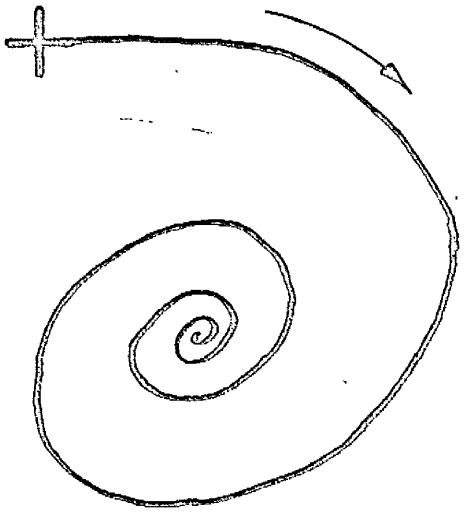

MOTION OF ROTOR

$\theta + \varphi$

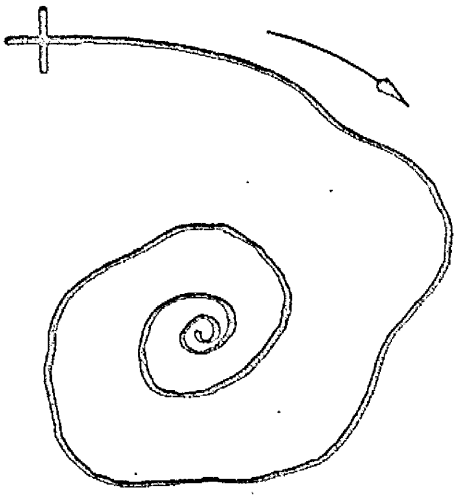

RELATIVE MOTION

φ

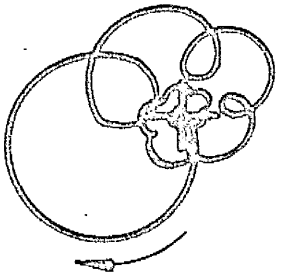

TRANSIENTS FOLLOWING AN IMPULSE IN THE x DIRECTION FOR $\mu = 0.1$ $\zeta = 0.5$.

FIG. 8

CHAPTER 5.

POSSIBLE SOURCES OF TANGENTIAL FORCES ON THE ROTOR

5.1. Effect of magnetic field of the driving motor

Fig.30 relates to a rotor tilted at an angle φ to the magnetic axis of the stator. At the instant being considered it is assumed that the displacement φ is in the plane of the magnetic field set up in the rotor by the three phase stator. The tangential force intensity due to the magnetic field will vary along the length of the rotor due to the variation in air gap g caused by the displacement φ . This variation will be non-linear, and may be represented as follows:-

$$F(g) = F_o + \Delta g \frac{dF}{dg} + \frac{\Delta g^2}{2} \frac{d^2F}{dg^2} + \text{- - -} \qquad (5.1)$$

where F(g) is the tangential force per unit length along one edge of the rotor, F_o is the value of F at the mean gap, g_o and $\Delta g = g - g_o = \varphi . x$. Fig.30 shows the variation of these three components of F along the length of the rotor, at both upper and lower edges. The arrows indicate the direction of the force components as they would appear in a plan view of the rotor.

It can be seen that while F_o and $\frac{\Delta g^2}{2} \frac{d^2F}{dg^2}$ simply produce driving torque about the rotor spin axis the $\Delta g \frac{dF}{dg}$ term produces a torque T_m about a vertical transverse axis, where:-

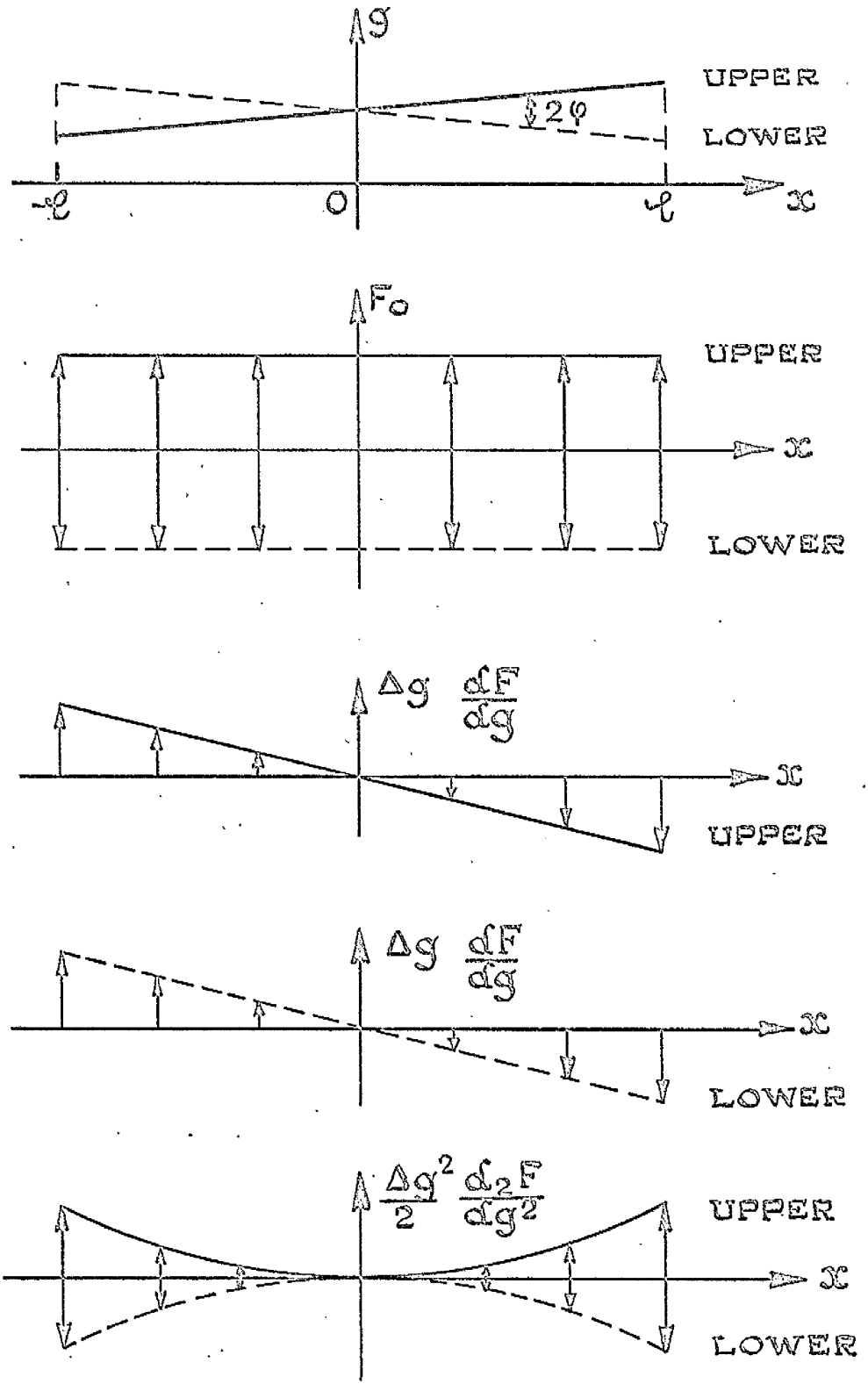

DISTRIBUTION OF AIR GAP AND TANGENTIAL FORCE INTENSITY ON A TILTED ROTOR.

FIG. 30.

$$T_m = 2 \int_{-l}^{l} F_x dx$$

$$= 2 \int_{-l}^{l} \Delta g \frac{dF}{dg} \times dx$$

$$= 2 \int_{-l}^{l} \frac{dF}{dg} \varphi x^2 dx$$

$$= \frac{4l^3}{3} \frac{dF}{dg} \varphi \qquad (5.2)$$

The quantity $\frac{dF}{dg}$ can be related to the variation in total motor torque with air gap under conditions where the air gap is uniform along the length of the motor.

The torque about the spin axis

$$T_s = 2R \int_{-l}^{l} F dx$$

and taking F as constant,

$$T = 4 l R F$$

and $$\frac{dT}{dg} = 4 l R \frac{dF}{dg} \qquad (5.3)$$

$\frac{dT}{dg}$ can be measured from torque/air gap curves of the motor and typical values, taken from a paper by Teare[11] give $\frac{dT}{dg}$ about 30 gm.cm/thou at 0.025 in. air gap.

Using this value in the expression

$$T_m = \frac{I^2}{3R} \frac{dT}{dg} \varphi \qquad (5.4)$$

gives

$$T_m \doteq 10^4 \varphi \text{ gm.cm. for } I = R = 1 \text{ in.}$$

5.2. Direction of T_m

For any configuration of gyroscope, whether the rotor surrounds the stator or vice versa the sense of T_m is the same as that of the torque produced by "oil whip" forces in the spin axis bearings.

5.3. Variation of T_m with rotation of rotor.

The above analysis holds for the instant when the rotating magnetic field is in the same plane as the displacement φ. When the magnetic field is at right angles to the plane of φ, T_m will be zero, so that T_m may be represented approximately by $T_m = \frac{10^4 \varphi}{2} \quad 1 + \cos(2\Omega t - \alpha)$

Where $\alpha = \tan^{-1} \frac{\varphi_y}{\varphi_x}$ is the angle between the planes of φ and φ_x, and Ωt is the angle between the plane of the rotating field and the plane of φ_x. Resolving T_m into torques about the OX, OY axes gives

$$T_{m_x} = \frac{10^4 \varphi}{2} \left[1 + \cos 2(\Omega t - \alpha)\right] \sin \alpha$$

$$T_{m_y} = -\frac{10^4 \varphi}{2} \left[1 + \cos 2(\Omega t - \alpha)\right] \cos \alpha \qquad (5.5)$$

5.4 Effect of type of motor

The above analysis will apply to synchronous hysteresis motors and also to asynchronous induction motors. In a D.C. motor the magnetic field does not rotate and the transverse magnetic torques T_{mx} and T_{my} will not be periodic with time, depending only on the orientation of the displacement φ relative to the magnetic field.

5.5 Kinematic analysis of angular contact ball bearing

This investigates the possibility of the existence in ball bearings of forces of the type which produce "oil whip" in journal bearings. Prentis[2] in his analysis assumes that the bearing reaction force has a radial component proportional to the radial relative velocity and a tangential component proportional to relative radial displacement, (see Fig. 26). The following approximate analysis investigates possible effects due to angular acceleration of the ball cage about the axis of shaft rotation. Angular velocities and accelerations of the cage about other axes are not considered.

In an angular contact ball bearing, the angular velocity of the cage about the spin axis of the shaft, assuming pure rolling, is a function of the contact angle, i.e.

$$\Omega_c = \frac{\Omega}{2}\left(1 - \frac{d}{D}\cos\Theta\right) \qquad (5.6)$$

where Ω_c is the cage speed, Ω is the shaft speed, d is the ball diameter, D the pitch circle diameter of the balls and Θ is the angle of contact.

If the angle of contact θ varies due to angular displacements of the rotor about axes transverse to the spin axis, this will tend to produce changes in the angular velocity of the cage, Ω_c. The following analysis seeks to establish a relationship between the angular acceleration $\dot{\Omega}_c$ and the angular velocity of the spin axis relative to the inner gimbal, $\dot{\varphi}$.

Fig. 31 (a) shows a cross section of a ball in contact with the races, the difference between ball and race curvatures being exaggerated. C_i and C_o are the centres of curvature of inner and outer races respectively. If rotor spin is ignored one possible kinematic model of the rotor-inner gimbal assembly is shown in fig. 31 (b). As shown, no relative angular displacement φ transverse to the spin axis is possible, but it can take place if the outer races are free to move axially, due for instance to elastic deflection of preload springs or the inner gimbal itself.

Fig. 32 shows one quarter of fig. 31 (b), in its original and deflected positions. O is a point on the spin axis, midway between the bearings, and the displacement φ moves the point C_i to C_i^1. As a result the point C_o moves axially to C_o^1 and the distance $C_o C_o^1$ represents the axial deflection of the bearing outer race away from O. At the opposite side of the same bearing, clearance will appear, and the cage speed will be mainly determined by conditions at the loaded side. The angular acceleration of the cage is obtained by differentiating eqn. 5.6, giving

$$\dot{\Omega}_c = \frac{\Omega}{2} \frac{d}{D} \sin\theta \cdot \dot{\theta} \qquad (5.7)$$

where θ is the angle of contact at the loaded side of the bearing. Referring to

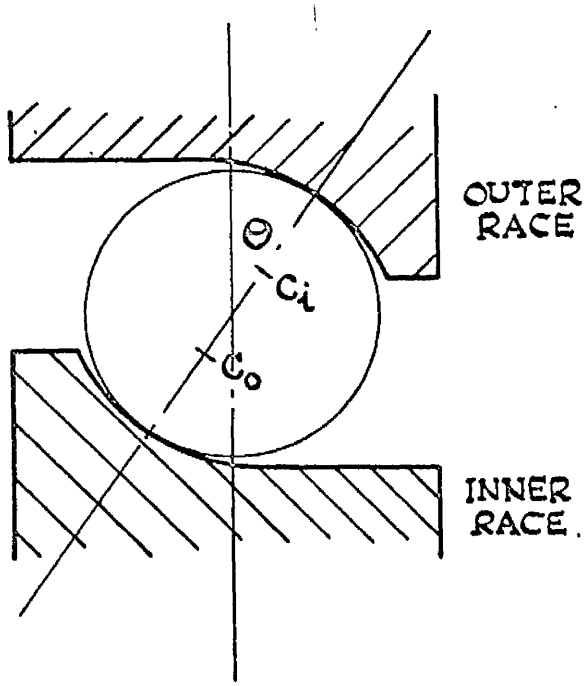

(a)

CROSS SECTION OF
BALL AND RACES.

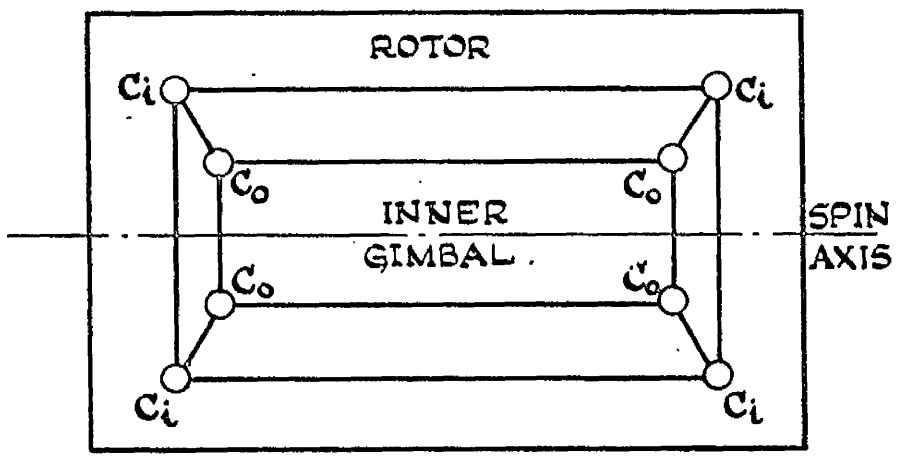

(b)

KINEMATIC MODEL, IGNORING SPIN.

FIG. 3

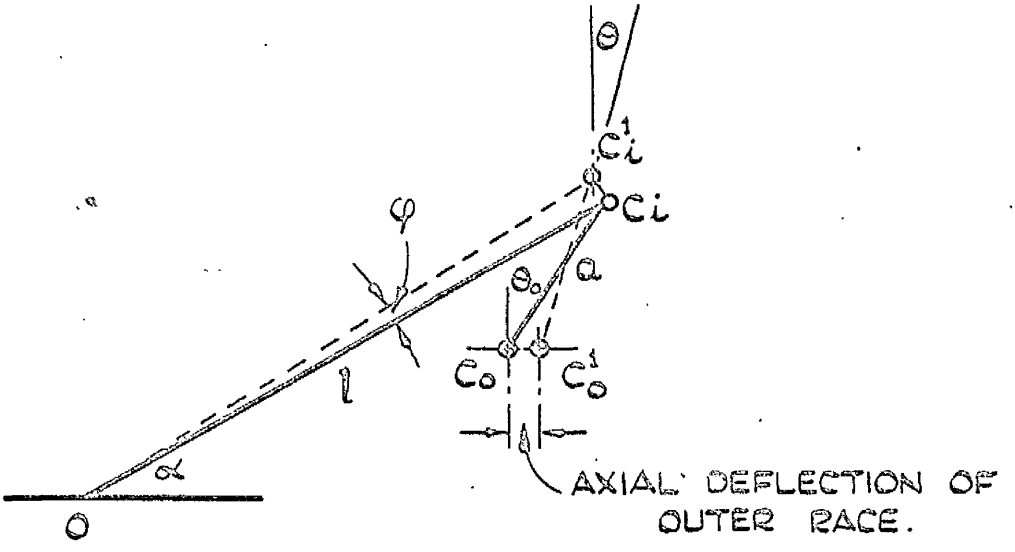

EFFECT OF ROTOR DISPLACEMENT ON CONTACT ANGLE

FIG. 32

fig. 32 again, $C_i C_i^1 \simeq \ell\varphi$, and the projection of $C_i C_i^1$ perpendicular to the spin axis is approximately $C_i C_i^1 \cos\alpha$.

Also,

$$C_i C_i^1 \cos\alpha = a(\cos\Theta - \cos\Theta_o)$$

where Θ_o is the angle of contact in the unloaded condition.

i.e. $\ell\varphi\cos\alpha = a(\cos\Theta - \cos\Theta_o)$

and $\ell\dot{\varphi}\cos\alpha = -a\sin\Theta\,.\,\dot{\Theta}$

Taking the axial pitch of the bearings as $L = 2\ell\cos\alpha$,

$$\dot{\varphi}_i = -\frac{2a}{L}\sin\Theta\,.\,\dot{\Theta}$$

and substituting in eqn. 5.7 gives

$$\dot{\Omega}_c = -\frac{\Omega}{2}\,.\,\frac{d}{D}\,.\,\frac{L}{2a}\,\dot{\varphi} \qquad (5.8)$$

for Barden 34 - 5B bearings, axially pitched at 2.25 ins, and a shaft speed of 400 rev/sec.

$$\dot{\Omega}_c = -\frac{2514}{2}\,.\,\frac{0.125}{0.388}\,.\,\frac{2.25\,\dot{\varphi}}{2\times 0.01}$$

$$= -45{,}700\dot{\varphi}\ \text{rad/sec}^2$$

It will be seen that this effect depends strongly on the conformity of the race curvatures with the ball curvature, i.e. the distance $a = C_i C_o$. Conformity is specififed by giving the radius of curvature of the race as a percentage of the ball radius so that a change of radius of race curvature from 52% to 54% ball radius makes 100% change in the value of a. The value of a used in the numerical work above assumes that the conformity is 54%.

5.6 Effect of cage acceleration

Fig. 33 shows the directions of the forces and couples acting on the cage and balls, and Fig. 33 shows a linear system equivalent to shaft, cage and gimbal.

M_c and M_b are the masses of cage and balls respectively and I_b is the total moment of inertia of those balls considered to be subject to the angular acceleration α_b. r_p is the pitch circle radius of the balls and r_b is the rolling radius = ball radius r. cos θ .

R_s and R_g are the reactions exerted on the balls by the shaft and gimbal respectively. Taking moments about the unknown reactions,

$$R_s = \frac{1}{2r_b}\left[(M_c + M_b)\dot{\Omega}_c r_p r_b + I_b \alpha_b\right]$$
$$R_g = \frac{1}{2r_b}\left[(M_c + M_b)\dot{\Omega}_c r_p r_b - I_b \alpha_b\right] \qquad (5.9)$$

and since $\alpha_b = \dot{\Omega}_c \cdot \frac{r_p}{r_b}$

$$R_s = \frac{\dot{\Omega}_c r_p}{2}\left[M_c + M_b + \frac{I_b}{r_b^2}\right] \qquad (5.10)$$

Assuming that 3 balls out of the total of 6 are in contact and subject to the angular acceleration α_b, and putting $I_b = M_b k_b^2$ where $k_b^2 = \frac{2}{5} r^2$

$$R_s = \frac{\dot{\Omega}_c r_p}{2}\left[M_c + M_b\left(1 + \frac{1}{5\cos^2\theta}\right)\right] \qquad (5.11)$$

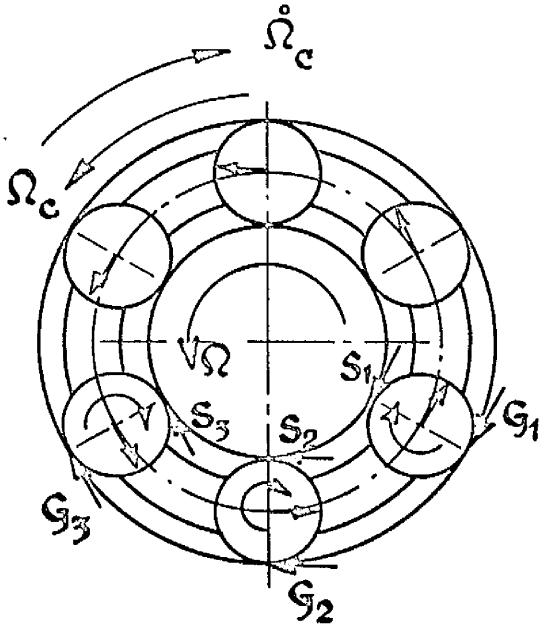

(a)

FORCES AND COUPLES DUE TO CAGE ACCELERATION

(b)

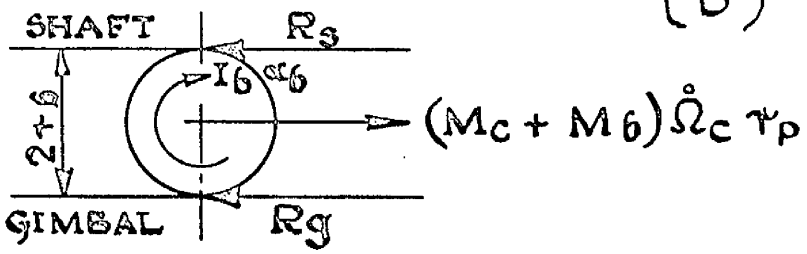

EQUIVALENT SYSTEM.

FIG. 33.

Substituting values appropriate to the Barden-34 5B bearing gives

$$R_s = \frac{45{,}700\ \dot{\varphi} \cdot \quad 0.194}{2 \times 386.4} \left[0.002 + 0.00063 \left(1 + \frac{1}{5 \cos^2 25^\circ}\right) \right]$$

i.e. $R_s = 0.032\ \dot{\varphi}$ lb. and $R_g = 0.0285\ \dot{\varphi}$ lb.

The sense of the corresponding force acting on the shaft is the same as that due to the wedge action in a hydrodynamic bearing.

On the other hand the force acting on the gimbal due to cage acceleration is in the same sense as that on the rotor whereas in the case of the hydrodynamic bearing the forces on shaft and bearing are in opposite senses.

The resultant of reactions S_1, S_2, S_3 at the three balls in contact can be shown to be $2S_1$ acting at a radius of $\frac{3}{2}\ r_i$, where r_i is the radius of the path of contact on the inner race, and similarly the resultant of $G_{1,2,3}$ is $2G_1$ acting at the radius $\frac{3}{2} r_o$. Since $S_1 = \frac{1}{3} R_s$ the total torque on the rotor about the spin axis is $2S_1 \times 1\frac{1}{2} r_i = 3\ S_1 r_i$ as would be expected. More important, however is the torque about the transverse axis which will be $2S_1 \times L = \frac{2}{3}\ R_s\ L$ where L is the axial distance between the bearings. It can be shown that if 2 balls are assumed in contact the above moment will be $\frac{3}{2} R_s L$ and for 1 ball in contact will be $R_s L$, ignoring the minor variation in I_c due to the different number of balls subject to angular acceleration.

A check on the direction of the moment $R_s L$ shows that it acts on the rotor in the same direction as the gyroscopic couple produced by the angular velocity $\dot{\varphi}$, so that in the case of a fixed casing or gimbals, the effect of cage acceleration is the same as an increase in polar moment of inertia of the rotor.

For an axial pitch L = 2.25 in, polar moment of inertia J = 1.525 gm. cm. sec^2 and rotor speed 400 rev/sec,

$$R_s L = 0.0721 \dot{\varphi} \text{ lb. in.}$$

and the gyroscopic couple $J\Omega\dot{\varphi} = 3.33\dot{\varphi}$ lb. in.

The effect of cage acceleration is therefore of the order of 2% of the gyroscopic couple. When the gimbals are free, the gyroscopic couple is proportional to $\dot{\theta} + \dot{\varphi}$ while the effect of cage acceleration remains proportional to $\dot{\varphi}$.

5.7 Effect of bearing slackness

Another possible cause of cage acceleration is the reduction in radial load and friction as the shaft passes across the clearance in a slack bearing. It will be particularly significant in the upper bearing of a vertical shaft gyro where the radial load will reduce to zero when the shaft is in the centre of the clearance and the thrust load will be small, or zero.

Two opposite effects are possible depending on the construction of the bearing.

If the bearing is made with the inner race separable, the cage and balls will be retained by the outer race and will slow down as the shaft and inner race pass across the clearance.

However, if the bearing is made with the outer race separable the cage will tend to speed up during the passage of the shaft across the clearance. On subsequent contact the cage will impart impulses to shaft and gimbals as it regains

its "epicyclic" speed.

The effect is not readily analysed since the magnitude of the effect depends on the time of passage across the clearance and the friction torques acting on the cage which will vary with the position of the shaft. The effect will be generally similar to that described in section 3.1 and formulated in equations 3.1.

The bearing with inner race separable will give an effect similar to μ positive in equations 3.1. and with the outer race separable μ will be negative.

CHAPTER 6.

THE EFFECT OF SHAFT AND BEARING COMPLIANCE

In this analysis it is assumed that the rotor bearings and/or shaft are elastic. Only those modes of vibration are considered in which the rotor centre of gravity remains at the intersection of the gimbal bearing axes. The rotor spin axis is assumed to rotate through angles φ_x and φ_y relative to the inner gimbal. This is the case dealt with by Maunder[12] from the point of view of natural frequency.

6.1. Frequency response analysis

In this section the frequency response of the gyro to applied forcing torques on the gimbals will be considered.

The equations of motion are:-

$$I(\ddot{\theta}_x + \ddot{\varphi}_x) + J\Omega(\dot{\theta}_y + \dot{\varphi}_y) + R_b\dot{\varphi}_x + k\varphi_x = 0$$

$$I(\ddot{\theta}_y + \ddot{\varphi}_y) - J\Omega(\dot{\theta}_x + \dot{\varphi}_x) + R_b\dot{\varphi}_y + k\varphi_y = 0 \qquad (6.1)$$

$$M_x\ddot{\theta}_x + R_g\dot{\theta}_x - R_b\dot{\varphi}_x - k\varphi_x = T_x$$

$$M_y\ddot{\theta}_y + R_g\dot{\theta}_y - R_b\dot{\varphi}_y - k\varphi_y = T_y$$

where Ω = angular velocity of spin.

T_x = applied forcing torque about the outer gimbal axis.

T_y = applied forcing torque about the inner gimbal axis.

If T_x and T_y are sinusoidal, of frequency ω radians/sec, the customary substitution of $d/dt \equiv j\omega$ can be made. The equations can then be written in matrix form as:-

$$\begin{bmatrix} k + R_b j\omega - \omega^2 I & J\Omega j\omega & j\omega I & J\Omega \\ -J\Omega j\omega & k + R_b j\omega - \omega^2 I & -J\Omega & j\omega I \\ -k - R_b j\omega & 0 & R_g + j\omega M_x & 0 \\ 0 & -k - R_b j\omega & 0 & R_g + j\omega M_y \end{bmatrix} \begin{bmatrix} \varphi_x \\ \varphi_y \\ \dot{\theta}_x \\ \dot{\theta}_y \end{bmatrix} = \begin{bmatrix} 0 \\ 0 \\ T_x \\ T_y \end{bmatrix} \qquad (6.2)$$

For $T_y = 0$, the fourth equation gives

$$\varphi_y = \frac{R_g + j\omega M_y}{k + R_b j\omega} \dot{\theta}_y$$

and the third,

$$\varphi_x = -\frac{T_x}{k + R_b j\omega} + \frac{R_g + j\omega M_x}{k + R_b j\omega}$$

Substituting these in the first and second equations and multiplying throughout by $k + R_b j\omega$ gives

$$\begin{bmatrix} j\omega I(k+R_b j\omega)+(k+R_b j\omega-\omega^2 I)(R_g+j\omega M_x) & J\Omega[k+R_b j\omega+j\omega(R_g+j\omega M_y)] \\ -J\Omega[k+R_b j\omega+j\omega(R_g+j\omega M_x) & j\omega I(k+R_b j\omega)+(k+R_b j\omega-\omega^2 I)(R_g+j\omega M_y) \end{bmatrix} \times \begin{bmatrix} \dot{\theta}_x \\ \dot{\theta}_y \end{bmatrix} = T_x \begin{bmatrix} k+R_b j\omega-\omega^2 I \\ -J\Omega j\omega \end{bmatrix} \qquad (6.3)$$

Using the abbreviations:-

$$\begin{bmatrix} a_x & b_y \\ b_x & a_y \end{bmatrix} \times \begin{bmatrix} \ddot{\theta}_x \\ \ddot{\theta}_y \end{bmatrix} = T_x \begin{bmatrix} c \\ d \end{bmatrix}$$

the transfer functions are:-

$$\frac{\ddot{\theta}_x}{T_x} = \frac{\begin{vmatrix} c & b_y \\ d & a_y \end{vmatrix}}{\begin{vmatrix} a_x & b_y \\ b_x & a_y \end{vmatrix}} = \frac{c.a_y - d.b_y}{a_x a_y - b_x b_y}$$

and (6.4)

$$\frac{\ddot{\theta}_y}{T_x} = \frac{\begin{vmatrix} c & a_x \\ d & b_x \end{vmatrix}}{\begin{vmatrix} a_x & b_y \\ b_x & a_y \end{vmatrix}} = \frac{d.a_x - c.b_x}{a_x a_y - b_x b_y}$$

Similarly it can be shown that:-

$$\frac{\ddot{\theta}_x}{T_y} = \frac{-d.a_y - c.b_y}{a_x a_y - b_x b_y}$$

and

$$\frac{\ddot{\theta}_y}{T_y} = \frac{d.b_x + c.a_x}{a_x a_y - b_x b_y}$$

If the damping is assumed to be zero these transfer functions can be "non-dimensionalised" as follows. First the requisite power of J is extracted so that all other inertias appear divided by J and the following inertia ratios

are defined :- $i = I/J$, $x = M_x/J$, $y = M_y/J$

Then the requisite power of Ω is extracted so that all frequencies are referred to Ω i.e. $\omega/\Omega = f$ and $k/J\Omega^2 = p^2$.

The transfer functions then reduce to:-

$$\frac{J\Omega\dot{\theta}_x}{T_x} = \frac{i\ f/x\left[i^2\left\{\frac{p^2(i+y)}{iy} - f^2\right\}\left(\frac{p^2}{i} - f^2\right) + \frac{p^2}{y} - f^2\right]}{\left[\left(\frac{p^2}{x} - f^2\right)\left(\frac{p^2}{y} - f^2\right) - i^2f^2\left\{\frac{p^2(i+x)}{ix} - f^2\right\}\left\{\frac{p^2(i+y)}{iy} - f^2\right\}\right]}$$

$$\frac{J\Omega\dot{\theta}_y}{T_x} = \frac{i/y\left[\left(\frac{p^2}{x} - f^2\right)\left(\frac{p^2}{i} - f^2\right) + f^2\left\{\frac{p^2(i+x)}{ix} - f^2\right\}\right]}{\left[\left(\frac{p^2}{x} - f^2\right)\left(\frac{p^2}{y} - f^2\right) - i^2f^2\left\{\frac{p^2(i+x)}{ix} - f^2\right\}\left\{\frac{p^2(i+y)}{iy} - f^2\right\}\right]}$$

$$= \frac{p^4}{\left[\left(\frac{p^2}{x} - f^2\right)\left(\frac{p^2}{y} - f^2\right) - i^2f^2\left\{\frac{p^2(i+x)}{ix} - f^2\right\}\left\{\frac{p^2(i+y)}{iy} - f^2\right\}\right]}$$

$$\frac{J\Omega\dot{\theta}_x}{T_y} = -\frac{p^4}{\left[\left(\frac{p^2}{x} - f^2\right)\left(\frac{p^2}{y} - f^2\right) - i^2f^2\left\{\frac{p^2(i+x)}{ix} - f^2\right\}\left\{\frac{p^2(i+y)}{iy} - f^2\right\}\right]}$$

$$\frac{J\Omega\dot{\theta}_y}{T_y} = \frac{i\ f/y\left[i^2\left\{\frac{p^2(i+x)}{ix} - f^2\right\}\left(\frac{p^2}{i} - f^2\right) + \frac{p^2}{x} - f^2\right]}{\left[\left(\frac{p^2}{x} - f^2\right)\left(\frac{p^2}{y} - f^2\right) - i^2f^2\left\{\frac{p^2(i+x)}{ix} - f^2\right\}\left\{\frac{p^2(i+y)}{iy} - f^2\right\}\right]}$$

(6.5)

6.2. General form of frequency response curves

6.2.1. Amplitude:

The equation $\left(\frac{p^2}{x} - f^2\right)\left(\frac{p^2}{y} - f^2\right) - i^2 f^2 \left\{\frac{p^2(i+x)}{ix} - f^2\right\}\left\{\frac{p^2(i+y)}{iy} - f^2\right\} = 0$

gives the poles of the transfer functions, i.e. the natural frequencies of the gyro. Since $\left(\frac{p^2}{x} - f^2\right)\left(\frac{p^2}{y} - f^2\right) - i^2 f^2 \left\{\frac{p^2(i+x)}{ix} - f^2\right\}\left\{\frac{p^2(i+y)}{iy} - f^2\right\}$ is a cubic function of f^2 there will be three natural frequencies. The bracketed parts of the numerators of $\frac{\dot{\theta}_x}{T_x}$ and $\frac{\dot{\theta}_y}{T_y}$ are quadratics in f^2 and give two zeros.

Because of the factor jf outside the brackets there is another zero at zero frequency.

At zero frequency $\frac{J\Omega\dot{\theta}_y}{T_x}$ and $\frac{J\Omega\dot{\theta}_x}{T_y}$ are both unity as would be expected.

At very high frequency, only the highest powers of f need be considered. Under these conditions $\frac{J\Omega\dot{\theta}_x}{T_x} \rightarrow \frac{1}{jfx}$ and the high frequency asymptote on a Bode plot has a slope of - 1. Similarly $\frac{J\Omega\dot{\theta}_y}{T_y} \rightarrow \frac{1}{jfy}$. In the case of $\frac{J\Omega\dot{\theta}_y}{T_x}$ and $\frac{J\Omega\dot{\theta}_x}{T_y}$, both tend to the value $\frac{p^4}{i^2 xy (jf)^6}$ but with opposite signs indicating that the asymptote slope is - 6.

6.2.2. Phase:

For $\frac{J\Omega\dot{\theta}_y}{T_x}$ and - $\frac{J\Omega\dot{\theta}_x}{T_y}$, the phase shift tends to zero at low frequency and on passing through each natural frequency there is a phase shift of - 180°, so that at very high frequency the total phase lag is 540 degrees.

In the case of $\frac{J\Omega\dot{\theta}_x}{T_x}$ and $\frac{J\Omega\dot{\theta}_y}{T_y}$ the phase shift diagram is more complex. At zero frequency the phase shift is + 90° and at each natural frequency the phase shift changes by - 180°. At each zero of the transfer function the phase changes by + 180° so that the form of the phase shift curve depends on the relative disposition of the poles and zeros. At high frequency the phase shift tends to - 90°.

6.3. The effect of damping

6.3.1. At zero frequency.

In the absence of damping, as shown in the preceding section, the gimbal to which torque is applied does not move in the direction of that torque and the other gimbal moves at a rate proportional to the torque. The steady state behaviour in the presence of damping can be obtained by putting $\dot{\varphi} = \ddot{\varphi} = 0$ and $\ddot{\theta} = 0$ in equations 6.1.

Hence

$$J\Omega\dot{\theta}_y + k\varphi_x = 0$$

$$-J\Omega\dot{\theta}_x + k\varphi_y = 0$$

$$R_g\dot{\theta}_x - k\varphi_x = T_x$$

$$-R_g\dot{\theta}_y - k\varphi_y = T_y$$

(6.6.)

i.e. $$Rg\,\dot{\theta}_x + J\Omega\,\dot{\theta}_y = T_x$$

$$-J\Omega\,\dot{\theta}_x + Rg\,\dot{\theta}_y = T_y$$

giving

$$\dot{\theta}_x = \frac{Rg\,T_x - J\Omega\,T_y}{(J\Omega)^2 + Rg^2}$$

and

$$\dot{\theta}_y = \frac{J\Omega\,T_x + RgT_y}{(J\Omega)^2 + Rg^2}$$

$$\text{for } T_y = 0,\ \frac{\dot{\theta}_x}{T_x} = \frac{Rg}{(J\Omega)^2 + Rg^2},\ \frac{\dot{\theta}_y}{T_x} = \frac{J\Omega}{(J\Omega)^2 + Rg^2}$$

$$\text{and for } T_x = 0,\ \frac{\dot{\theta}_x}{T_y} = -\frac{J\Omega}{(J\Omega)^2 + Rg^2},\ \frac{\dot{\theta}_y}{T_y} = \frac{Rg}{(J\Omega)^2 + Rg^2} \qquad (6.7)$$

6.3.2. At other frequencies

The effect of damping will be to limit amplitudes at the three natural frequencies and also prevent the amplitude responses of $\frac{J\Omega\,\dot{\theta}_x}{T_x}$ and $\frac{J\Omega\,\dot{\theta}_y}{T_y}$ dropping to zero. The phase shift graphs will become continuous instead of having step changes of $\pm 180^\circ$.

6.4. Frequency response curves from analogue simulation

Fig.34. shows an analogue computer simulation of a gyro with compliance between rotor and gimbal. The frequency response curves shown

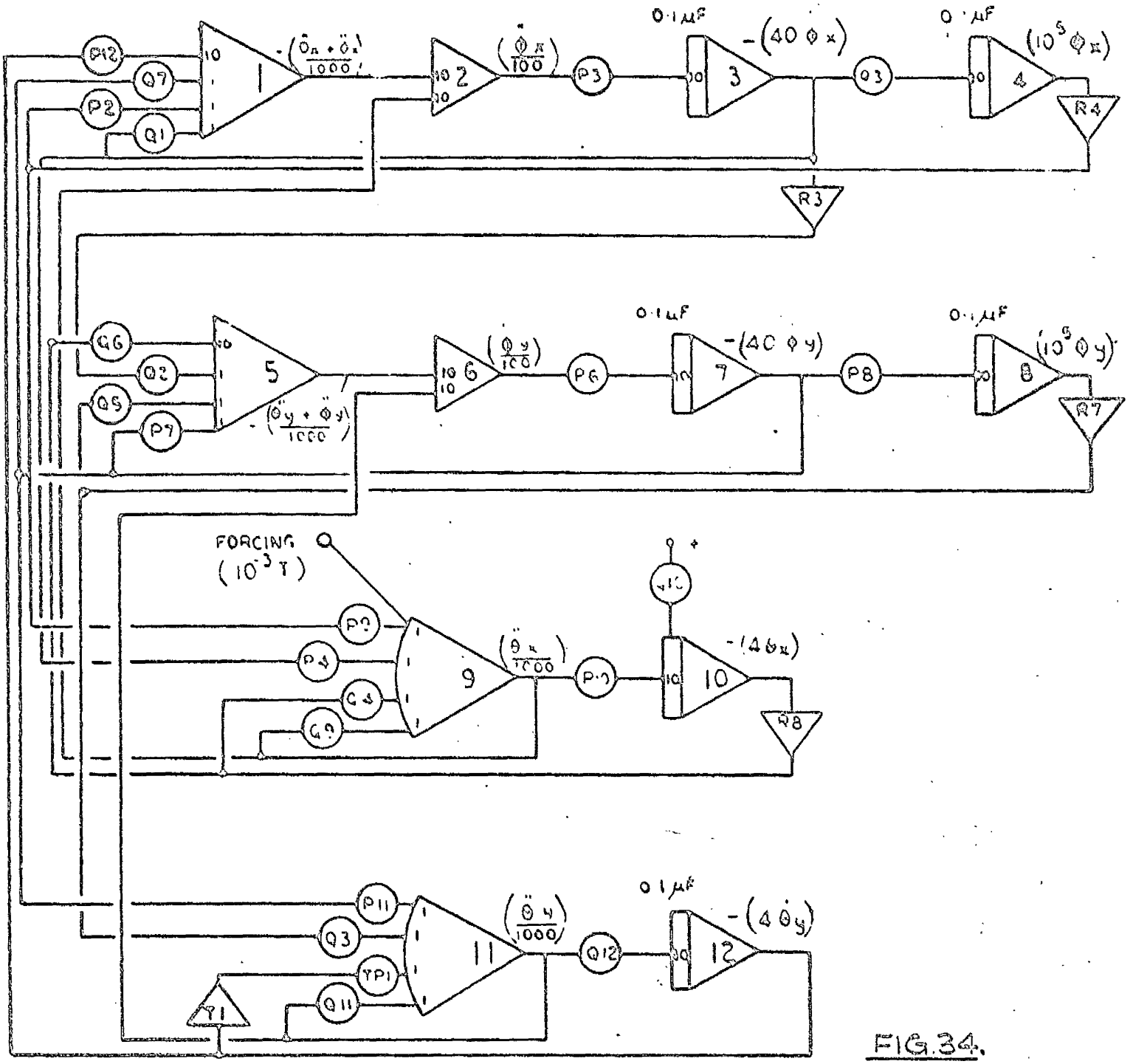

FIG.34.

COMPUTER DIAGRAM - GYRO WITH SHAFT/BEARING COMPLIANCE

in Fig. 35 were obtained by forcing the simulation with a transfer function analyser in a manner similar to that described in sec. 2.7.

The three resonances can be clearly seen in the response of both gimbal velocities to applied torque at the outer gimbal, and the lower frequency zero is also apparent in the curves of $\frac{J \Omega \dot{\theta}_x}{T_x}$. The effect of the upper zero is masked by its proximity to the third natural frequency.

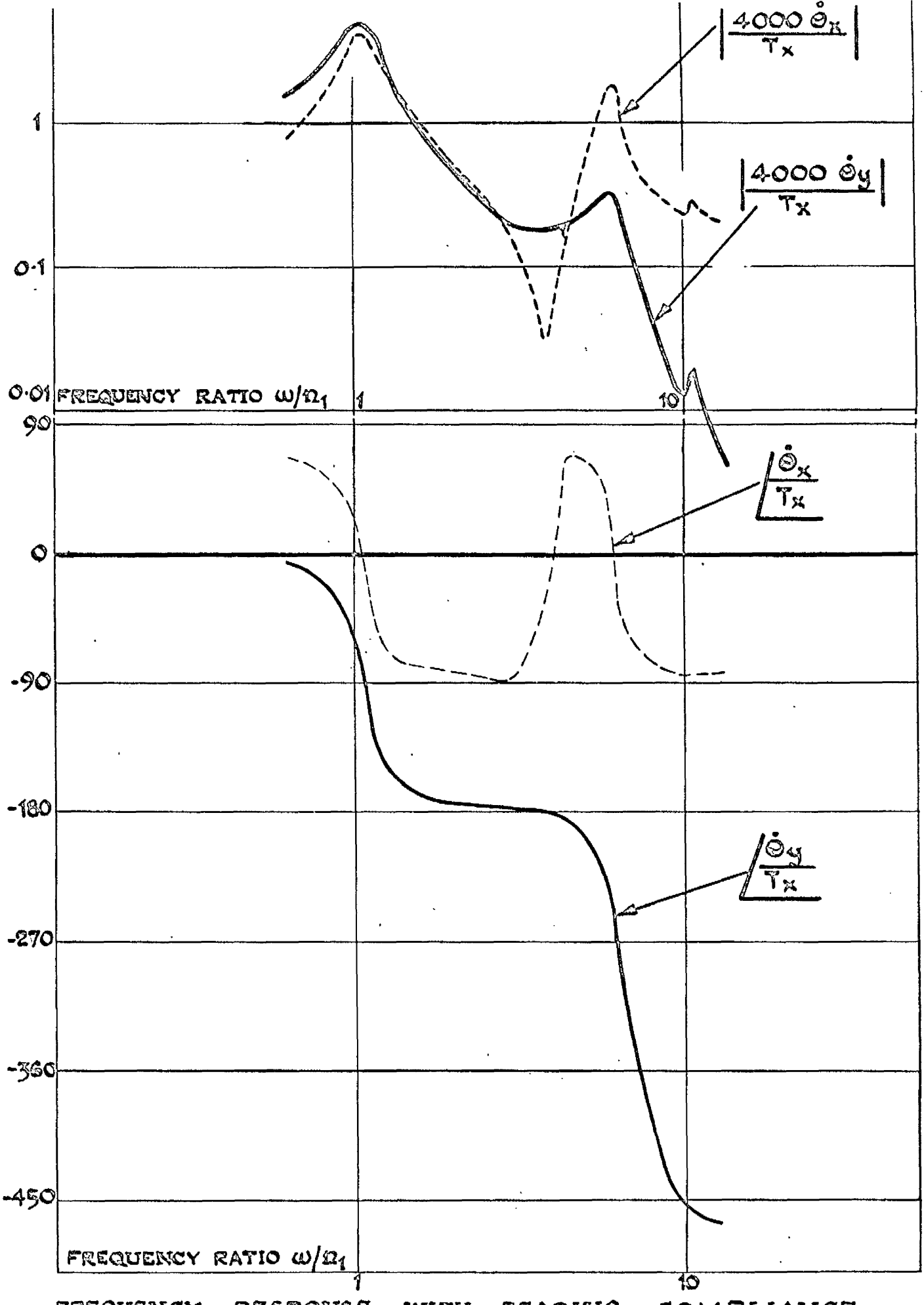

FREQUENCY RESPONSE WITH BEARING COMPLIANCE AND SYMMETRICAL ROTOR.

FIG. 35

6.4.1 Alternative method of obtaining the frequency response

The frequency response can also be obtained numerically by inverting the matrix on the left hand side of equation 6.2. The resulting 4 x 4 complex matrix contains the response of each of the displacements φ_x, φ_y, θ_x, θ_y to each of the torques T_{rx}, T_{ry}, T_x, T_y where T_{rx}, T_{ry} are forcing torques applied to the rotor - assumed zero in equation 6.2.

Since the matrix to be inverted is complex, it is necessary to convert it into a real matrix of double the size before inversion and select the appropriate quarters of the inverted matrix to give the real and imaginary parts of the result.

i.e. if $A + jB$ is the original matrix and $C + jD$ its inverse then

$$(A + jB)(C + jD) = 1 + jO$$

i.e. $$AC - BD = 1; \quad BC + AD = O$$

It can easily be shown that if the matrix

$$\begin{bmatrix} A & -B \\ B & A \end{bmatrix}$$

is inverted, the result is the matrix

$$\begin{bmatrix} C & -D \\ D & C \end{bmatrix}$$

Appendix 4 shows an Algol programme which carries out this process for the case of the symmetrical gyro with compliant shaft or bearings. A

typical set of results is also shown. Use of the "time now" procedure has indicated that the inversion process takes approximately 2 to 3 seconds for this size of matrix. Since the ICT 1905 computer used for this problem is a time sharing machine, the actual computing time may be even less.

Bearing in mind that the process gives the amplitude and phase relations between the torques and displacements plus a hard copy of the results it can be seen to compare very favourably with the analogue computer/ transfer function analyser approach, in which a single response of one displacement to one torque may take 30 seconds or more to obtain. Agreement between the digital results and the analogue results plotted in fig. 35 is excellent.

6.4.2 Extension to the unsymmetrical case

By including the effect of shaft/bearing compliance in equations 2.17 and manipulating the resulting equations in a fashion similar to section 8.2, the equations for the forced unsymmetrical gyro with a flexible shaft can be expressed in the form

$$\frac{dy}{dt} = ay + \mu f y + T$$

where a is a complex frequency dependent matrix - and f is a matrix containing periodic terms at the frequency 2Ω . T is a column vector of sinusoidal forcing torques frequency ω and μ is a small constant, here

proportional to the asymmetry of the rotor. Expressing y in a series form:-

$$y = y_o + \mu y_1 + \mu^2 y^2 + \text{-----}$$

and putting $\mu = 0$ gives yo as the solution of

$$\frac{dy}{dt} = a\,y + T$$

i.e. $$\frac{dy_o}{dt} = a\,y_o + T$$

and hence $$\frac{y_o}{T} = \left[a - j\,\omega I\right]^{-1}$$

Now if μ^2 and higher powers are neglected,

$$y = y_o + \mu y_1$$

$$\frac{dy}{dt} = \frac{dy_o}{dt} + \mu \frac{dy_1}{dt}$$

but $$\frac{dy}{dt} = a(y_o + \mu y_1) + \mu f(y_o + \mu y_1) + T$$

$$= a\,y_o + T + \mu(a\,y_1 + f\,y_o + \mu f\,y_1)$$

Equating the two expressions for dy/dt, neglecting the last term, and cancelling μ gives

$$\frac{dy_1}{dt} = a y_1 + f\,y_o$$

and $$\frac{y_1}{f\,y_o} = \left[(a - j\,\omega I)\right]^{-1}$$

i.e. fy_o becomes the forcing for the second approximation y_1. In block diagram form:-

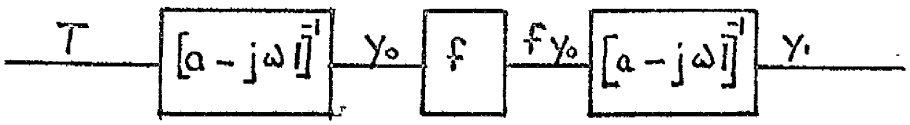

The matrix product fy_o contains terms with frequencies $\omega + 2\Omega$ and $\omega - 2\Omega$ and so at each step in the successive approximation process the waveform y becomes more complicated. By restricting attention to the case of a single forcing torque T_x or T_y the problem is much simplified and repeated use of the inversion procedure with appropriate frequencies inserted into the matrix $(a - j\omega I)$ gives a reasonable method of obtaining the solution y.

6.5 Natural frequencies of the system

The introduction of bearing elasticity gives rise to natural frequencies other than the normal nutation frequency of the gyro. The normal nutation frequency is reduced due to bearing elasticity and two other frequencies appear which are, for the parameters chosen, higher than the spin frequency of the rotor.

The natural frequencies can be easily found by substitution of appropriate sinusoidal functions in the equations of motion, and eliminati on of the amplitudes, or from the poles of the transfer functions in equations 6.5.

Shortly after this work was carried out, a paper by Maunder (12) appeared describing this case in considerable detail.

Fig. 36 shows for the case $M_x = M_y = M$, the variation of the three calculated natural frequencies with gimbal inertia for two values of the bearing stiffness k. The value of k affects the two upper frequenc ies, mainly, the lowest nutation frequency being only slightly altered by varying k between 10^7 gm.cm/radian and infinity.

6.6 The effect of bearing eccentricity

In this analysis the rotor bearings are assumed to be eccentric, in such a way that the rotor C. G. is not displaced but the equilibrium position of the shaft centre line generates a conical surface at an angular velocity of ω_1, the angular velocity of the ball cage, the semi angle of

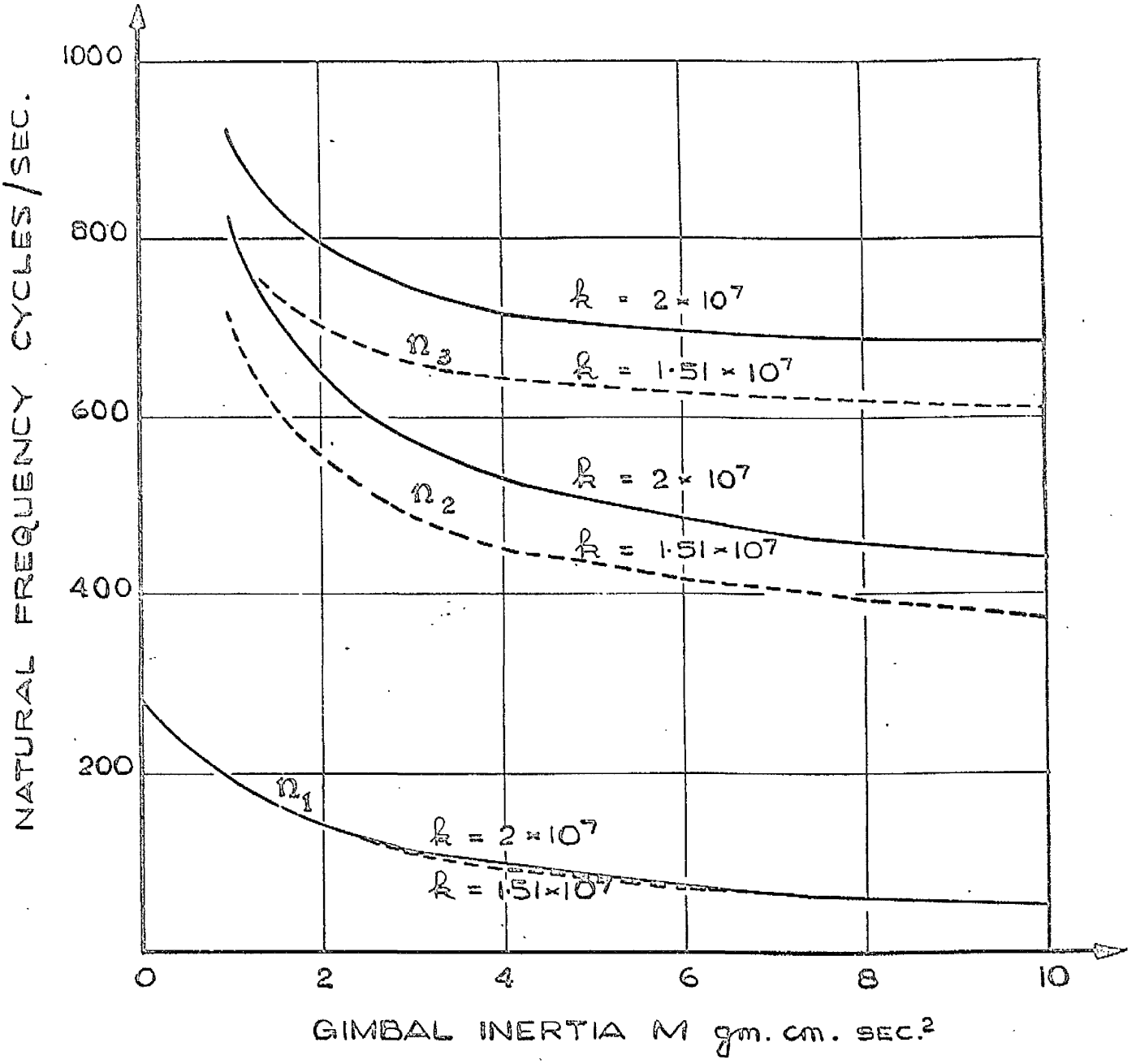

NATURAL FREQUENCIES OF GYRO WITH SHAFT OR BEARING COMPLIANCE.

FIG. 36

the cone being e (Fig. 37). For the angular contact bearings used in the experimental work the ratio $\dot{\omega}_1/\Omega$ was about 0.37.

The bearings are also assumed to be elastic, giving an equivalent angular stiffness k.

The equations of motion of this sytem are:-

$$I(\ddot{\theta}_x + \ddot{\varphi}_x) + J\Omega(\dot{\theta}_y + \dot{\varphi}_y) + R_b\dot{\varphi}_x + k\varphi_x - ke\cos\omega_1 t = 0$$
$$I(\ddot{\theta}_y + \ddot{\varphi}_y) - J\Omega(\dot{\theta}_x + \dot{\varphi}_x) + R_b\dot{\varphi}_y + k\varphi_y - ke\sin\omega_1 t = 0 \qquad (6.8)$$
$$M_x\ddot{\Theta}_x + Rg\dot{\Theta}_x - R_b\dot{\varphi}_x - k\varphi_x + ke\cos\omega_1 t = 0$$
$$M_y\ddot{\Theta}_y + Rg\dot{\Theta}_y - R_b\dot{\varphi}_y - k\varphi_y + ke\sin\omega_1 t = 0$$

It can be seen that the moments $ke\cos\omega_1 t$ and $ke\sin\omega_1 t$ act on rotor and gimbals and if the frequency ω_1 should coincide with a natural frequency of the system, large amplitudes of oscillation could be expected.

This system was simulated on an analogue computer, the computer diagram being shown in Fig. 38.

Fig. 39 shows the build up of a resonant oscillation, obtained by plotting θ_y against θ_x on an X-Y plotter. Also shown is the rotor motion, generated by two additional summing amplifiers, connected to sum the X and Y components of θ and φ.

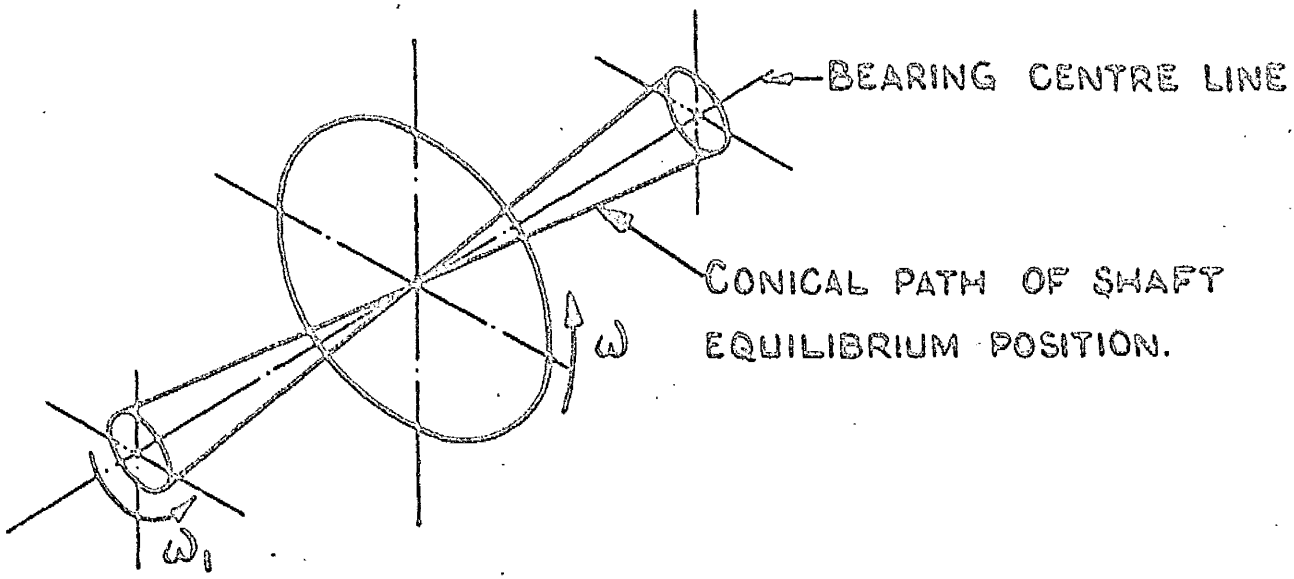

ASSUMED EFFECT OF ECCENTRIC SPIN AXIS BEARINGS.

FIG. 37.

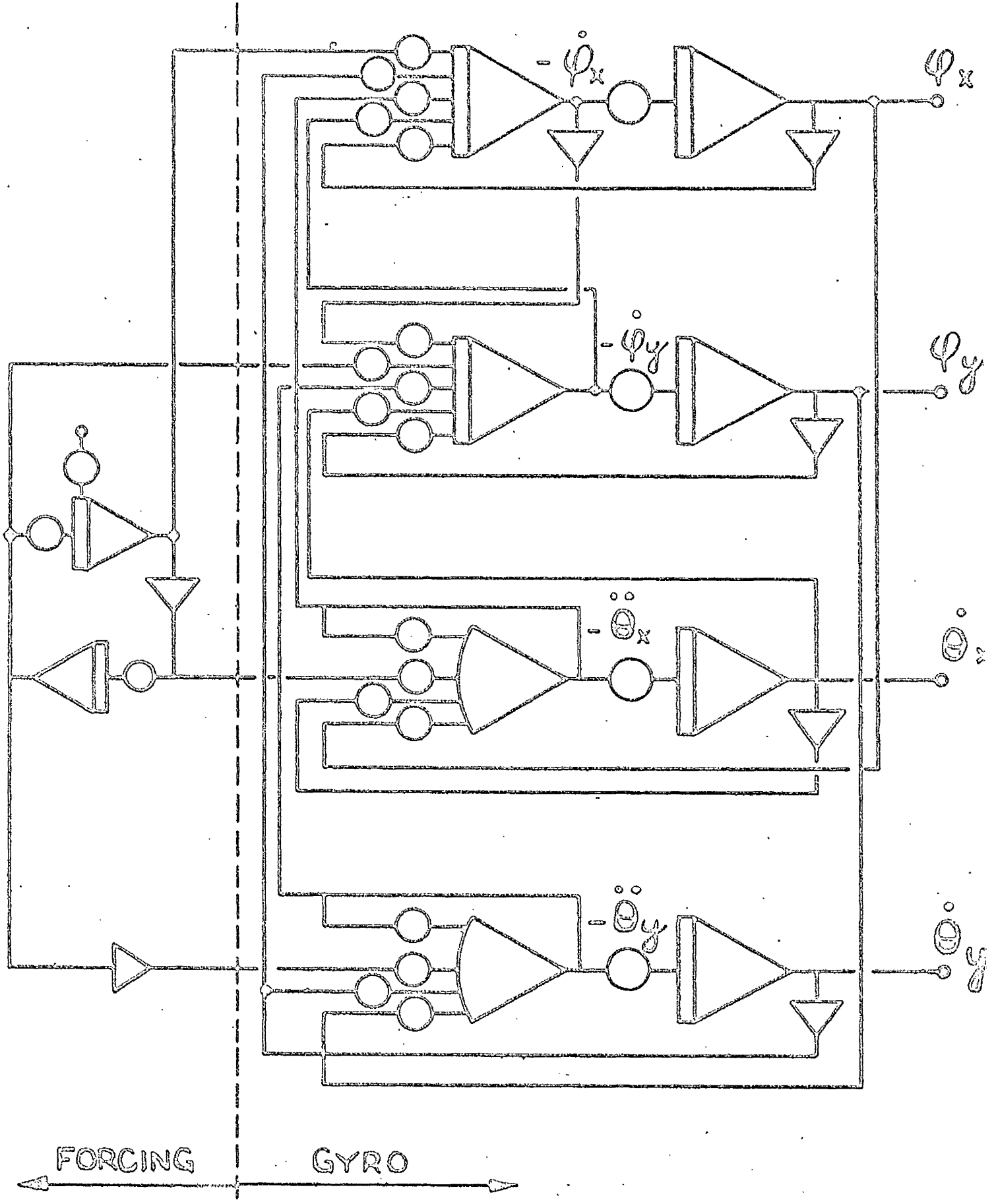

COMPUTER DIAGRAM - ECCENTRIC BEARINGS.

PIG. 38.

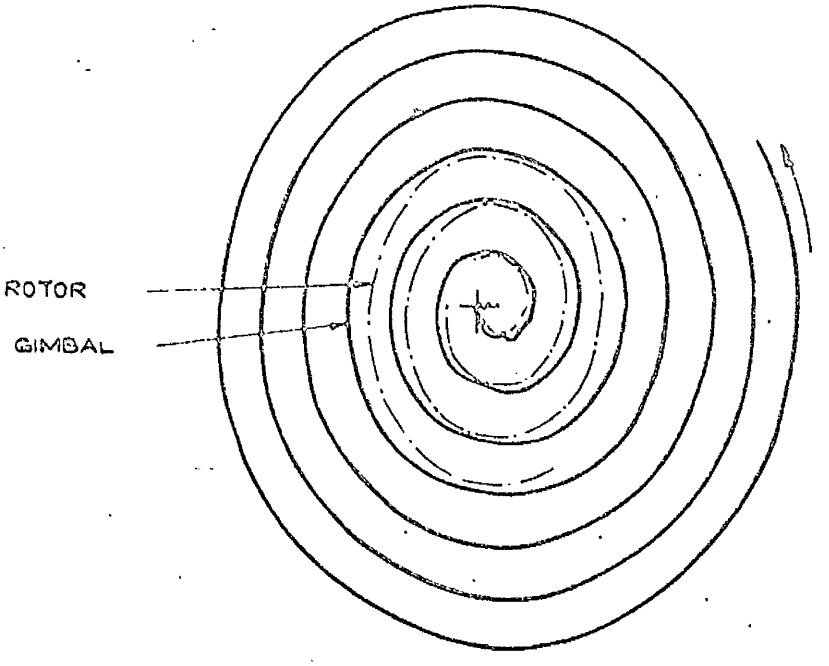

BUILD UP OF RESONANT OSCILLATION DUE TO ECCENTRIC BEARINGS.

FIG. 39.

CHAPTER 7.

THE EFFECT OF VARIATION OF RADIAL STIFFNESS IN THE SPIN AXIS BEARINGS

7.1. Assumptions and Equations of Motion

Variation of radial stiffness could arise due to the presence of an oversize ball, causing the radial stiffness of the bearing to be greater in the direction of the oversize ball and less in the direction at right angles to it. The effect is represented diagrammatically in Fig.40 and it will be seen that the axes of maximum and minimum stiffness rotate at the speed of the ball cage ω_1. The equations of motion are as follows:-

$$
\begin{aligned}
&I(\ddot{\theta}_x + \ddot{\varphi}_x) + J\Omega(\dot{\theta}_y + \dot{\varphi}_y) + k\varphi_x + \Delta k(\varphi_x \cos 2\omega_1 t + \varphi_y \sin 2\omega_1 t) = 0 \\
&I(\ddot{\theta}_y + \ddot{\varphi}_y) + J\Omega(\dot{\theta}_x + \dot{\varphi}_x) + k\varphi_y + \Delta k(\varphi_x \sin 2\omega_1 t - \varphi_y \cos 2\omega_1 t) = 0 \\
&M_x \ddot{\theta}_x - k\varphi_x - \Delta k(\varphi_x \cos 2\omega_1 t + \varphi_y \sin 2\omega_1 t) = 0 \\
&M_y \ddot{\theta}_y - k\varphi_y - \Delta k(\varphi_x \sin 2\omega_1 t - \varphi_y \cos 2\omega_1 t) = 0
\end{aligned}
\qquad (7.1)
$$

7.2. Analogue Simulation

Fig.41 shows the part of the computer set up concerned with the effects of stiffness variation, the remainder of the simulation being the same as that shown in Fig.34. A three amplifier loop oscillates the two multiplier shafts M 1 and M 2 in quadrature at the frequency $2\omega_1$.

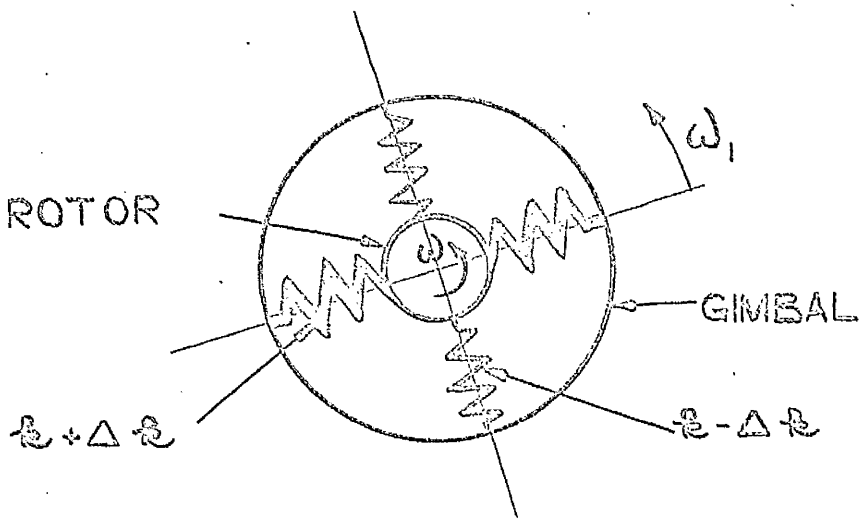

DIAGRAMMATIC REPRESENTATION OF STIFFNESS VARIATION EFFECT IN SPIN AXIS BEARINGS.

Fig. 40.

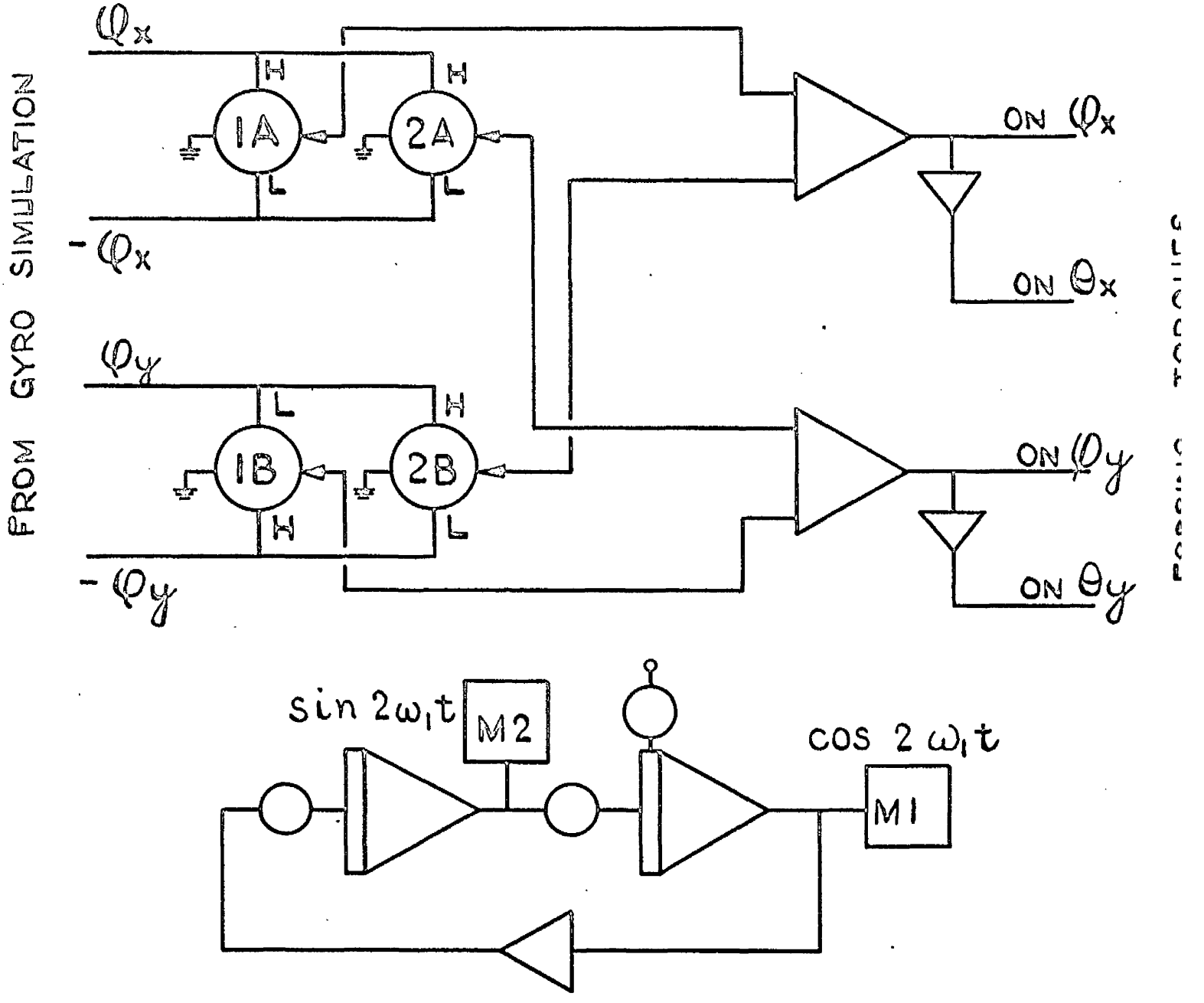

SIMULATION OF EFFECT OF STIFFNESS VARIATION.

FIG. 4

Traces obtained from the computer indicated instability when the gyro parameters were adjusted to make the nutation frequency equal to the ball cage frequency ω_1. Although the gimbal inertias were varied over a wide range this was the only condition where instability was noticed.

7.3. Digital simulation

The previously existing Atlas programme (Appendix 1) was modified to include the effect of bearing stiffness variation, giving the version shown in Appendix 2.

As previously, the time variation of the total energy, (strain + kinetic), in the motion was used as a measure of the relative stability of the system under various conditions. This is tabulated in the computer results as log (E/IE), where E is the total energy and IE is the initial energy. As a rough measure of stability the average value of log (E/IE) was also computed.

Three sets of computer runs were taken, one with equal gimbal inertias, one with the total moment of inertia of the gimbals about the outer gimbal axis, $M_x = 4\ M_y$ about the inner axis, and the third set with $M_y = 4M_x$. The average log (E/IE) over the first 40 milliseconds of the vibration is shown plotted in Fig. 42 to a base of equivalent gimbal inertia. In the case of unequal gimbal inertias, the equivalent inertia is taken as that value of M which would give the same nutation frequency.

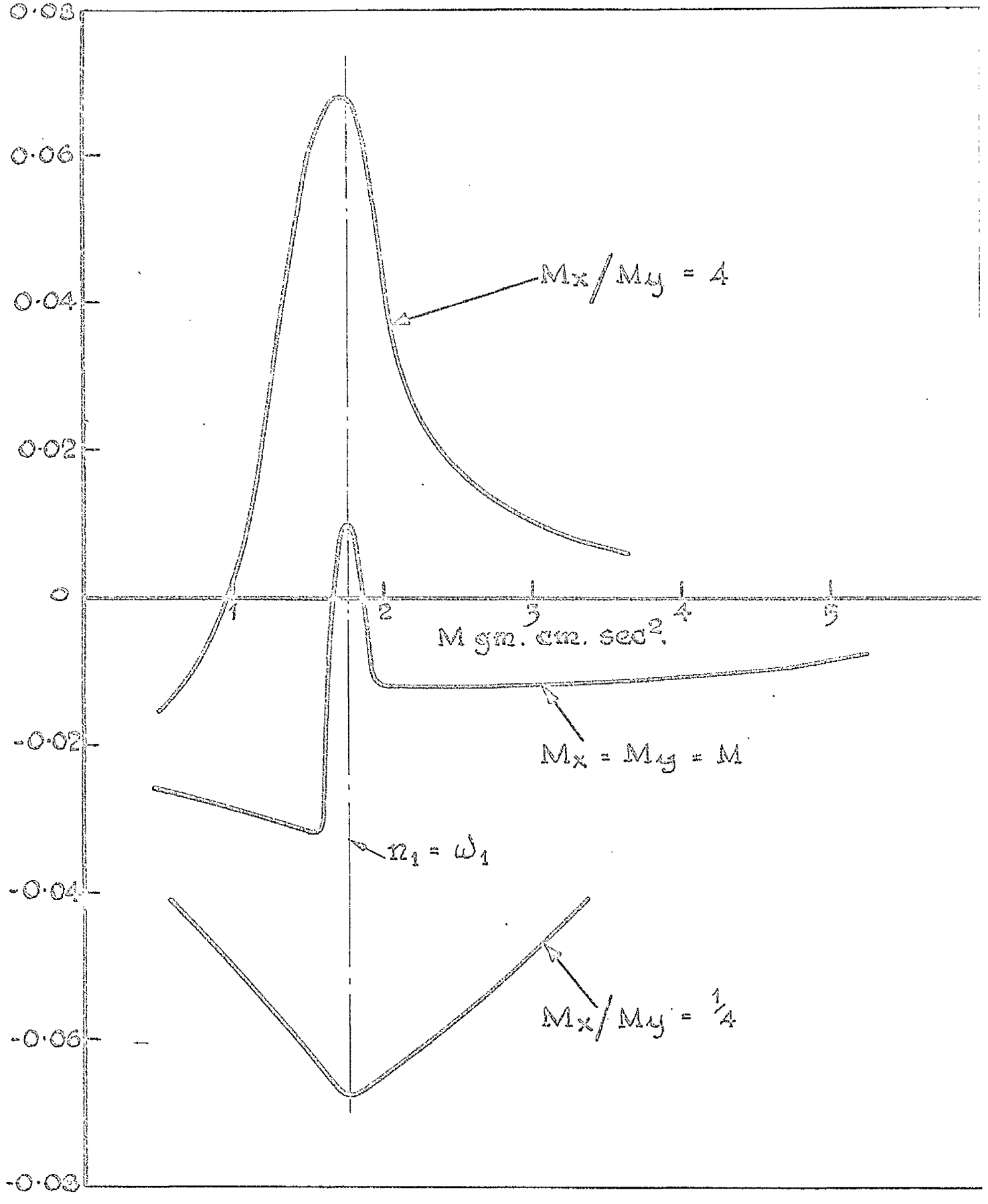

EFFECT OF GIMBAL INERTIA ON STABILITY FOR VARIOUS GIMBAL INERTIA RATIOS.

FIG. 42.

These results were sufficient to confirm that something significant occurs when the first natural frequency of nutation is the same as the ball cage frequency.

7.4 Effect of unequal gimbal inertias

Fig.42 indicates considerable differences in the behaviour of the system with variation in the ratio M_x/M_y. This is further illustrated by Fig. 43 which shows the variation of log (E/IE) with time for $M_x = M_y = 1.57$; $M_x = 2.63$, $M_y = 0.66$; and $M_x = 0.66$, $M_y = 2.63$, all units being gm.cm.sec^2. These are values which give $n_1 = \omega_1$.

The reason for the difference in average log (E/IE) is seen to be mainly the difference in phase of the low frequency variation in log (E/IE) the variations for $M_x/M_y = 4$ and $M_x/M_y = \frac{1}{4}$ being 180° out of phase. For $M_x/M_y = 1$ the frequency of the variation is higher, being three times that of the variations in the other two cases.

In each case, however, the trend is upwards, indicating instability.

7.5 Effect of initial conditions

The results presented up till now were all obtained using fixed initial conditions, viz. $\varphi_{xo} = 10^{-4}$ radians, $\dot{\Theta}_{xo} = 0.5$ rad/sec, $\dot{\varphi}_{xo} = -0.5$ rad/sec.

Fig.44 shows the effect of varying the initial velocities in the case where $M_x = 2.63$, $M_y = 0.66$. The three curves show that the main, low

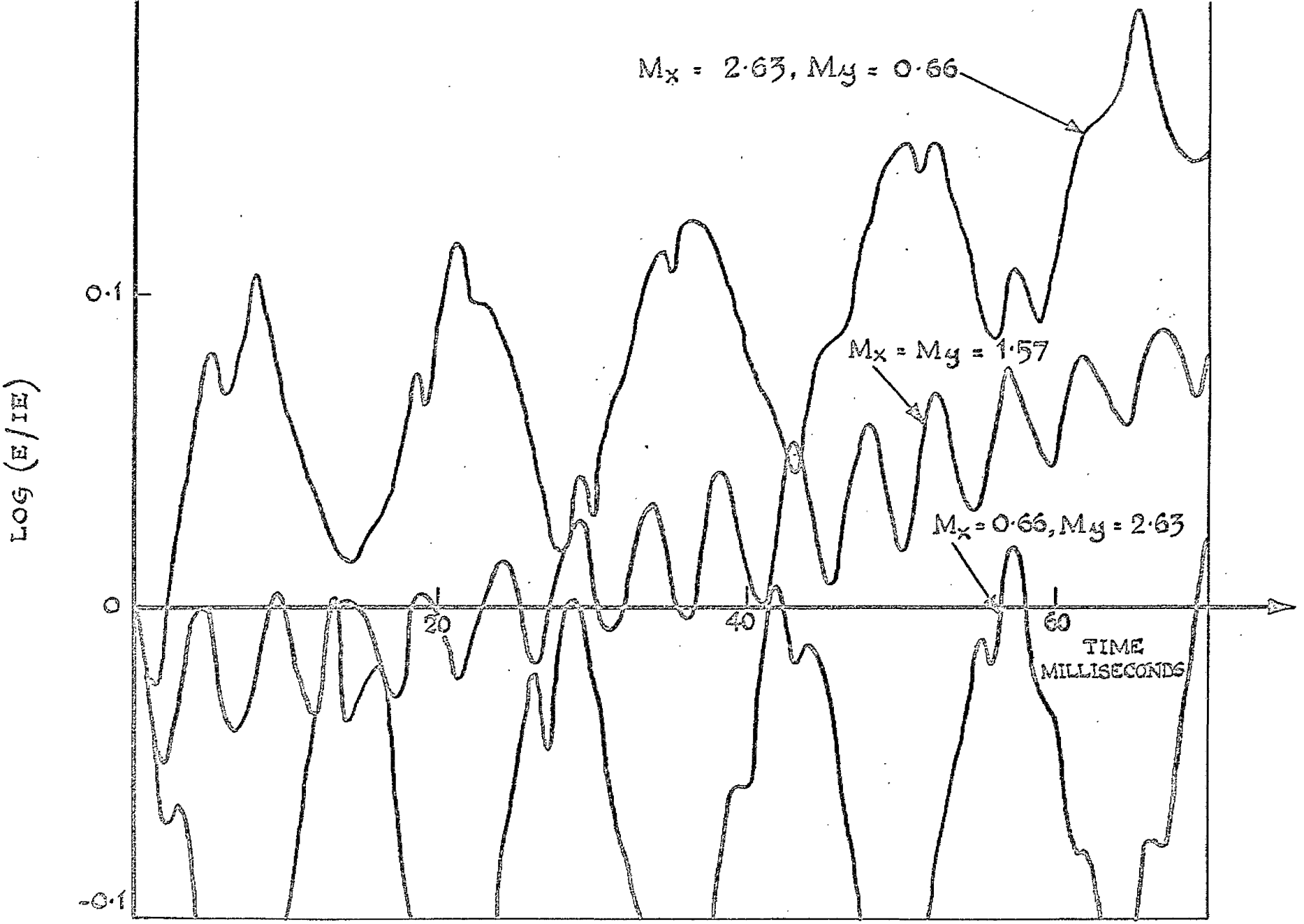

EFFECT OF GIMBAL INERTIA RATIO FOR CONSTANT INITIAL CONDITIONS.

FIG 43

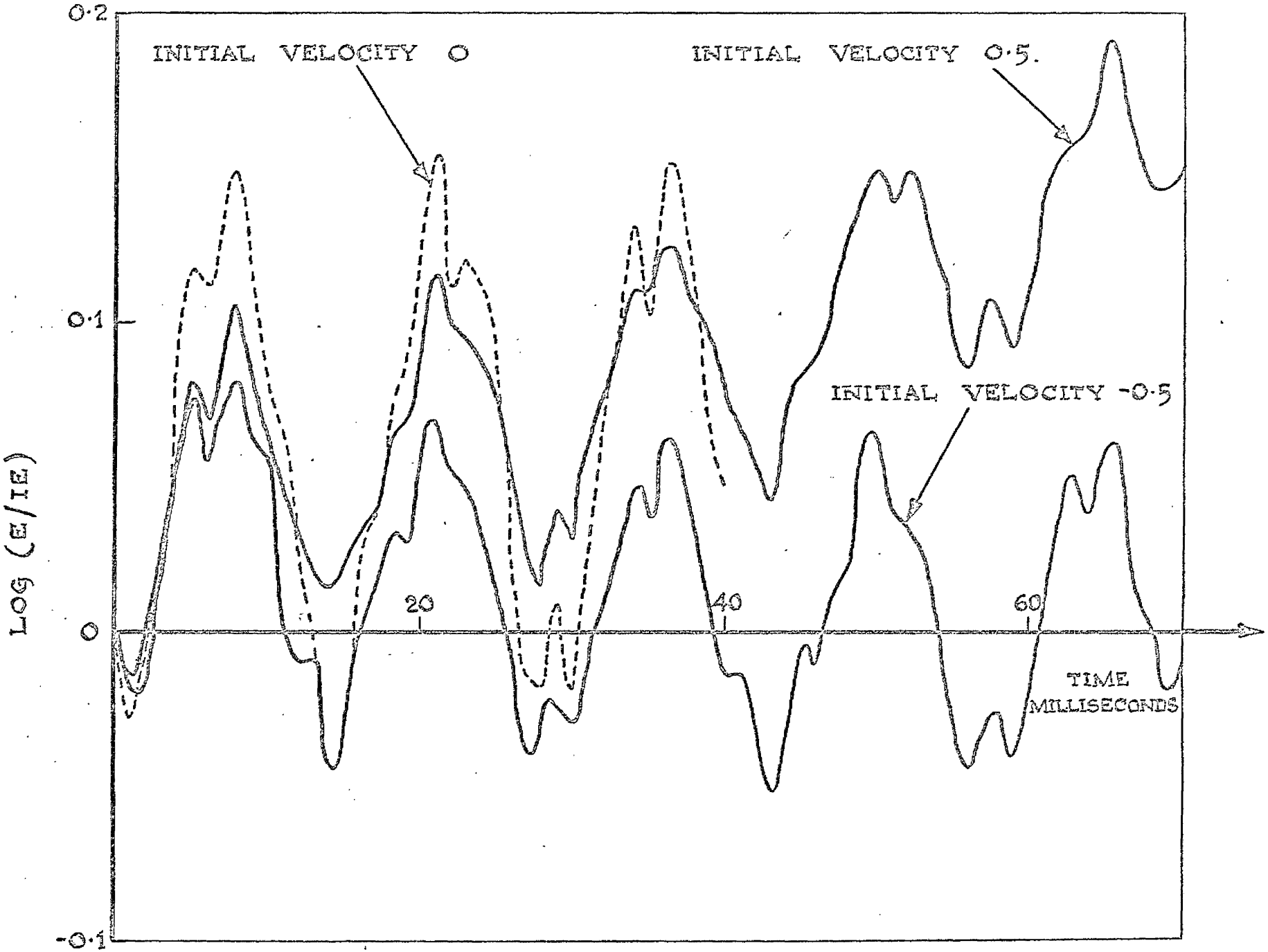

EFFECT OF INITIAL VELOCITY FOR $M_X = 2{\cdot}63$, $M_Y = 0{\cdot}66$.

FIG. 44.

frequency variations remain in phase and that the amplitude of the variation is largest for zero initial velocity.

More important however is the difference in average slope of the curves. For $\dot{\theta}_{x_o} = 0.5$ the trend is markedly upwards indicating a pronounced instability whereas with the initial velocity in the opposite direction the trend is downwards at first.

Presumably this is due to the fact that, of the several modes of vibration possible not all are unstable and in the case of $\dot{\theta}_{x_o} = -0.5$ the unstable mode is inhibited, at least at first.

7.6. Parametric resonance

The theory outlined in Chapter 8 indicates that parametric resonances or zones of instability occur when the sum of, or difference between, any two natural frequencies is an integer multiple of the frequency of variation of the parameters.

Taking the natural frequency data from Fig.36, figures 45 and 46 were constructed, showing these sums and differences plotted to a base of gimbal inertia M for two different values of bearing stiffness. Also plotted are horizontal lines at $2\omega_1$, $4\omega_1$, etc. being the fundamental and harmonics of the parameter variation frequency.

The intersections are shown by circles and these indicate the locations of the parametric resonances.

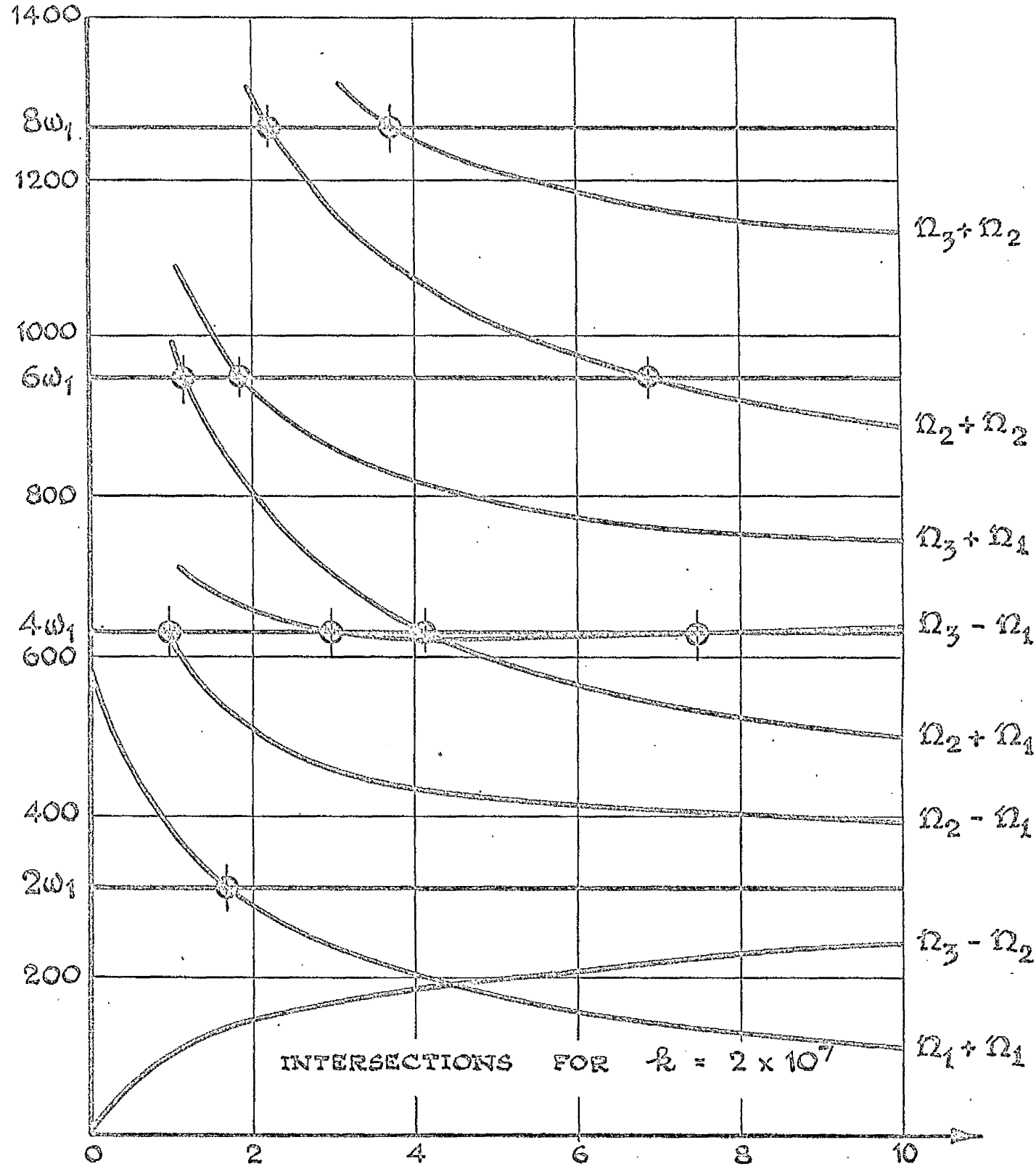

LOCATION OF PARAMETRIC RESONANCES

FOR $k = 1.51 \times 10^7$ GMCM / RADIAN.

FIG. 45.

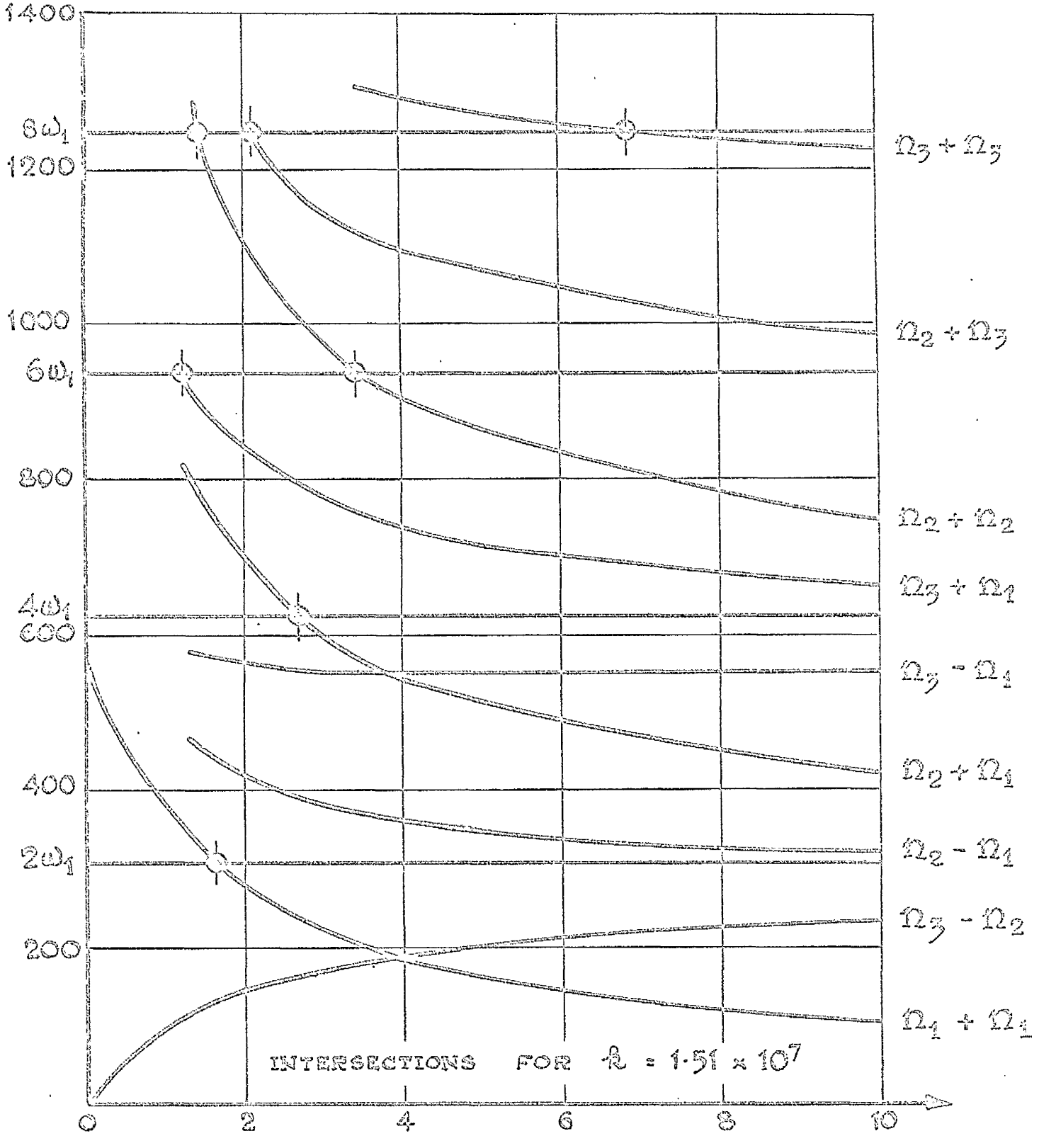

LOCATION OF PARAMETRIC RESONANCES

FOR $\mathfrak{K} = 2 \times 10^7$ GM. CM. / RADIAN.

FIG. 46.

Of particular interest is the curve for $n_3 - n_1$ which is almost horizontal over a wide range of gimbal inertia. If the unstable zone were sufficiently wide, it is possible that the gyro represented by Fig.45 might be unstable over the entire range from M = 2.5 to 10, or greater.

7.7. Effect of bearing slackness

It is possible also that the gyroscope described by Quartley[1] had its effective bearing stiffness reduced by slackness to the extent that a parametric resonance of this type occurred over a wide range of high gimbal inertia.

Yamamoto[6] describes in Chapter VI of his 1957 paper, the effect of bearing fit on the synchronous backward precession of a whirling shaft. He concludes that a medium fit is worse than either a tight or a slack fit since the variation of radial stiffness is greater. This is in line with the theory of Chapter 8 since the width of the unstable zone or the magnitude of the positive characteristic exponent are both proportional to the quantity μ, which, as indicated in Sec.8.9, is equal to the ratio of the stiffness variation Δk to the mean stiffness k.

CHAPTER 8.

CHARACTERISTIC EXPONENTS AND ZONES OF INSTABILITY IN LINEAR DIFFERENTIAL EQUATIONS WITH PERIODIC COEFFICIENTS

8.1. First Method

Vide Chapter III. Sec.11 of Ref.(14)

The form of the equations dealt with is

$$\frac{dx_s}{dt} = (a_{s1} + \mu f_{s1}) x_1 + \ldots\ldots\ldots\ldots + (a_{sn} + \mu f_{sn}) x_n \qquad (s = 1, \ldots\ldots, n) \tag{8.1}$$

where the n x n matrices $\begin{bmatrix} a_{11} & \cdots & a_{1n} \\ \vdots & & \vdots \\ a_{n1} & \cdots & a_{nn} \end{bmatrix}$ and $\begin{bmatrix} f_{11} & \cdots & f_{1n} \\ \vdots & & \vdots \\ f_{n1} & \cdots & f_{nn} \end{bmatrix}$ are

respectively constant and periodic with period $T = \frac{2\pi}{\omega_0}$. (There will be minor departures from Malkin's notation). μ is a small quantity representing the amplitude of the periodic variation in the system parameters.

For $\mu = 0$ the system reduces to :-

$$\frac{dx_s^{\,o}}{dt} = \sum_{j=1}^{n} a_{sj}\, x_s^{\,o} \tag{8.2}$$

The characteristic exponents of the system are of the form

$$\alpha_i = \lambda_i + \bar{a}_i \tag{8.3}$$

where $\bar{a}_i$ reduces to zero when $\mu = 0$, leaving $\alpha_i = \lambda_i$, which are the values of the characteristic exponents of the system i.e. the eigen values of the matrix a.

The equations (8.1) will have at least one solution of the form

$$x_s = e^{(\lambda_i + \bar{a}_i)t} \varphi_s(t) \tag{8.4}$$

where φ_s is periodic, period T. Hence if the change of variables $x_s = e^{(\lambda_i + \bar{a}_i)t} y_s$ is made in equations (8.1) the transformed system

$$\frac{dy_s}{dt} = \sum_{j=1}^{n} (a_{sj} + \mu f_{sj}) y_j - (\lambda_i + \bar{a}_i) y_s \tag{8.5}$$

must have a periodic solution, period T. The zero-th approximation to y_s is given by putting $\mu = 0$ in eqns.(8.5) i.e.

$$\frac{dy_s^{\circ}}{dt} = \sum_{j=1}^{n} a_{sj} y_j^{\circ} - \lambda_i y_s^{\circ} \tag{8.6}$$

The roots of the characteristic equation of this system are:-

$$\lambda_1 - \lambda_i,\ \lambda_2 - \lambda_i,\ \ldots\ldots\ldots\ldots,\ \lambda_n - \lambda_i$$

so that one root at least must be zero giving a solution of the form $y_s^{\circ} = \text{const.}$ which can be regarded as periodic of arbitrary period. Also if any of the differences $(\lambda_j - \lambda_i)$ is an integer multiple of $i\omega_o = \frac{2\pi i}{T}$ then there will be another periodic solution, period T.

Assuming there are m such solutions,

$$y_s^{\circ} = M_1^* \varphi_{s1} + \ldots\ldots\ldots + M_m^* \varphi_{sm} \qquad (8.7)$$

where M_i^* are arbitrary constants.

The recurrence formula describing successive approximations to the true solution y_s is

$$\frac{dy_s^{(k)}}{dt} = \sum_{j=1}^{n} a_{sj} y_j^{(k)} - \lambda_i y_s^{(k)} + \sum_{j=1}^{n} f_{sj} y_j^{(k-1)} - \bar{a}_i^{(k)} y_s^{(k-1)} \qquad (8.8)$$

where (k) denotes the k-th approximation.

Putting k = 1 gives a system of equations for $y_s^{(1)}$ and in order that they may have a periodic solution the following conditions apply:-

$$(B_{r1} - \bar{a}_i^{(1)} A_{r1}) M_1^* + \ldots\ldots\ldots + (B_{rm} - \bar{a}_i^{(1)} A_{rm}) M_m^* = 0 \qquad (8.9)$$

$$(r = 1, \ldots\ldots\ldots, m)$$

where

$$B_{rj} = \int_0^T \sum_{\alpha,\beta=1}^{n} f_{\alpha\beta} \varphi_{\beta j} \psi_{\alpha r} \, dt \qquad (8.10)$$

and $A_{rj} = T \cdot \sum_{\alpha=1}^{n} \varphi_{\alpha j} \psi_{\alpha r}$

$\psi_{s1}, \ldots\ldots\ldots, \psi_{sm}$ are periodic solutions of the equations conjugate to the system (8.6)

viz. $$\frac{dz_s}{dt} + \sum_{j=1}^{n} a_{js} z_j - \lambda_i z_s = 0 \qquad (8.11)$$

(To obtain the conjugate system the coefficient matrix is transposed and changed in sign. The resulting eigen values are opposite in sign to those of the original system).

Since $\bar{a}_i^{(1)}$ is required to vanish for $\mu = 0$, it may conveniently be replaced by $\mu\, a_i^{(1)}$.

The above conditions for periodicity may then be written in matrix notation as:-

$$(B - a_i^{(1)} \quad A)\ M^* = 0 \qquad (8.12)$$

where A and B are mx n matrices and M* an m x 1 column vector. Hence for a non-trivial solution, the determinant $|B - a_i^{(1)} \quad A|$ is zero, which gives the value of $a_i^{(1)}$.

First, putting $\mu = 0$ gives an intermediate approximation to $a_i^{(1)}$ - say a_i^*. The value of a_i^* can be refined to $a_i^{(1)}$ by putting $\mu = \mu$ in the matrix B.

Provided μ is small, further approximation gives little improvement in the value of a_i and the functions y_s° are close to the true solutions.

8.2 Application to gyro with unsymmetrical rotor

The equations used are those from section 2.7 viz:-

$$(I + M_x)\ddot{\theta}_x + J\Omega\dot{\theta}_y + R_g\dot{\theta}_x + rl(\ddot{\theta}_x \cos 2\Omega t + \ddot{\theta}_y \sin 2\Omega t) \qquad (8.13)$$
$$+ 2rl\Omega(-\dot{\theta}_x \sin 2\Omega t + \dot{\theta}_y \cos 2\Omega t) = 0$$

$$(I + M_y)\ddot{\theta}_y - J\Omega\dot{\theta}_x + R_g\dot{\theta}_y + rl(\ddot{\theta}_x \sin 2\Omega t - \ddot{\theta}_y \cos 2\Omega t)$$
$$+ 2rl\Omega(\dot{\theta}_x \cos 2\Omega t + \dot{\theta}_y \sin 2\Omega t) = 0$$

To put these equations in the form of eqns. 8.1 it is necessary to obtain explicit expressions for $\ddot{\theta}_x$ and $\ddot{\theta}_y$. Rearranging 8.13 gives:-

$$\ddot{\theta}_x(I+M_x+rl\cos 2\Omega t) + \ddot{\theta}_y . rl \sin 2\Omega t = \dot{\theta}_x(2rl\Omega \sin 2\Omega t - R_g) - \dot{\theta}_y(J\Omega + 2rl\Omega \cos 2\Omega t)$$

$$\ddot{\theta}_x . rl \sin 2\Omega t + \ddot{\theta}_y(I+M_y - rl\cos 2\Omega t) = \dot{\theta}_x(J\Omega - 2rl\Omega \cos 2\Omega t) - \dot{\theta}_y(2rl\Omega \sin 2\Omega t + R_g)$$

These have the form

$$\alpha \ddot{\theta}_x + \beta \ddot{\theta}_y = \gamma \dot{\theta}_x - \delta \dot{\theta}_y$$

$$\beta \ddot{\theta}_x + \varepsilon \theta_y = \zeta \dot{\theta}_x - \eta \dot{\theta}_y \qquad (8.14)$$

so that $$\ddot{\theta}_x = \frac{(\gamma\varepsilon - \beta\eta)\dot{\theta}_x - (\delta\varepsilon - \beta\eta)\dot{\theta}_y}{\alpha\varepsilon - \beta^2}$$

and $$\ddot{\theta}_y = \frac{(\beta\gamma - \alpha\zeta)\dot{\theta}_x - (\beta\delta - \alpha\eta)\dot{\theta}_y}{\beta^2 - \alpha\varepsilon}$$

$$= \frac{(\alpha\zeta - \beta\gamma)\dot{\theta}_x - (\alpha\eta - \beta\delta)\dot{\theta}_y}{\alpha\varepsilon - \beta^2}$$

The common denominator $\alpha\varepsilon - \beta^2$ is:-

$$(I+M_x)(I+M_y)\left[1 - \frac{rl(M_x - M_y)\cos 2\Omega t}{(I+M_x)(I+M_y)} - \frac{r^2 l^2}{(I+M_x)(I+M_y)}\right]$$

If r is assumed small, the term is r^2 may be neglected in this expression and also in subsequent working. The $(1 - r\Delta M \cos 2\Omega t)$ in the denominator is replaced by a factor $(1 + r\Delta M \cos 2\Omega t)$ in the numerator, which is then multiplied into the coefficient matrix, ΔM being an abbreviation for:

$$\frac{I\,(M_x - M_y)}{(1 + M_x)\,(1 + M_y)}$$

When this has been carried out, the coefficient matrices reduce to:-

$$a = \frac{\Omega}{(1+M_x)(1+M_y)} \begin{bmatrix} 0 & -J\,(1 + M_y) \\ J\,(1 + M_x) & 0 \end{bmatrix} \qquad (8.15)$$

$$\mu f = \frac{r\,\Omega}{(1+M_x)(1+M_y)} \begin{bmatrix} I\left[2(1 + M_y) - J\right] \sin 2\Omega t - R_g'\,(1+M_y) & -\left\{J\,\Delta M\,(1 + M_y) + I\left[2(1+M_y)-J\right]\right\} \cos 2\Omega t \\ \left\{J\,\Delta M\,(1 + M_x) + I\left[J-2(1+M_x)\right]\right\} \cos 2\Omega t & I\left[J - 2\,(1 + M_x)\right] \sin 2\Omega t - R_g'\,(1 + M_x) \end{bmatrix}$$

where R_g is replaced by $r\Omega R'_g$ to assist factorisation. The damping terms have been grouped with the periodic terms in the matrix f to facilitate calculation of the damping in a later section. The quantity r is taken as the parameter μ.

The eigen values of the matrix a are $\pm$ in, where $n = \dfrac{J\Omega}{\sqrt{(I+M_x)(I+M_y)}}$, is the natural frequency of nutation of the symmetrical gyro. The matrix a can be further condensed using the substitution:-

$$R = \sqrt{\frac{I + M_x}{I + M_y}}$$

and hence

$$a = \begin{bmatrix} 0 & -n/R \\ nR & 0 \end{bmatrix} \qquad (8.16)$$

The equations 8.6 then become:-

$$\frac{dy_1^o}{dt} = -\text{in}\, y_1 - \frac{n}{R} y_2$$

$$\frac{dy_2^o}{dt} = nRy_1 - \text{in}\, y_2 \qquad (8.17)$$

having roots zero and -2 in. The solutions are therefore

$$y_1^o = M^*_1 + M^*_2 e^{-2\,\text{in}t}$$

$$y_2^o = M^*_1 P + M^*_2 Q e^{-2\,\text{in}t} \qquad (8.18)$$

it can be easily shown that $P = -iR$, $Q = iR$

so that $\varphi = \begin{bmatrix} 1 & e^{-2\,int} \\ -iR & iRe^{-2\,int} \end{bmatrix}$ (8.19)

putting $\psi = \begin{bmatrix} 1 & e^{2\,int} \\ P & Q\,e^{2\,int} \end{bmatrix}$ (8.20)

P and Q must be chosen to satisfy the conjugate equations to 8.17, viz.

$$\frac{dz_1}{dt} = inz_1 - nRz_2$$

$$\frac{dz_2}{dt} = \frac{n}{R} z_1 + i n z_2 \qquad (8.21)$$

hence $\psi = \begin{bmatrix} 1 & e^{2\,int} \\ \frac{i}{R} & -\frac{i}{R} e^{2\,int} \end{bmatrix}$ (8.22)

Using the expressions (8.10),

$$A_{11} = T(1+1) = 2T$$

$$A_{12} = T(e^{-2int} - e^{-2int}) = 0$$

$$A_{21} = T(e^{2int} - e^{2int}) = 0$$

$$A_{22} = T(1+1) = 2T$$

so that $A = 2T \begin{bmatrix} 1 & 0 \\ 0 & 1 \end{bmatrix}$ (8.23)

$$B_{11} = \int_o^T (f_{11}\varphi_{11}\psi_{11} + f_{12}\varphi_{21}\psi_{11} + f_{21}\varphi_{11}\psi_{21} + f_{22}\varphi_{21}\psi_{21})\, dt$$

$$= \int_o^T (f_{11} - iRf_{12} + \frac{i}{R} f_{21} + f_{22})\, dt$$

Only the constant terms will contribute to this integral, so that

$$B_{11} = - \frac{\Omega T R_g' (21 + M_x + M_y)}{(1 + M_x)(1 + M_y)} \qquad (8.24)$$

$$B_{12} = \int_o^T (f_{11}\varphi_{12}\psi_{11} + f_{12}\varphi_{22}\psi_{11} + f_{21}\varphi_{12}\psi_{21} + f_{22}\varphi_{22}\psi_{21})\, dt$$

$$= \int_o^T [e^{-2 int} (f_{11} + i R f_{12} + \frac{i}{R} f_{21} - f_{22})]\, dt$$

If we assume that the gyro is tuned so that $n = \Omega$, only the periodic terms in f contribute to this integral and since $\int_o^T e^{-2i\Omega t} \cos 2\Omega t = T/2$

(8.25)

and $\int_o^T e^{-2i\Omega t} \sin 2\Omega t = -iT/2$

$$B_{12} = \frac{i I \Omega T}{2(1+M_x)(1+M_y)} \left[\begin{array}{l} 2J - 2(1 + M_x) - 2(1 + M_y) \\ - 4\sqrt{(1+M_x)(1+M_y)} + J R + J/R \end{array} \right]$$

(8.26)

In a similar fashion it can be shown that

$B_{21} = - B_{12}$, and $B_{22} = B_{11}$

Applying the periodicity condition, $\left| B - a_i^{(1)} A \right| = 0$

gives the quadratic equation:-

$$4T^2 (a_i^{(1)})^2 - 4 T B_{11} a_i^{(1)} + B_{11}^2 + B_{12}^2 = 0 \qquad (8.27)$$

For zero damping, $B_{11} = 0$

and $a_i^{(1)} = \pm \frac{B_{12}}{2iT}$

The characteristic exponent $\bar{a}_i^{(1)} = \mu a_i^{(1)}$

$$\text{i.e. } \bar{a}_i^{(1)} = \pm \frac{rB_{12}}{2iT} \qquad (8.28)$$

Strictly, according to Malkin's notation the quantity $a_i^{(1)}$ above should be written a_i^* since the matrix f is derived by neglecting terms in r^2 and r^3. However provided r is small the difference is not significant.

For the gyroscope configuration used in chapter 2, $I/J = 0.55$, $r = 0.0909$, $M_x = 3gJ$, $M_y = gJ$, $\Omega = 10$ The parametric resonance occurs when $g = 0.2393$, and thus $\frac{I + M_x}{J} = 1.2679$

$$\frac{I + M_y}{J} = 0.7893$$

$$R^2 = 1.606, \quad R = 1.2679, \quad 1/R = 0.7893$$

Substituting these values in eqn. 8.26 gives

$$B_{12} = \frac{i \times 0.55 \times 10.T}{2 \times 1.2679 \times 0.7893} \left[\begin{matrix} 2 - 2\,(1.2679) - 2\,(0.7893) \\ -4 + 1.2679 + 0.7893 \end{matrix} \right]$$

$$= -2.75\, i\, T\, (4.0572)$$

$$\bar{a}_i^{(1)} = \pm \frac{0.0909 \times 2.75 \times 4.0572}{2}$$

$$= \pm 0.5072 \text{ sec}^{-1}$$

This value is in good agreement with the results obtained in sec. 2.6. and sec. 2.10.

8.3 Alternative Method

Reference - Malkin, Chapter V, Sec. 7.

In this method the original equations are first transformed by a change of time scale.

If the original equations in terms of real time τ are:-

$$\frac{dx_s}{d\tau} = \sum_{\alpha=1}^{n} (a_{s\alpha} + \mu f_{s\alpha}) x_\alpha(\tau) \qquad (8.29)$$

$$(s = 1, \ldots\ldots, n)$$

where the functions f are periodic with period T in terms of τ, $(T = \frac{2\pi}{\omega_o})$, the non dimensional time t is chosen so that $t = \frac{1}{2}\omega_o \tau = \frac{\pi\tau}{T}$.

The equations then become

$$\frac{dx_s}{dt} = \frac{1}{\frac{1}{2}\omega_o} \frac{dx_s}{d\tau} = \lambda \sum_{\alpha=1}^{n} (a_{s\alpha} + \mu f_{s\alpha}) x_\alpha(t) \qquad (8.30)$$

where $\lambda = \frac{2}{\omega_o}$ and the coefficients f now have period π

To find the limits of stability the characteristic exponents are calculated for different values of the quantity σ where $\lambda = \lambda_o + \mu\sigma$ and λ_o is taken as one of the values producing parametric resonance.

i.e. If $\omega_1, \omega_2, \omega_3, \ldots\ldots, \omega_m$ where $m = n/2$ are the natural frequencies of the original system for $\mu = 0$ the eigen values of the matrix a are $\pm i\omega_1, \pm i\omega_2, \ldots\ldots, \pm i\omega_m$ The condition for parametric resonance is that the difference between any two eigen values shall be an integer multiple of $i\omega_o$.

i.e. $i(\omega_j \pm \omega k) = N i\omega_o (N = \pm 1, \pm 2, \ldots..)(j, k, = 1, \ldots.., m)$ (8.31)

or, dividing by i

$$\lambda(\omega_j \pm \omega k) = 2N \tag{8.32}$$

For simple parametric resonance $k = j$ and $2\omega_j = \omega_o$. For $k \neq j$ combination resonance occurs if the above condition is satisfied.

The characteristic exponent of equations (8.30) is expressed in the form $\alpha = \lambda_o i\omega_j + \mu a$ where λ_o satisfies relation (8.32) above. Making as before the change of variable $x_s = e^{\alpha t} y_s$, the following system of equations is obtained which must admit 2 periodic solutions.

$$\frac{dy_s}{dt} = (\lambda_o + \mu\sigma) \sum_{\beta=1}^{n} (a_{s\beta} + \mu f_{s\beta}) y_\beta - (\lambda_o i\omega_j + \mu a) y_s \tag{8.33}$$

Proceeding as before putting $\mu = 0$ gives

$$\frac{dy_s^o}{dt} = \lambda_o \sum_{\beta=1}^{n} (a_{s\beta} + \mu f_{s\beta}) y_\beta - \lambda_o i\omega_j y_s \tag{8.34}$$

and $y_s^{\circ} = M_o \varphi_{s1} + N_o \varphi_{s2}$ (8.35)

where the φ_{s1} are constants and the φ_{s2} are periodic period 2π.

Again ψ_{s1} and ψ_{s2} are the periodic solutions of the system conjugate to equations (8.33).

The next approximation $y_s^{(1)}$ is defined by a recurrence relation similar to equations (8.8) and the condition for periodicity is:-

$$\left[\sigma A + \left(1 + \frac{\mu\sigma}{\lambda_o}\right) B - a^{(1)} \cdot I\right] \cdot m = 0 \qquad (8.36)$$

where m is the 2 x 1 column vector M_o, N_o

I is a 2 x 2 unit matrix and A and B are 2 x 2 matrices defined by Malkin as follows:-

$$A_{ij} = \sum_{\alpha,\beta=1}^{n} \int_0^{2\pi} a_{\beta\alpha} \varphi_{\alpha i} \psi_{\beta j} \, dt$$

$$B_{ij} = \sum_{\alpha,\beta=1}^{n} \int_0^{2\pi} \lambda_o f_{\beta\alpha} \varphi_{\alpha i} \psi_{\beta j} \, dt \qquad (8.37)$$

The matrix equation (8.36) is also subject to the condition that the ψ_{sj} are chosen so that the product $\psi' \varphi$ gives a unit 2 x 2 matrix.

The matrix equation (8.36) can be further simplified by putting $\mu = 0$, giving

$$(\sigma A^{\circ} + B^{\circ} - a^* I) m^* = 0 \qquad (8.38)$$

and putting the determinant $|\sigma A^{\circ} + B^{\circ} - a^* I| = 0$ gives the quadratic equation

$$a^{*2} - \left[\sigma(A_{11}^{\circ} + A_{22}^{\circ}) + B_{11}^{\circ} + B_{22}^{\circ}\right] a^{*}$$

$$+ (\sigma A_{11}^{\circ} + B_{11}^{\circ})(\sigma A_{22}^{\circ} + B_{22}^{\circ}) - (\sigma A_{21}^{\circ} + B_{21}^{\circ})(\sigma A_{12}^{\circ} + B_{12}^{\circ}) = 0 \qquad (8.39)$$

Putting $\sigma = 0$ gives a first approximation to the values of the characteristic exponents a^* at the centre of the resonance zone, and putting $a^* = 0$ gives the width of the resonance zone in terms of σ. This leads easily to an expression for the unstable zone in terms of frequency.

This second method would therefore appear to be superior to the first, giving information both on the limits of the unstable zone and the degree of instability.

8.4 Modes of vibration associated with characteristic exponents

If it is assumed that the system is tuned to a combination resonance so that:-

$$\omega_j - \omega_k = N\omega_o$$

as in the relation (8.31), the first approximation y_s° to the solution of equations (8.34) is of the form $y_s^{\circ} = K_1 + K_2 e^{-2iNt}$ where K_1 and K_2 are complex constants. Returning to x_s° via the transformation

$$x_s = e^{(\lambda_o i\omega_j + \mu a)t} y_s$$

and recalling that a has two values a_1 and a_2 (i.e. the roots of the quadratic equation (8.39) the solution x_s° is seen to be of the form

$$x_s^{\circ} = K_1 e^{\mu a_1 t} e^{\lambda_o i\omega_j t} + K_2 e^{\mu a_1 t} e^{(\lambda_o i\omega_j - 2iN)t}$$

$$+ K_1' e^{\mu a_2 t} e^{\lambda_o i\omega_k t} + K_2' e^{\mu a_2 t} e^{(\lambda_o i\omega_k - 2iN)t} \qquad (8.40)$$

Making the time scale change to real time τ by the substitutions $t = \frac{1}{2}\omega_o\tau$ and $\lambda_o = \frac{2}{\omega_o}$ the solution becomes

$$x_s^o(\tau) = K_1 e^{\frac{\mu a_1 \omega_o \tau}{2}} \cdot e^{i\omega_j \tau} + K_2 e^{\frac{\mu a_1 \omega_o \tau}{2}} \cdot e^{(i\omega_j - i N\omega_o)\tau}$$
$$+ K_1^1 e^{\frac{\mu a_2 \omega_o \tau}{2}} \cdot e^{i\omega_k \tau} + K_2^1 e^{\frac{\mu a_2 \omega_o \tau}{2}} \cdot e^{(i\omega_k - i N\omega_o)\tau} \qquad (8.41)$$

Hence there appear to be four frequencies affected by the characteristic exponents viz. $\omega_{j'}$ $\omega_j - N\omega_o$ associated with a_1

and $\omega_{k'}$ $\omega_k - N\omega_o$ associated with a_2

In fact the frequency $\omega_j - N\omega_o = \omega_k$ because of the resonance condition so that we have the higher of the two natural frequencies associated with a_1, the lower associated with both a_1 and a_2, and a third frequency $\omega_k - N\omega_o$ associated with a_2.

Although in the simple case of the gyro with an unsymmetrical rotor a_1 and a_2 are equal in magnitude and opposite in sign, it is not certain that this will be true in general. However, assuming that a_1 and a_2 are at least of opposite sign, it is not certain that the unstable positive exponent will be associated with the two natural frequencies ω_j and ω_k rather than the lower natural frequency ω_k and the difference frequency $\omega_k - N\omega_o$, although intuitively it may seem more likely.

8.5 Application to gyro with unsymmetrical rotor

In the original equations (2.17) the frequency of the periodic variation is 2Ω and if a time scale change is made as in section 8.3, the quantity $\lambda = 1/\Omega$. The matrix a (eqn. 8.15) is unchanged, as is the matrix f except that the periodic terms contain sin 2t or cos 2t instead of sin 2Ω t or cos 2Ω t.

The matrices φ and ψ are similar to those given in equations 8.19 and 8.20, except that the indices of the exponential terms do not contain n. Also, the matrix ψ has a multiplying factor of $\frac{1}{2}$ in order to satisfy the condition $\psi^{t} \varphi$ = unit 2 x 2 matrix.

i.e.

$$\varphi = \begin{bmatrix} 1 & e^{-2it} \\ -iR & iRe^{-2it} \end{bmatrix}$$

$$\psi = \frac{1}{2} \begin{bmatrix} 1 & e^{2it} \\ \frac{i}{R} & \frac{i}{R} e^{2it} \end{bmatrix} \qquad (8.42)$$

Evaluating the integrals in the expressions 8.37, the matrix A becomes:-

$$A = 2\pi \begin{bmatrix} i\Omega & 0 \\ 0 & -i\Omega \end{bmatrix} \qquad (8.43)$$

The matrix B is similar to that developed for the first method in sec. 8.2, except that there is a multiplying factor of $\lambda_o/2$ because of the scale change and because of the factor $\frac{1}{2}$ outside the matrix $\sqrt{}$ (eqn. 8.42). Also, the period T has become 2π. Making these alterations to eqns. 8.24 and 8.26, and noting again that $\lambda_o = 1/\Omega$,

$$B_{11} = -\frac{2\pi R_g' (2I + M_x + M_y)}{2(I + M_x)(I + M_y)}$$

$$B_{12} = \frac{2\pi i I}{4(I + M_x)(I + M_y)} \left[2J - 2(I + M_x) - 2(I + M_y) - 4\sqrt{(I+M_x)(I+M_y)} + JR + J/R \right] \tag{8.44}$$

In applying the equation 8.39 which is derived from the periodicity conditions, it is convenient to take particular cases rather than obtain a general solution in terms of the system parameters.

For comparison with the results obtained in sec. 8.2 using the first method we put $R_g = 0$, $\sigma = 0$ to give the characteristic exponents at the centre of the region of instability. Since $A_{12} = A_{21} = 0$ and $B_{11} = B_{22} = 0$ for zero damping, equation 8.39 reduces to:-

$$a^{*2} - B_{12} B_{21} = 0 \tag{8.45}$$

since B_{12} and B_{21} are conjugate imaginary this reduces to:-

$$a^* = \frac{B_{12}}{i} = 2\pi \cdot \frac{I}{4(I+M_x)(I+M_y)} \left[\text{-----} \right] \tag{8.46}$$

the contents of the square bracket being the same as in eqns. 8.44 and 8.26.

Because of the change in time scale, a* must be multiplied by Ω before comparison with the $a_i^{(1)}$ of section 8.2. When this is done, it is seen that the results of Malkin's two methods disagree by the factor of 2π.

The limits of stability for zero damping are obtained by solving equations 8.39 for a* = 0 and $B_{11} = B_{22} = 0$. Equation 8.39 then reads:-

$$\sigma^2 A_{11} A_{22} - B_{21} B_{12} = 0$$

which reduces to

$$\sigma = \frac{B_{12}}{2\pi i \Omega} = \frac{a^*}{2\pi\Omega} \qquad (8.47)$$

The stability boundaries are given by

$$\lambda = \lambda_o \pm \mu\sigma = \frac{1}{\Omega}\left(1 \pm \frac{ra^*}{2\pi}\right)$$

This is equivalent to the statement that the limits of the unstable zone occur when the nutation frequency

$$n = \Omega\left(1 \pm \frac{ra^*}{2\pi\Omega}\right)^{-1} \doteq \Omega\left(1 \mp \frac{ra^*}{2\pi\Omega}\right) \qquad (8.48)$$

since r is small.

Using the parameters of chapter 2,

$$\frac{ra^*}{2\pi} = \frac{ra_i^{(1)}}{\Omega} = 0.5072/\Omega$$

so that the region of instability lies between the values of g which give n = 9.4928 and 10.5072 rad/sec.

These values of g are given by the equations:-

$$\frac{1}{\sqrt{(0.55+3g)(0.55+g)}} = 0.94928 \text{ or } 1.05072$$

i.e. $$g = 0.2125 \text{ or } 0.269$$

This is in agreement with the analogue computer results obtained both by solution of Magnus' equations and the equations 2.17.

8.6 Characteristic exponents

In the previous section it has been shown that Malkin's two methods disagree by a factor of 2π in the value of the characteristic exponent, the first method giving a result which agrees with the analogue computations of chapter 2.

Also the second method gives the limits of stability, which agree with the analogue computer results, apparently because the factor 2π cancels.

Further examination of Malkin's work indicates that the periodicity conditions used to derive the equations 8.9 and 8.39 are based on Malkin's chapter II, equation 4.13, p.118.

This gives the condition that the set of equations:-

$$\frac{dx_s}{dt} = a_{s1}\,x_1 + a_{s2}\,x_2 + \cdots + a_{sn}\,x_n + f_s(t)$$

$$s = 1, 2, \cdots, n$$

has a periodic solution of the same period as the functions $f_s(t)$.

The condition is:-

$$\int_0^T \sum_{\alpha=1}^{n} f_\alpha(\tau)\,\psi_{\alpha i}(\tau)\,d\tau = 0$$

$$(i = 1, \cdots, m)$$

where T is the period of the functions $f_s(t)$, $\psi_{\alpha i}$ are the periodic solutions, period T, of the conjugate equations:-

$$\frac{dy_s}{dt} + a_{1s}\,y_1 + a_{2s}\,y_2 + \cdots a_{ns}\,y_n = 0$$

and m is the number of such periodic solutions. When this is applied in section 6 of Malkin's chapter V, the time scale has been changed to give a period of 2π. In Malkin's equations 6.21 on p.411, he applies the conditions 6.22 with a view to giving a unity coefficient for the characteristic exponent a_1. In doing so Malkin has overlooked the integration from zero to 2π and this error is repeated in section 7 of his chapter V, on which section 8.3 of this thesis is based.

The most convenient way of correcting this error is to apply a factor $\frac{1}{2\pi}$ to the matrices A and B specified by equations 8.37, and this will be done in subsequent parts of this thesis.

The derivation of the periodicity conditions 8.9 and 8.36 is given in more detail in Appendix 3.

8.7 Effect of inequality of gimbal inertia

If the gimbal inertias M_x and M_y are equal, the condition of parametric resonance occurs at $M_x = M_y = 0.45J$, if $I = 0.55\,J$. In this case the characteristic exponent as computed in sec. 8.2 becomes:-

$$a_i^{-(1)} = \pm \frac{0.0909 \times 2.75}{2} \qquad \left[2 - 2 - 2 - 4 + 1 + 1\right]$$

$$= \pm 0.5 \text{ sec}^{-1}$$

In general, if $\sqrt{(I + M_x)(I + M_y)} = R$

$$a_i^{(1)} = \pm \frac{r\, I\, \Omega}{2J} \quad (2 + R + 1/R)$$

which is a minimum at $R = 1$ and is $12\frac{1}{2}\%$ greater at $R = 2$ or $R = \frac{1}{2}$.

8.8 Effect of damping

The amount of damping required just to assure stability at the centre of the resonance zone can be calculated by including the terms B_{11} and B_{22} in equation 8.39 and putting $\sigma = 0$. Equation 8.39 then becomes:-

$$a^{*2} - (B_{11} + B_{22})\, a^* + B_{11}\, B_{22} - B_{12}\, B_{21} = 0 \qquad (8.49)$$

Since $B_{11} = B_{22}$, (and both are negative for positive R_g), a will have one zero and one negative root when $B_{11}\, B_{22} = B_{12}\, B_{21}$.

Using the expressions 8.44 for B_{11} and B_{12}, applying the condition that $n = \Omega$, and including the factor $\frac{1}{2\pi}$ discussed in sec. 8.6,

$$B_{11} = -\frac{R'_g (R + 1/R)}{2J} = B_{22} \qquad (8.50)$$

$$B_{12} = -B_{21} = -\frac{il}{4J} (2 + R + 1/R)$$

and hence $$R'_g = \frac{1}{2} \frac{(2 + R + 1/R)}{(R + 1/R)}$$

but since $$R_g = R'_g \, r\Omega$$

$$R_g = \frac{rl\Omega}{2} \frac{(2 + R + 1/R)}{(R + 1/R)} \qquad (8.51)$$

For the parameters used in Chapter 2, i.e.

$r = 0.0909$, $l/J = 0.55$, $\Omega = 10$, $R = 1.2679$,

$$\frac{R_g}{J} = \frac{0.0909 \times 0.55 \times 10}{2} \cdot \frac{4.0572}{2.0572}$$

$$= 0.494 \text{ sec}^{-1}$$

Also for $R = 1$, $\frac{R_g}{J} = 0.5 \text{ sec}^{-1}$

which is again in good agreement with the results of sec. 2.11.

It is interesting to note that, because of the factor $R + 1/R$ in the denominator of the expression for R_g, the damping required just to stabilise the gyro is a maximum at $R = 1$. Hence as the inequality in gimbal inertia increases, although the undamped gyro becomes more unstable, the damping required to stabilise it decreases.

8.9. Application to gyro with bearing stiffness variation

If the equations (7.1) which describe the effect of bearing stiffness variation are put into the form of equations (8.1) the coefficient matrices are as follows:-

$$a = \begin{bmatrix} 0 & 1 & 0 & 0 & 0 & 0 \\ -\left(\frac{k}{M_x} + \frac{k}{I}\right) & 0 & 0 & -\frac{J\Omega}{I} & 0 & -\frac{J\Omega}{I} \\ 0 & 0 & 0 & 1 & 0 & 0 \\ 0 & \frac{J\Omega}{I} & -\left(\frac{k}{M_y} + \frac{k}{I}\right) & 0 & \frac{J\Omega}{I} & 0 \\ \frac{k}{M_x} & 0 & 0 & 0 & 0 & 0 \\ 0 & 0 & \frac{k}{M_y} & 0 & 0 & 0 \end{bmatrix} \tag{8.52}$$

$$f = \begin{bmatrix} 0 & 0 & 0 & 0 & 0 & 0 \\ -\left(\frac{k}{M_x} + \frac{k}{I}\right)\cos 2\omega_1 t & 0 & -\left(\frac{k}{M_x} + \frac{k}{I}\right)\sin 2\omega_1 t & 0 & 0 & 0 \\ 0 & 0 & 0 & 0 & 0 & 0 \\ -\left(\frac{k}{M_y} + \frac{k}{I}\right)\sin 2\omega_1 t & 0 & \left(\frac{k}{M_y} + \frac{k}{I}\right)\cos 2\omega_1 t & 0 & 0 & 0 \\ \frac{k}{M_x}\cos 2\omega_1 t & 0 & \frac{k}{M_x}\sin 2\omega_1 t & 0 & 0 & 0 \\ \frac{k}{M_y}\sin 2\omega_1 t & 0 & -\frac{k}{M_y}\cos 2\omega_1 t & 0 & 0 & 0 \end{bmatrix} \tag{8.53}$$

where the variables $x_1 \ldots\ldots x_6$ correspond to φ_x, $\dot{\varphi}_x$, φ_y, $\dot{\varphi}_y$, $\dot{\theta}_x$, $\dot{\theta}_y$, respectively and $\mu = \frac{\Delta k}{k}$.

Following the method of Sec.8.3. for the simple parametric resonance where the first natural frequency n_1 is equal to the ball cage frequency ω_1, the solutions of the equations corresponding to (8.34) are:-

$$y_s^{\,o} = M_o P_s + N_o Q_s e^{-2it} \tag{8.54}$$

The vectors P and Q are easily shown to be as follows.

$$P_1, \ldots P_6 = 1,\ in_1,\ -\frac{in_1\left[n_1^2 - \left(\frac{k}{M_x} + \frac{k}{I}\right)\right]}{\frac{J\Omega}{I}\left(n_1^2 - \frac{k}{M_y}\right)},\ \frac{n_1^2\left[n_1^2 - \left(\frac{k}{M_x} + \frac{k}{I}\right)\right]}{\frac{J\Omega}{I}\left(n_1^2 - \frac{k}{M_y}\right)},$$

$$-\frac{ik}{M_x n_1},\ \frac{\frac{J\Omega}{I} \cdot \frac{k}{M_y}\left(n_1^2 - \frac{k}{M_x}\right)}{n_1^2\left[\left(\frac{k}{M_y} + \frac{k}{I}\right) - n_1^2\right]} \tag{8.55}$$

while $Q_1, \ldots\ldots Q_6$ are the conjugates of $P_1, \ldots\ldots P_6$ respectively.

The vectors R and S of the negative transpose of a make up the function matrix ψ, and like P and Q they are complex conjugates. They are similar in form to those shown above for P and it will be apparent that it would be rather unwieldy to form the products $\psi' \varphi$, $\varphi' a' \psi$ and $\varphi' f' \psi$ analytically.

8.10 Numerical solution - simple resonance

Using the parameters of Chapter 7 with $M_x = M_y = 1.57$ the first natural frequency is found to be $n_1 = 984.1016$ rad/sec.

Taking the case of simple parametric resonance where the ball cage frequency is equal to the first natural frequency, n_1, the vectors P and Q were found by putting $P_1 = 1$ and solving 5 of the equations:

$$(a - in_1)\ P = 0 \qquad (8.56)$$

using a standard Sirius library programme, S 1510.

Since P_2, P_3 and P_5 are imaginary, they are replaced by iP_2', iP_3' and iP_5' giving a set of 5 real linear equations for P_2', P_3', P_4, P_5' and P_6. The vector Q, corresponding to the eigen value - in, is the solution of $(a + in_1)\ Q = 0$. and is thus the conjugate of P.

The vectors R and S were similarly found from $(a' - in)\ R = 0$ and $S = \bar{R}$. The vectors P and R were found to be as follows:-

$P_1 = 1$	$R_1 = 1$
$P_2 = 984.1016i$	$R_2 = 0.00125144i$
$P_3 = -i$	$R_3 = i$
$P_4 = 984.1016$	$R_4 = -0.00125144$
$P_5 = -9774.8i$	$R_5 = 0.00226760i$
$P_6 = -9774.8$	$R_6 = -0.00226760$

The matrix φ is then

$$\begin{bmatrix} P_1 & Q_1 e^{-2it} \\ \vdots & \vdots \\ P_6 & Q_6 e^{2it} \end{bmatrix} \qquad (8.57)$$

and ψ =

$$\begin{bmatrix} R_1 & S_1 e^{2it} \\ \vdots & \vdots \\ R_6 & S_6 e^{2it} \end{bmatrix}$$

First the matrix $\psi' \varphi$ was computed:-

$$\begin{bmatrix} \Sigma PR & \Sigma QR e^{-2it} \\ \Sigma PS e^{2it} & \Sigma QS \end{bmatrix}$$

It is found that $\Sigma PS = \Sigma QR = 0$

and that $\Sigma PR = \Sigma QS = \text{const} = 43.8673$

and if the matrix ψ is divided by this constant

$$\psi' \varphi = \begin{bmatrix} 1 & 0 \\ 0 & 1 \end{bmatrix}$$

The matrix $A = \varphi' a' \psi$ was then computed, (using the new value of ψ),

and was found to be $\begin{bmatrix} in_1 & 0 \\ 0 & -in_1 \end{bmatrix}$ correct to 6 decimal places.

That this is a general result and not particular to this case is shown below in Sec. 8.14.

The matrix B was then computed and found to be

$$B = \begin{bmatrix} 0 & -i.44.866 \\ i.44.866 & 0 \end{bmatrix}$$

Substituting in the quadratic equation (8.39) gives

$$a^* = \pm \quad 44.866\ \lambda_o \quad \text{for } \sigma = 0$$

and $$\sigma = \pm \quad 44.866\ \lambda_o/n \text{ for } a^* = 0$$

The characteristic exponent referred to real time is $\frac{\mu\, a^*\, \omega_o}{2}$, $= 44.866\mu$

since $\lambda_o = \frac{2}{\omega_o}$. As a percentage of critical damping this is

$$\frac{44.866 \times 100}{984.1016} = 4.5577 \ \% = \underline{0.456\%} \quad \text{for} \quad = \frac{\Delta k}{k} = 0.1$$

The width of the unstable zone is given by the values of σ for $a^* = 0$. Let these limiting values of σ be $\pm\ \sigma_1$ and recall that in equations (8.30)

$\lambda = \lambda_o + \mu\sigma$, The limits of stability therefore correspond to

$$\lambda = \lambda_o \pm \mu\sigma_1$$

or $$\frac{2}{\omega} = \frac{2}{\omega_o} \pm \mu\sigma_1$$

where ω is the frequency of variation of the coefficients f and ω_o is the value at the centre of the parametric resonance.

This gives $$\frac{\omega}{\omega_o} = \frac{1}{1 \pm \frac{\mu\sigma_1\ \omega_o}{2}} \qquad (8.58)$$

and hence for the particular case considered

$$\frac{\omega}{\omega_o} = \left(1 \pm \frac{44.866}{n_1}\right)^{-1}$$

$$\doteq 1 \mp \frac{44.866}{n_1}$$

for μ small.

This means that the system is unstable when the natural frequency matches the ball cage frequency to within 0.5% approx. for $\frac{\Delta k}{k} = 0.1$. It can be seen therefore that this is a small and 'highly tuned' effect.

8.11 Combination resonance

A study of Figs. 45 and 46 shows that there is only one parametric resonance at the fundamental parameter variation frequency, viz. the simple resonance just dealt with in the previous section.

If, however, a resonance is being considered where $\omega_i - \omega_k = N\omega_o$, for $N \neq 1$, the functions

$$\varphi_s(t) = P_s + Q_s e^{-2iNt}$$
$$\text{and } \psi_s(t) = R_s + S_s e^{2iNt} \qquad (8.59)$$

If the terms of the coefficient matrix contain neither constants nor harmonics of order N, then the matrix B will be zero and no instability will arise.

This is the case in the equations (7.1) so that the simple resonance computed in Sec. 8.10 is the only unstable one.

In an actual system, however, harmonics of the ball cage frequency are likely to be present, particularly that corresponding to the number of balls.

8.12 Comparison with digital simulation

The Atlas programme described in 7.3 was used with initial conditions defined by the vectors P preceding eqn. 8.57.

$$\text{i.e.} \quad X_s^{\circ} = P_s e^{in_1\tau} + Q_s e^{-in_1\tau} \tag{8.60}$$

and for

$$\tau = 0, \; X_s^{\circ} = P_s + Q_s = 2P_s \text{ for } P_s \text{ real}$$

$$= 0 \text{ for } P_s \text{ imaginary}$$

since P_s and Q_s are conjugate .

In fact, φx_o was taken as 10^{-4} radians, $\dot{\varphi} y_o$ was taken as 0.09841 rad/sec. and $\dot{\theta} y_o$ as - 0.9775 rad/sec. This choice of initial conditions excites motion in the mode of the first natural frequency.

Fig. 47 shows $\log_{10}(E/IE)$ plotted to a base of time. The curve is smooth and the slope tends to a value about 5% below that calculated from the characteristic exponent obtained in Sec. 8.10.

To check if this discrepancy depended on $\mu = \Delta k/k$, computer transients were also obtained for $\mu = 0.1$ and $\mu = 0.05$ for the case $M_x = M_y = 1.57$ gm. cm. sec^2. Very long transients were required before the term with the negative exponent died away sufficiently to indicate the slope due to the positive exponent. Since graphical estimation of slope is never very satisfactory, the exponents were calculated as follows:-

Assuming the variation of E to be of the form

$$E = \frac{IE}{2}\left(e^{2at} + e^{-2at}\right) \tag{8.61}$$

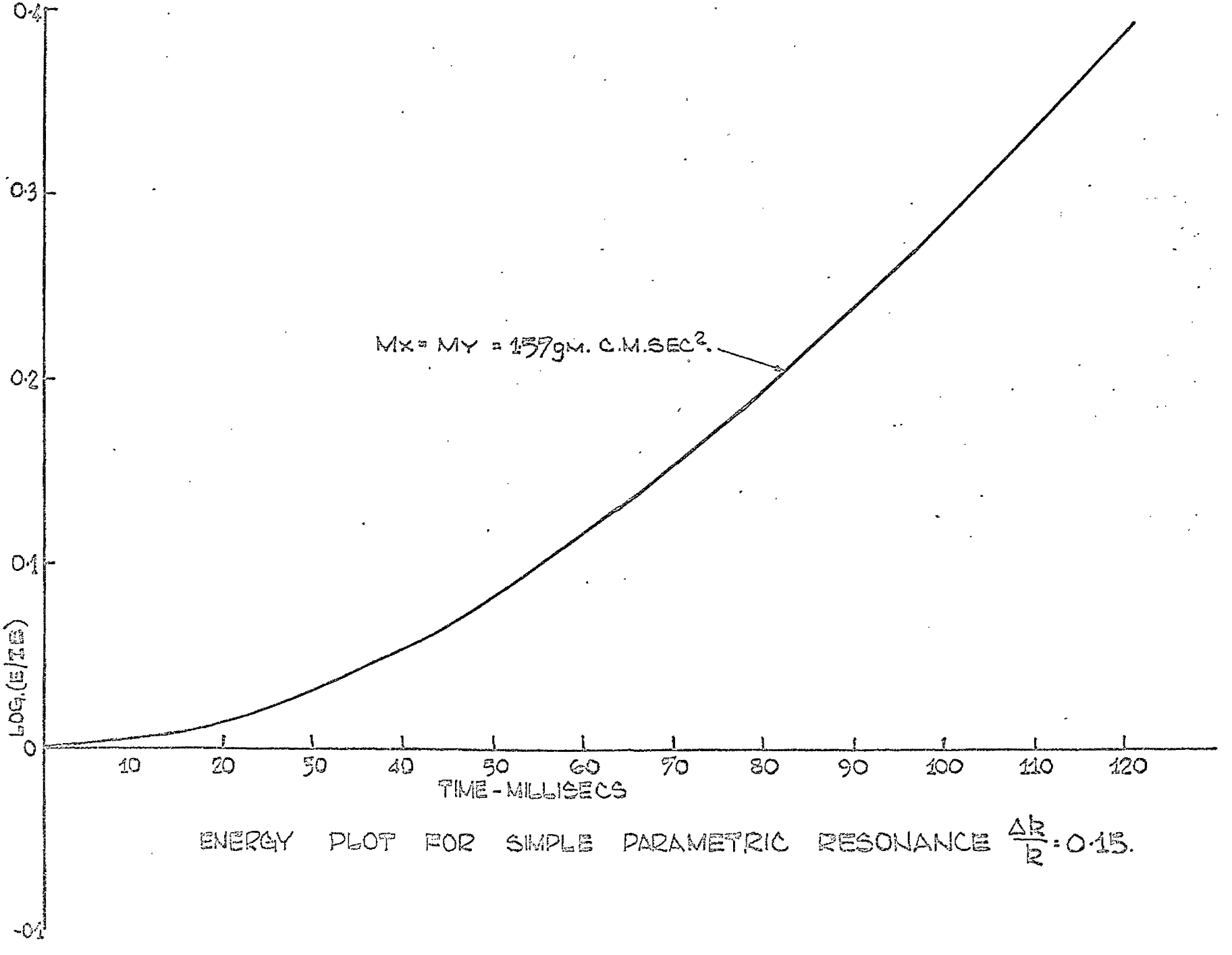

ENERGY PLOT FOR SIMPLE PARAMETRIC RESONANCE $\frac{\Delta R}{R} = 0{\cdot}15$.

FIG. 417

where a and -a are the characteristic exponents (E is a quadratic function of the variables x_s)

$$z + \frac{1}{z} = \frac{2E}{1E} \quad \text{where } z = e^{2at}$$

Using the computer values for E/1E at 120 m.. . values of z could be found and hence a. The validity of the assumed expression for E was checked by back substitution at other values of t.

Fig. 48 shows the values of a thus obtained from the computer transients, plotted against $\mu = \Delta k/k$ and for comparison the theoretical values, proportional to μ, obtained by the method of Section 8.3. The percentage difference between the two values of the characteristic exponent is found to increase with μ and it seems likely that the difference is due to the approximation involved in the method of Sec. 8.3.

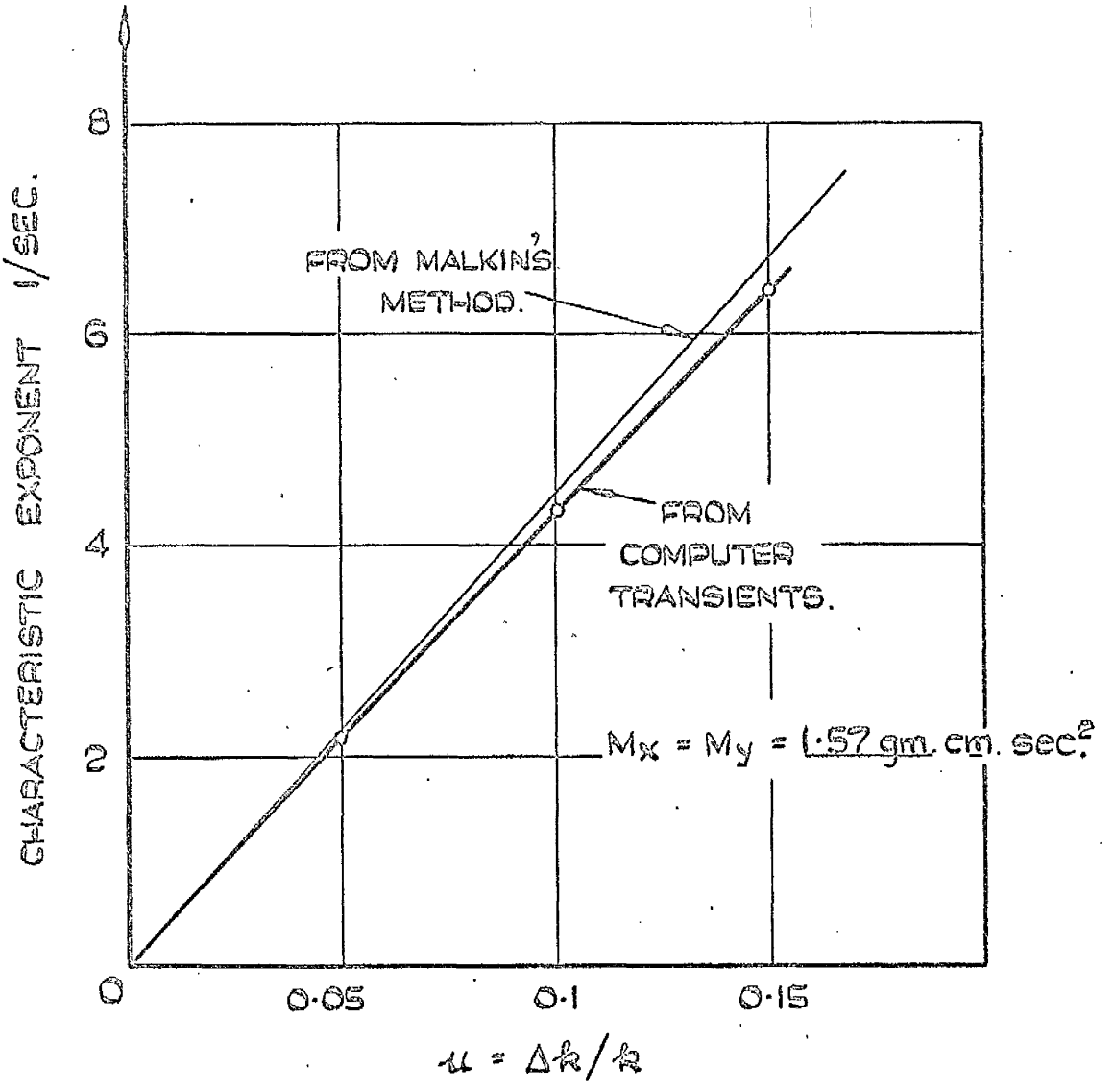

EFFECT OF USING THE FIRST APPROXIMATION IN CALCULATING THE CHARACTERISTIC EXPONENT.

FIG. 48.

8.13. Extension of the method to more complex cases.

The method is, in principle, applicable to systems with any number of simultaneous equations of the type shown in equation 8.1. However, even with the system of six equations (equations (7.1)) which describe the effect of bearing stiffness variation, analytical expression of the functions φ and ψ becomes too unwieldy.

The method would lend itself well to numerical solution, using well established matrix procedures on a digital computer.

The first stage would be to find the latent roots and vectors of the matrix a over the desired range of system parameters. The location of any resonances could then be found using the relation (8.32).

The two vectors forming the matrix φ are the latent vectors of the matrix a corresponding to the two latent roots which satisfy the relation (8.32). The two vectors forming the matrix ψ are the latent vectors of the transpose a' for the same two latent roots. A scalar adjustment requires to be made to ψ to satisfy the condition that $\psi' \varphi = 1$.

8.14. Formation of matrix A.

$$\text{The matrix } A = \frac{1}{2\pi} \int_0^{2\pi} (\varphi' a' \psi) dt \qquad (8.62)$$

but because of various properties of the matrices φ, a, and ψ the $\frac{1}{2\pi} \int_0^{2\pi}$ can be discarded since the only non zero terms in the product

are constants.

Using the expression $A_{ij} = \sum_{\alpha,\beta=1}^{n} a_{\beta\alpha}\, \varphi_{\alpha i}\, \psi_{\beta j}$ (8.63)

and writing $\varphi_s = P_s + Q_s e^{-2iNt}$

$$\psi_s = R_s + S_s e^{2iNt} \tag{8.64}$$

$$\begin{aligned} A_{11} = {} & R_1(a_{11}P_1 + a_{12}P_2 + \ldots\ldots + a_{1n}P_n) \\ & + R_2(a_{21}P_1 + \ldots\ldots + a_{2n}P_n) \\ & + \ldots\ldots\ldots\ldots\ldots\ldots \\ & + R_n(a_{n1}P_1 + \ldots\ldots + a_{nn}P_n) \end{aligned} \tag{8.65}$$

but, since P is the latent vector corresponding to the eigen value $i\omega_i$, Q the latent vector for $-i\omega_i$, R corresponds to $i\omega_k$, and S to $-i\omega_k$,

$$(a - i\omega_i I)P = 0$$

$$(a - i\omega_i I)Q = 0$$

$$(a' + i\omega_i I)R = 0$$

$$(a' + i\omega_k I)S = 0$$

$$\therefore\ A_{11} = R_1 \cdot i\omega_i P_1 + R_2 \cdot i\omega_i P_2 + \ldots\ldots + R_n\, i\omega_i P_n$$

$$= i\omega_i \Sigma PR = i\omega_i$$

Similarly it can be shown that

$$A_{22} = i\omega_k \cdot \Sigma QS = i\omega_k$$

$$A_{12} = A_{21} = 0$$

i.e. the matrix $A = \begin{bmatrix} i\omega_i & 0 \\ 0 & i\omega_k \end{bmatrix}$ (8.66)

provided $\chi' \varphi = \begin{bmatrix} 1 & 0 \\ 0 & 1 \end{bmatrix}$

8.15 Formation of matrix B.

B is defined by relation (8.37) viz.

$$B_{ij} = \frac{1}{2\pi} \sum_{\alpha,\beta=1}^{n} \int_0^{2\pi} \lambda_0 f_{\beta\alpha} \varphi_\alpha i \chi_{\beta i} dt$$

where $f_{\beta\alpha}$ may contain constants, terms in cos 2 Nt, or terms in sin 2 Nt (for N = 1,2 ...)

i.e. let $f_{\beta\alpha} = f_{1\beta\alpha} + f_{2\beta\alpha} \cos 2Nt + f_{3\beta\alpha} \sin 2Nt$

$$B_{11} = \frac{\lambda_0}{2\pi} \sum_{\alpha,\beta=1}^{0} \int_0^{2\pi} f_{\beta\alpha} P_\alpha R_\beta dt$$

$$= \lambda_0 \sum_{\alpha,\beta=1}^{n} f_{1\beta\alpha} P_\alpha R_\beta dt$$

$$B_{22} = \frac{\lambda_0}{2\pi} \sum_{\alpha,\beta=1}^{n} \int_0^{2\pi} f_{\beta\alpha} Q_\alpha S_\beta dt$$

$$= \lambda_o \sum_{\alpha,\beta=1}^{n} f_{1\beta\alpha}\, Q_\alpha\, S_\beta$$

$$B_{12} = \frac{\lambda_o}{2\pi} \sum_{\alpha,\beta=1}^{n} \int_0^{2\pi} f_{\beta\alpha}\, P_\alpha\, S_\beta\, e^{2iNt}\, dt$$

$$= \frac{\lambda_o}{2} \sum_{\alpha,\beta=1}^{n} (f_{2\beta\alpha} + if_{3\beta\alpha}) P_\alpha\, S_\beta$$

$$B_{21} = \frac{\lambda_o}{2\pi} \sum_{\alpha,\beta=1}^{n} \int_0^{2\pi} f_{\beta\alpha}\, Q_\alpha\, R_\beta\, e^{-2iNt}\, dt$$

$$= \frac{\lambda_o}{2} \sum_{\alpha,\beta=1}^{n} (f_{2\beta\alpha} - if_{3\beta\alpha})\, Q_\alpha\, R_\beta$$

If $\varphi' f_1' \psi = F$

$\varphi' f_2' \psi = G$

$\varphi' f_3' \psi = H$

then

$$B = \lambda_o \begin{bmatrix} F_{11} & \frac{1}{2}(G_{12} + iH_{12}) \\ \frac{1}{2}(G_{21} - iH_{21}) & F_{22} \end{bmatrix} \qquad (8.67)$$

Having computed B as above it would then only remain to solve the quadratic equation (8.39) for σ or a^*

Damping could best be taken into account by including it in the constant matrix f_1 as illustrated in Sec.8.8 for the case of the gyro with an unsymmetrical rotor.

CHAPTER 9.

EXPERIMENTAL WORK

The object of the experimental work was to investigate the relationship between the bearing reaction forces and moments and the relative displacements of inner and outer races of the bearings, under various conditions of speed and preload.

9.1 Description of first experimental rig.

Since the deflections were very small rigid mountings for the probes were required. Also, because a wide speed range was desired the apparatus took the form shown in Fig. 49. This shows the rotor and stator coils from an existing gyroscope mounted in a heavy casing with an end cover. Holes are provided with insulated bushes for inserting capacitance probes. These are placed to permit measurement of radial and transverse angular displacement of the rotor in two directions and also axial displacement.

The mean of the axial displacements measured at two diametrically opposite probes gave the axial movement of the rotor while the difference was proportional to the tilt of the rotor. The preload was provided by a spring and was not varied.

The complete assembly was mounted on a vibrator instead of gimbals and rectilinear vibrations of different amplitudes and frequencies were imposed on the case, transverse to the spin axis. A block diagram of the forcing and measuring system is shown in Fig 50 (a). This

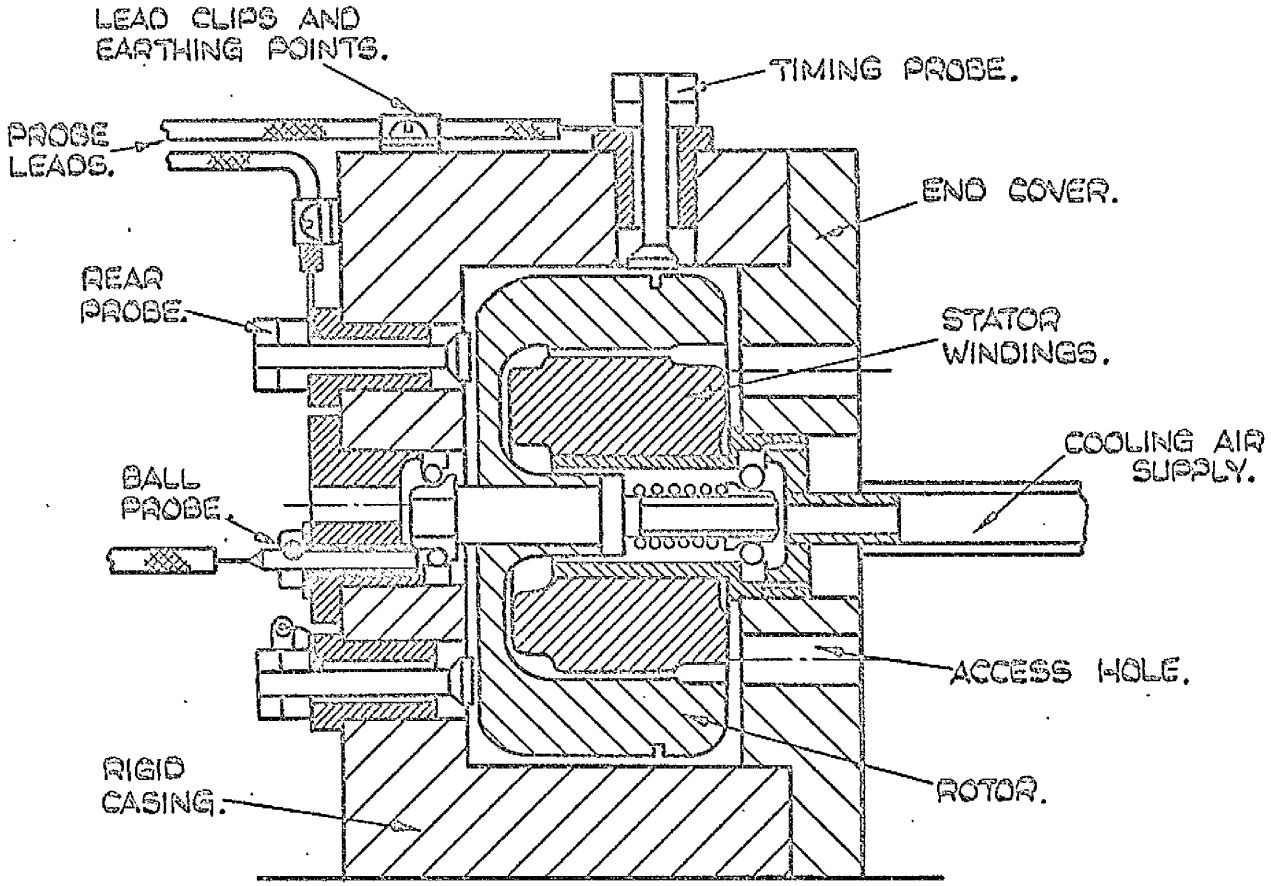

FIRST EXPERIMENTAL ASSEMBLY.

FIG. 49.

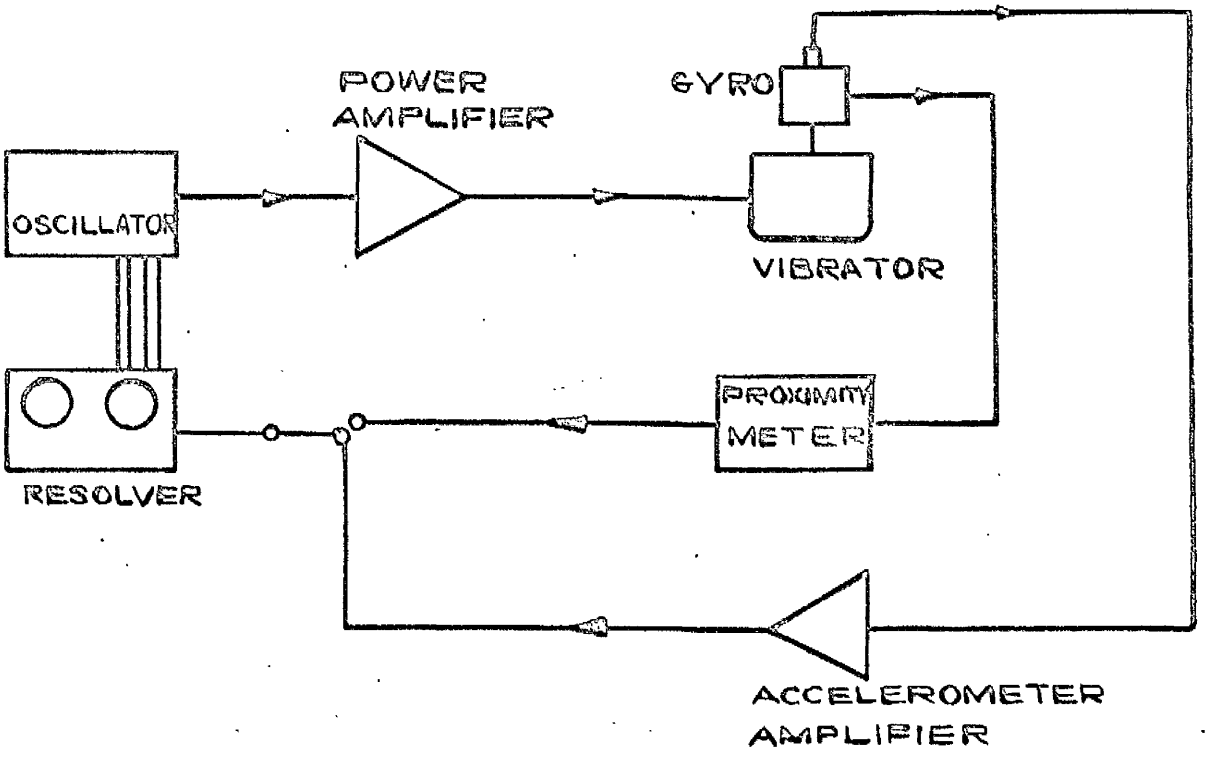

(a) ORIGINAL

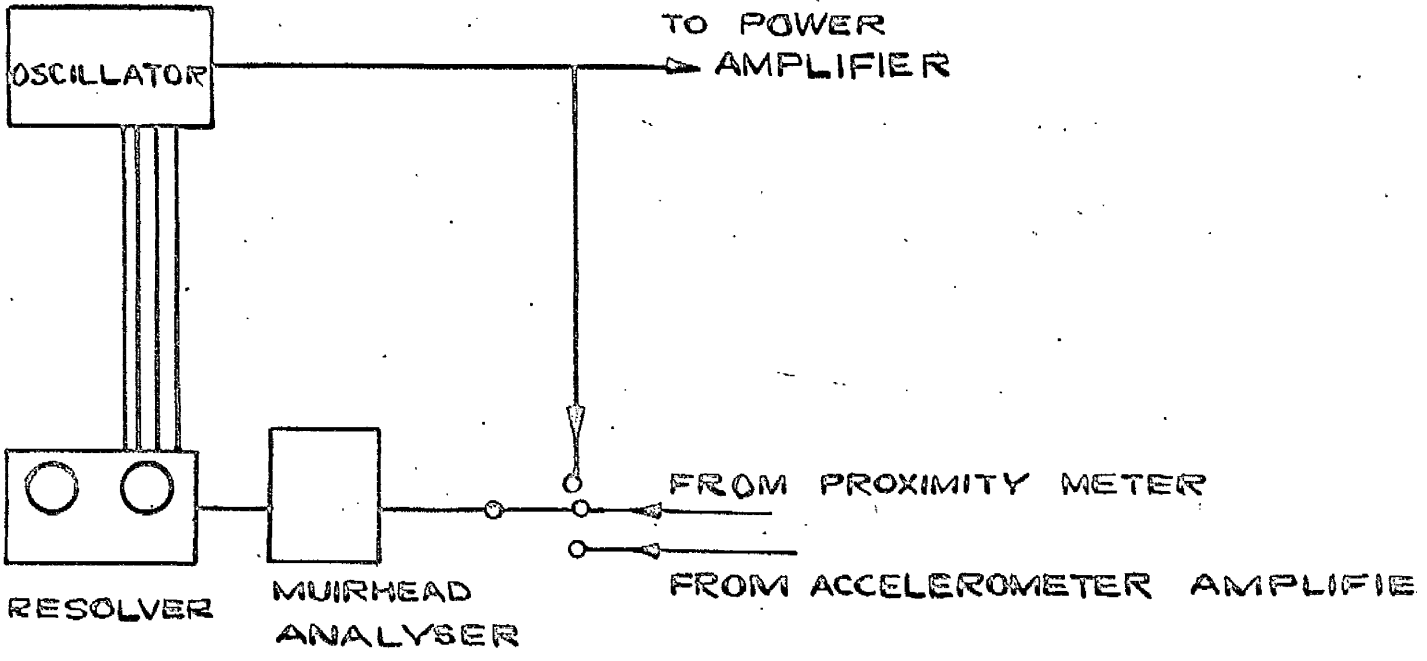

(b) LATER

EXPERIMENTAL SET UP

FIG. 5(

comprised the oscillator of a Solartron transfer function analyser feeding the power amplifier of the vibrator, this in turn producing the vibration of the gyro casing. The casing vibration was measured by an accelerometer with its associated amplifier and the "gain" and phase shift between the oscillator and the relative displacements of motor and casing could be obtained. By dividing the gains and subtracting the phase shifts the response of relative displacement to casing acceleration could be obtained. Because of the non-linearity of the system, the response was amplitude dependent and series of tests were run at different constant acceleration amplitudes.

It was found possible to obtain reasonably repeatable results as long as the rotor was stationary but when the rotor was running the meter pointers of the transfer function analyser wandered all over the scales and gave no useful results whatsoever.

The waveforms emanating from the relative displacement pick ups were extremely complex when the rotor was rotating and although the rejection of unwanted frequencies by the TFA is good (better than 40 db) it would appear that in this case the analyser was swamped by the unwanted signals. In an attempt to overcome this difficulty a Muirhead type D-489 DM frequency analyser was included in the set up to act as a tunable filter at the input to the resolver, as shown in Fig.50b. On setting the oscillator to each new frequency the analyser was switched to the oscillator output and tuned so that the resolver showed no

phase shift. The analyser was then switched to read the outputs from the proximity meter and accelerometer amplifier in turn.

Even with this refinement however, the readings were subject to random variation when the rotor was running.

The sensitivity of the proximity meter was such that the slightest movement of the leads between the probes and the meter was sufficient to affect the readings and accordingly this rig was abandoned in favour of an apparatus with a fixed casing.

9.2 Description of second rig.

The second apparatus is shown in Fig. 51and comprised a rather larger (4 in. diam) rotor mounted with axis vertical in a casing about $\frac{1}{2}$ in. thick, clamped to a heavy baseplate. Capacity probes were mounted as before and a pneumatic method was chosen to apply an easily controlled preload to the bearings. An additional probe mounted opposite a balancing hole in the rotor provided a pulse to operate a Racal digital frequency meter, giving a convenient speed measurement. Recordings of two displacements and the speed were made on a magnetic tape recorder for subsequent analysis, and the displacements were also displayed on an oscilloscope.

The method adopted was to run the gyro up to speed and then switch off the power. Keeping the preload constant, the gyro was allowed to run down, two channels of displacement being recorded along with a spoken record of the speed readings and comments on any interesting events appearing on the

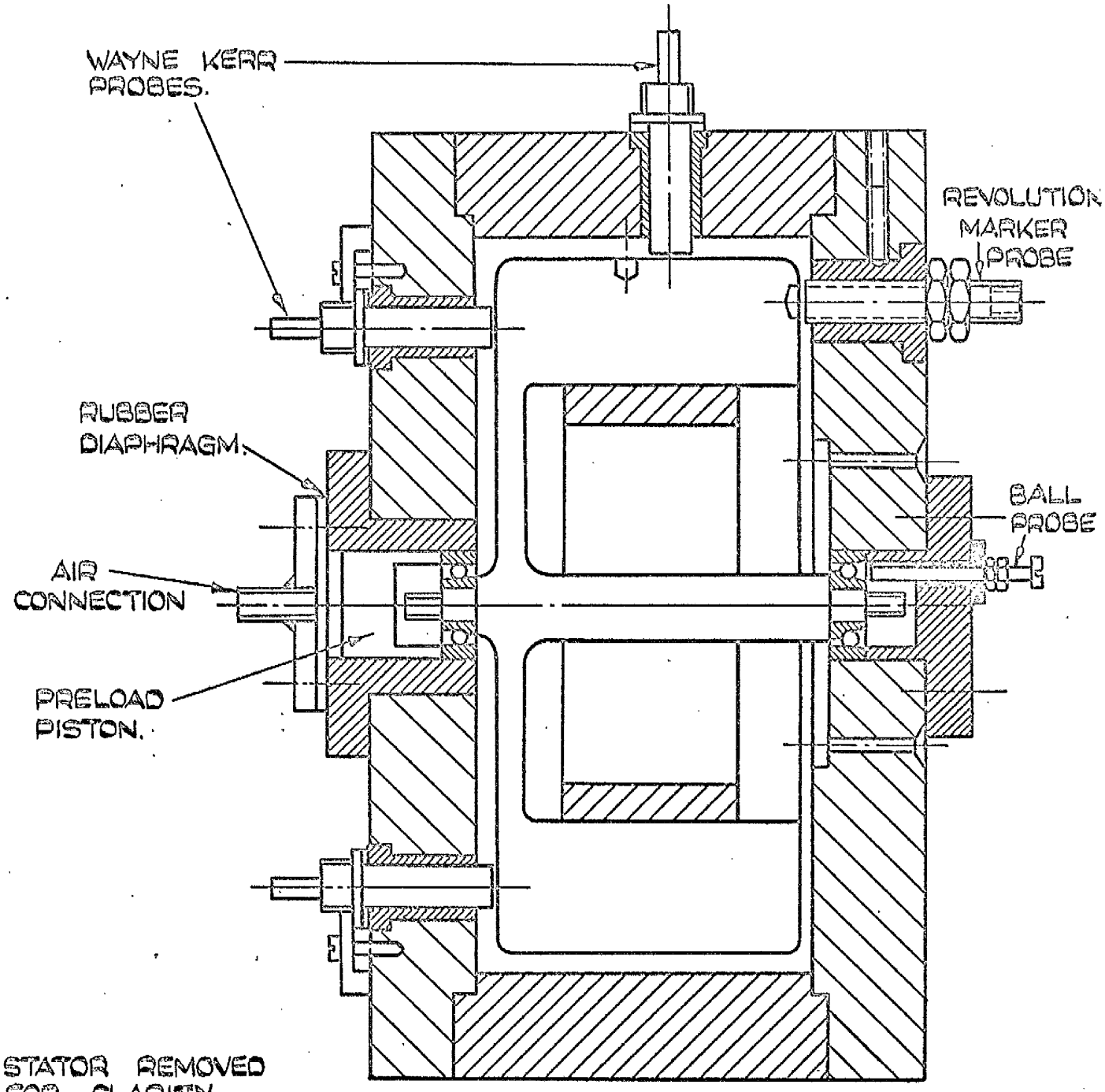

SECOND EXPERIMENTAL ASSEMBLY.

FIG. 51.

oscilloscope. The recordings could then be played back as often as desired for re-examination of the traces and for frequency analysis.

Normally in work of this kind one would attempt to keep the speed constant but the low torque/inertia ratio of the gyro motor and the characteristics of the alternator supplying the motor did not lend themselves to close control over a wide speed range. Because of the high rotor inertia and low bearings friction the rotor deceleration was small - of the order of $\frac{1}{2}$ rev/s^2 at 250 rev/s.

Two pairs of angular contact bearings were used in these tests - first a pair of high quality Barden 34 - 5B bearings, 5 mm bore x 5 mm wide x 16 mm o/d to rather better than ABEC 5 tolerances. Each bearing had six 1/8 in dia. balls in a phenolic retainer.

The other bearings used were Hoffmann A5 bearings of commercial quality having 5 balls in a brass cage.

Tests were run with the preload air pressure varied between 0 and 30 lb/in^2, corresponding to axial loads of 0 - 9.33 lb. The axial load on the lower bearings would be greater than this due to the rotor weight, which was 3.93 lb.

9.3. Analysis of recordings

Various methods of analysis were tried using a Bruel and Kjaer type 2107 analyser with a type 2305 level recorder. The analyser can be coupled by a flexible drive to the recorder and made to sweep automatically through the frequency range, recording the spectrum of the signal on paper which may

be plain or graduated logarithmically in terms of frequency. A variety of chart speeds, sweep speeds and writing speeds are available and some trial and error is necessary to achieve an optimum combination. (Writing speed is a measure of the speed of response of the recorder pen to changes in signal level)

At first short, continuous loops of tape on a second recorder were recorded from the main tape in order to pinpoint the signals at a certain speed. These were then played back continuously to get the normal form of spectrum at that one speed. Some difficulty was experienced in tensioning the tape properly and there were also transients due to the tape join and the gap left in the signal when recording on to the loop was stopped. This gap was due to the distance between the erase and record heads.

For a quick survey of the signals the analyser was set to a fast sweep speed and the complete signal tape played back. Notes were made on the chart of the speed from the speech channel on the tape. The disadvantages of this method were the lag of the resonance peak behind the true value, and the attenuation of the peak, both of which increased with the sweep speed. The peaks on the recorder chart did not therefore exactly match the speed with which they were associated.

A more accurate method, but much more time consuming, was to leave the analyser at a fixed frequency and run through the tape, or the part of interest, as often as required at different frequencies. This was more suited to the detailed

analysis of parts of the tape, e.g. in the region of a jump phenomenon.

9.4. Results of frequency analysis

Typical results of such an analysis are shown in Fig. 52 which shows contours of constant vibration level plotted on a field of log frequency v. log speed. On this plot, ridges running at 45° across the plot represent vibrations of the same order i.e. the same ratio vibration frequency/rotational speed. Ridges, or lines of peaks running across these lines represent the variation of natural frequency with speed. A disadvantage of this form of plot, however, is that the analyser cannot distinguish between forward and backward precession, since information regarding the relative phase of two displacements at right angles is required to establish this.

9.5. Jump phenomenon

This occurred predominantly in the axial motion at low preload with the Hoffmann A5 bearings. At zero preload and a speed of 71 rev/s. the amplitude of the signal at 203.5 c/s, (order 2.86) suddenly dropped by about 10 db while a sudden upward jump of approximately the same magnitude occurred at a frequency of 221.5 c/s (order 3.13). An overall reading of the vibration signal i.e. with the analyser in the wide band, non-selective condition, showed a drop of 7 db at this point. Fig.53 shows details of the spectra during the run down through 71 rev/s., while Fig.54 shows, in contour map form, the run down through a similar jump which occurred with a preload pressure of 5 lb/in^2. The rotor speed at which the jump took place was slightly higher than with no preload,

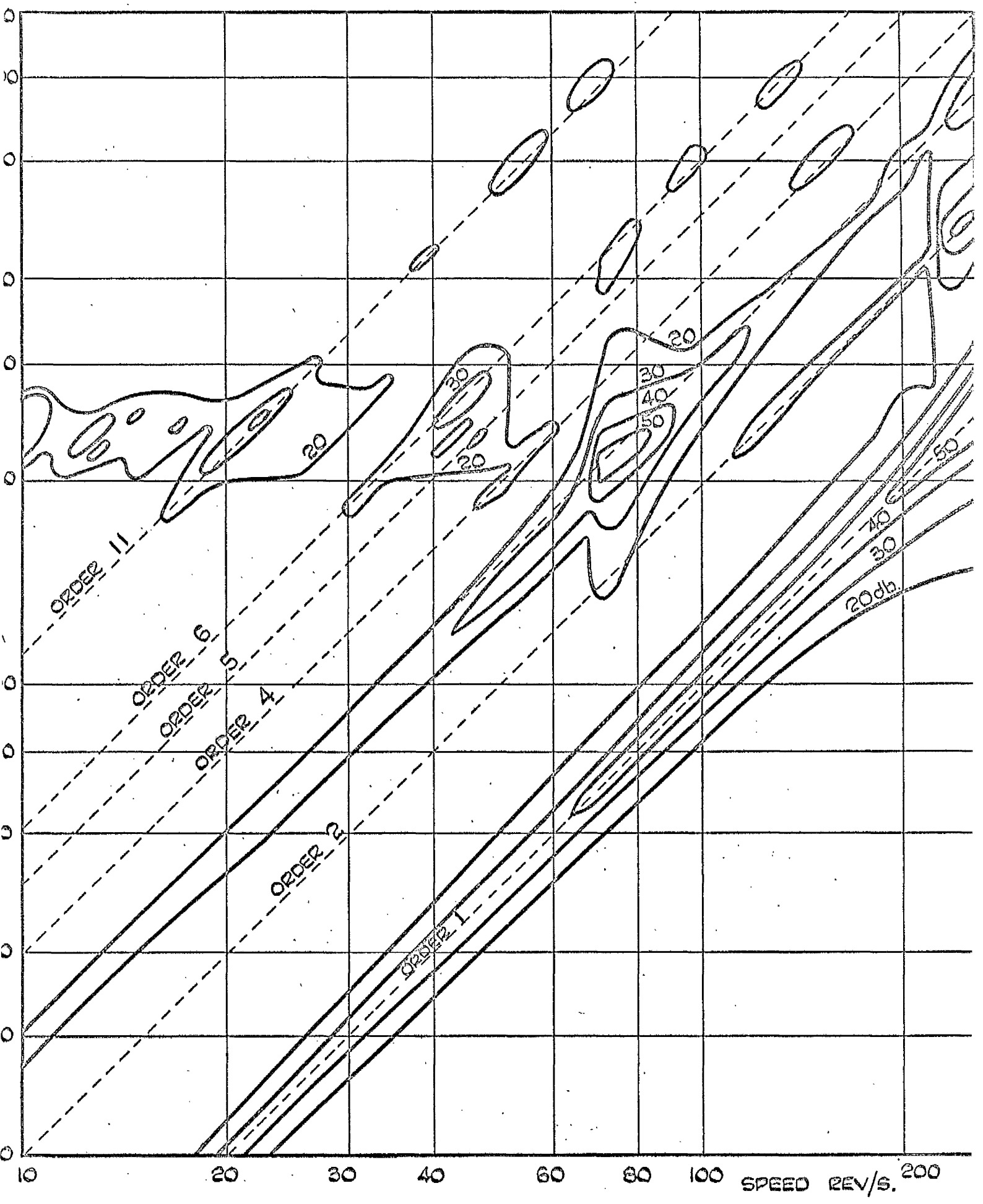

CONSTANT AMPLITUDE CONTOURS - HOFFMANN A5 BEARINGS
AXIAL DISPLACEMENT - 5 LB/IN^2 PRELOAD.

FIG. 52.

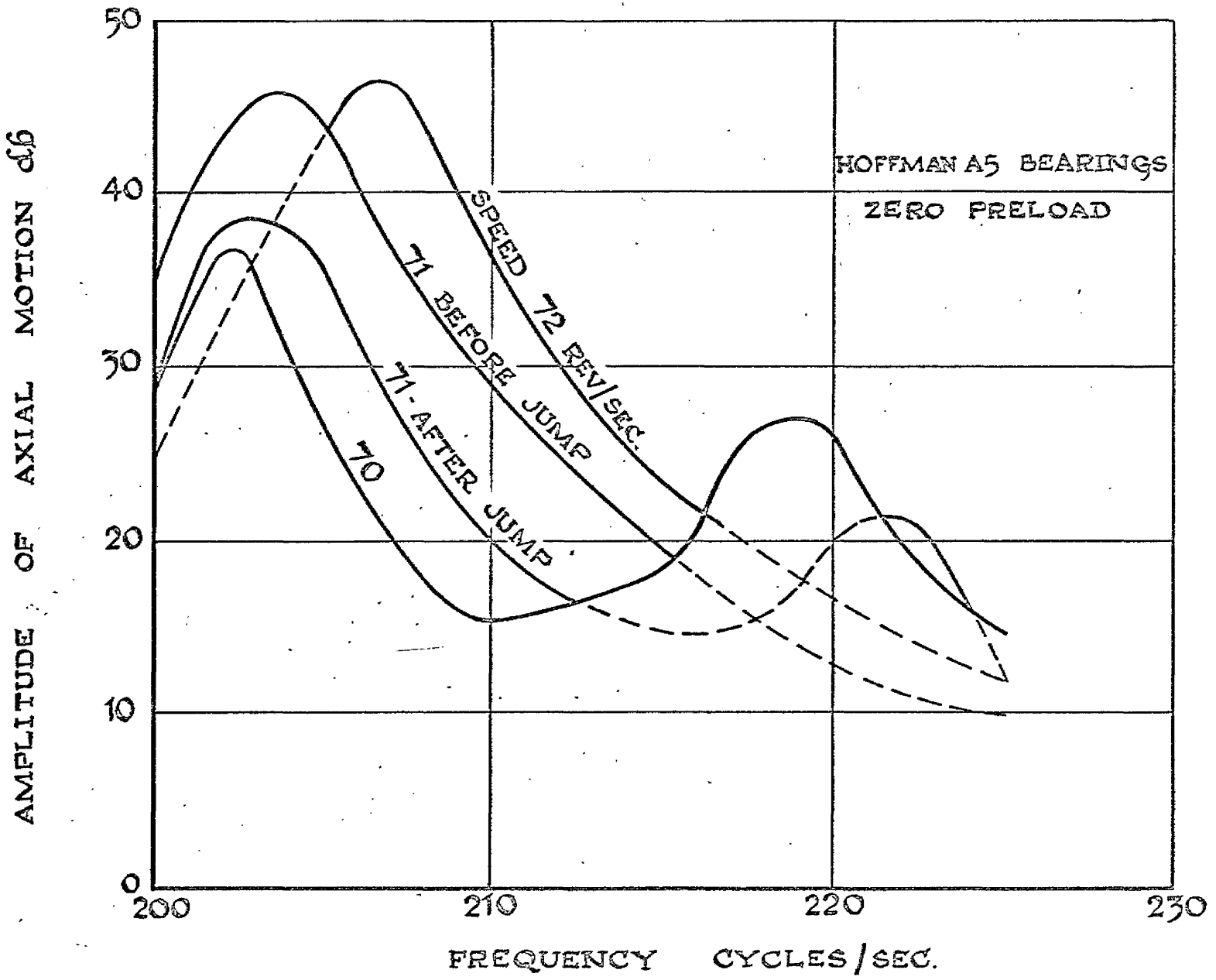

FIG 53.

SPECTRA DURING RUN DOWN THROUGH JUMP PHENOMENON.

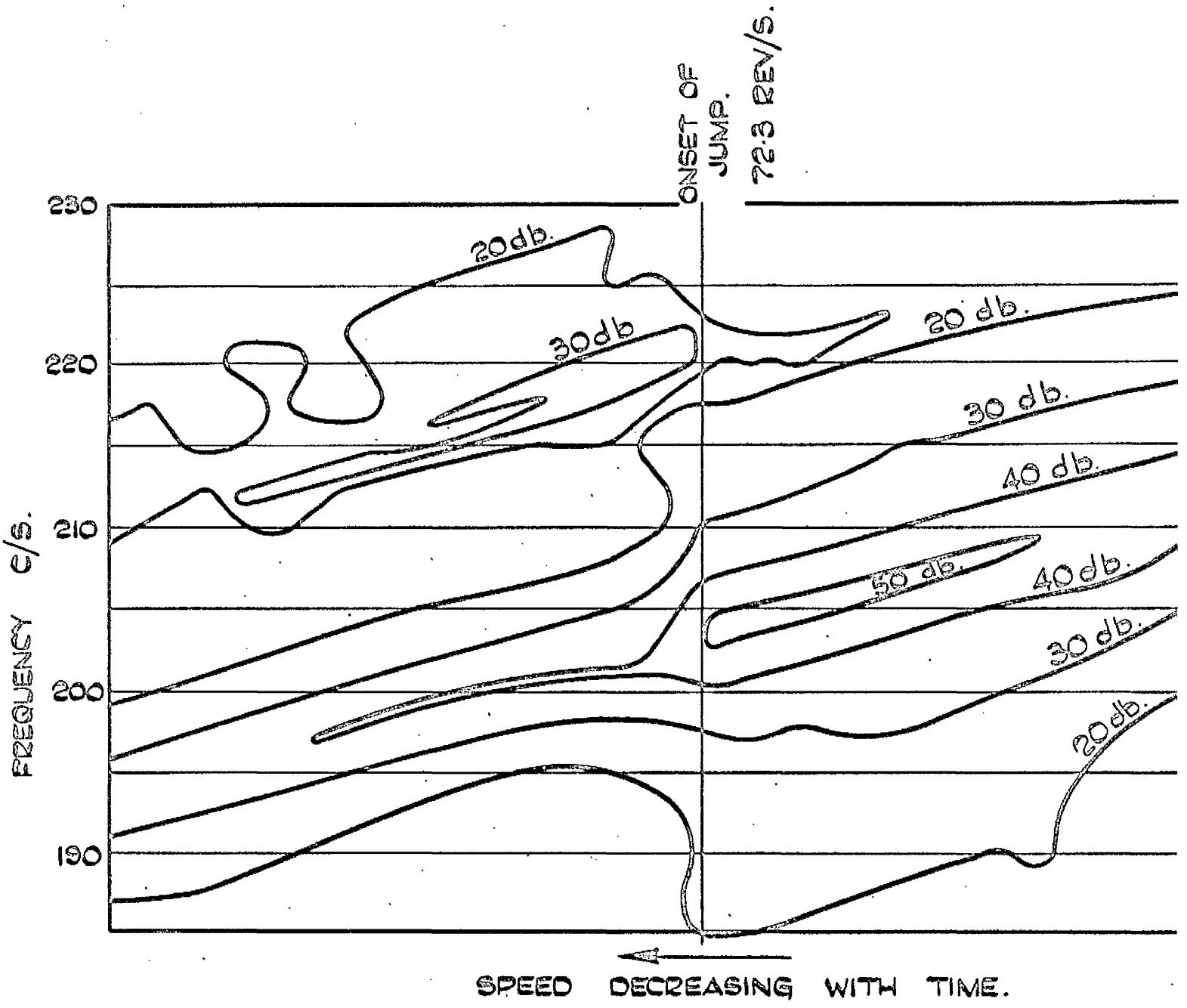

CONSTANT AMPLITUDE CONTOURS
NEAR JUMP RESONANCE. (5 LB/IN² PRELOAD)

FIG. 54.

but the two vibration frequencies involved in the change were virtually the same as those with no preload.

In a single degree of freedom system with non-linear restoring force a jump of this nature i.e. downwards in amplitude with decreasing speed, suggests springing of the soft type i.e. stiffness reducing with deflection. This case is not so simple, however, since the system has several degrees of freedom and since there may be coupling between the motions due to the bearing characteristics and gyroscopic effects. Comparison between the axial and radial displacements in the region of the jump, however, shows much less build up of the signals of order 2.86 in the radial displacement.

Other prominent signals apart from the fundamental are 6th and 11th order vibrations at around 250 c/s.

9.6. Suggested improvements to experimental apparatus

The chief difficulty with the present apparatus lies in the measurement of small high frequency vibrations of a flexible rotating body. No direct measurement of the forces in the bearings is possible and the nature of these forces requires to be inferred from the complex motions of the rotor.

An ideal apparatus would be a rotor, capable of running over a wide range of easily controlled speeds, mounted in bearings of infinite stiffness, and completely free of vibration. The bearing to be tested would be mounted on this shaft and the non rotating outer race could then be subjected to a variety of forms of loading in order to determine the relationship between forces, moments

and displacements in the ball bearing.

Fig. 55 shows a block diagram of the ball bearing in which x, y and z represent displacements of the inner race relative to the outer, z being the axial direction. θ_x, θ_y and θ_z are the corresponding rotations, and superimposed on all these displacements there may be fluctuations due to imperfections in the bearing. $F_{x,y,z}$ are the forces and $M_{x,y,z}$ are the moments impressed on the bearing. To specify the bearing completely transfer functions or frequency responses relating each of the displacements to each of the forces and moments are required, along with the nature of the disturbances due to manufacturing errors.

The responses will be non linear with amplitude and will be affected by rotational speed and conditions of lubrication.

This obviously is not an easy task and the experimental work described in the foregoing sections represents only the beginning. A stiff rotor supported in gas bearings seems to offer the only feasible approach to the ideal apparatus outlined above, and indeed, were it not for their high cost, gas bearings would possibly have replaced ball bearings for many gyro applications.

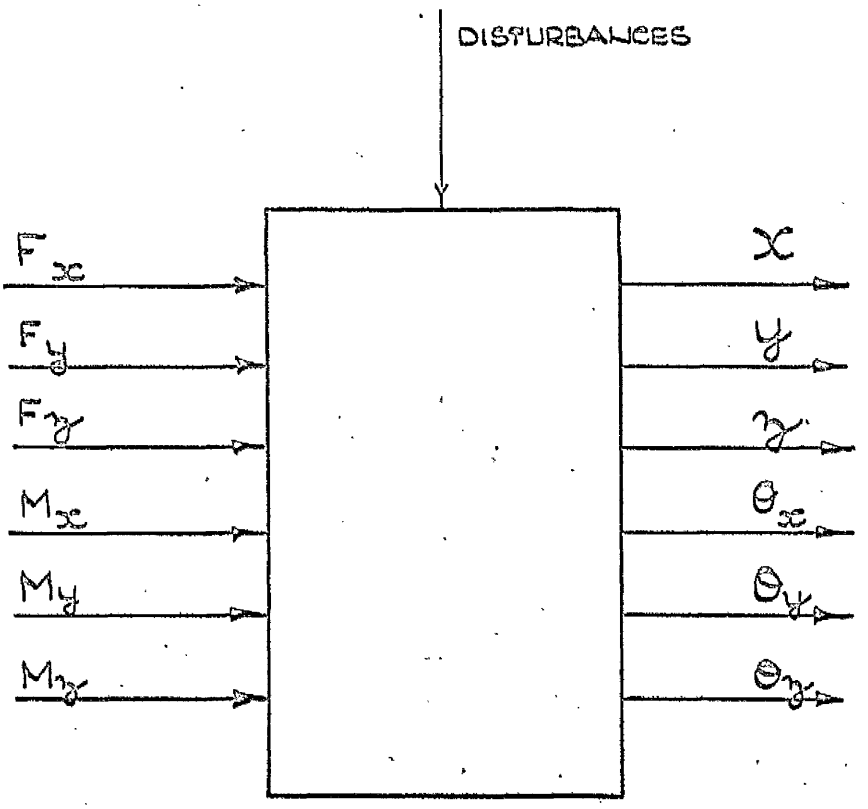

BLOCK DIAGRAM OF BALL BEARING.

FIG. 55.

CHAPTER 10.

CONCLUSIONS

The effect of rotor asymmetry has been studied, the most significant effect being a parametric resonance which occurs when the natural frequency of nutation of the gyro is close to the spin frequency of the rotor. This implies a "flat" rotor with small length/diameter ratio and light gimbals.

Empirical solutions have been developed for the equations of motion in both stable and unstable zones.

The frequency response curves of an unsymmetrical gyro are shown to be distorted in comparison with those of a symmetrical gyro and beating of the forcing frequency and the spin frequency occurs when these frequencies are close together.

The response of the unsymmetrical gyro to a constant torque applied at the gimbals is shown to contain an oscillatory component at double spin frequency, and an expression for the amplitude of this oscillation is given.

By studying the transient behaviour of the total vibratory energy in the system, and the energy dissipated by damping the destabilising effect of rotor asymmetry is shown to extend beyond the region of parametric resonance. The effects of unequal gimbal inertia, initial gimbal velocities and initial rotor position on the stability of the system have also been shown.

Slackness in the spin axis bearings has a stabilising effect, but tangential forces in either direction tend to produce instability.

The "oil whip" forces assumed by Prentis do produce instability with increasing gimbal inertia, and increase of bearing clearance increases the degree of instability up to a point where the nutation frequency has been very markedly reduced.

Possible sources of tangential forces on the rotor have been considered, namely the magnetic field of the driving motor, and cage accelerations in the bearings. The tangential forces produced by the magnetic field of the motor are shown to correspond to a mean torque about a transverse axis of the order of $\frac{1}{2} \times 10^{4} \varphi$ gm. cm. where φ is the angular deflection of the rotor relative to the bearing axis.

This is equivalent to a value of μ (as defined in eqns. 3.1) of about 5×10^{-4} and is thus a small effect. The sense of the torque corresponds to μ negative, thus giving effects similar to "oil whip" forces in the spin axis bearings.

The effect of cage accelerations is to produce a torque similar in nature and direction to the gyroscopic couple produced by rotor spin except that the couple is proportional to the relative transverse angular velocity $\dot{\varphi}$ of rotor and inner gimbal instead of the absolute angular velocity of the rotor.

In magnitude the couple produced by cage acceleration is of the order of 2% of the gyroscopic couple.

The effect of shaft and bearing compliance on frequency response has been considered analytically and found to be in good agreement with the results obtained by forcing an analogue simulation of the system. Both are in

agreement with the work of Maunder[12] in respect of the natural frequencies obtained. A method of obtaining frequency response data by digital computation is also described and its extension to take account of rotor asymmetry suggested.

The variation of the three natural frequencies of the system with variation of gimbal inertia has been obtained by digital computation.

Bearing eccentricity has been shown to produce a forced nutation at the frequency of rotation of the bearing cages.

Variation of radial stiffness in the bearings has been shown to produce a parametric resonance when the nutation frequency of the gyro approaches the bearing cage rotation frequency. Other resonances are possible if harmonics of the ball cage frequency are present in the stiffness variation, and if in addition the gyro has a non-uniform shaft, the likelihood of parametric resonance is increased due to the increase in the number of natural frequencies from three to five (vide Wippell and Maunder[17]).

Parametric resonance has been considered analytically and a method due to Malkin[14] of obtaining characteristic exponents and the width of zones of instability has been developed into a practical computational procedure. This has been applied to the case of the gyro with an unsymmetrical rotor and also to the case of bearing stiffness variation. The results of these computations have been found to be in excellent agreement with direct computer solution of the equations, provided a factor of 2π, omitted by Malkin, is introduced.

Experimental work has been carried out, mainly on the vibration of a gyro rotor in a fixed casing. The results are similar to those described by Yamamoto in his 1957 paper, with the addition of an interesting jump resonance phenomenon at low values of preload. A predominantly axial motion at a frequency of 2.86 times the rotor speed suddenly dropped in amplitude as the speed decreased, a corresponding sudden increase in amplitude appearing at a frequency of 3.13 times rotor speed. This phenomenon is as yet unexplained but is possibly connected with the non-linearity in axial stiffness. The stiffness in the downward direction is large but for small preloads the stiffness in the upward direction will be small.

The experimental method of tape recording and subsequent analysis is convenient but a recorder with at least 6 signal channels would assist materially in identifying the many and varied modes of vibration. A new design of apparatus is suggested which might simplify the problem of establishing the relationships between forces, moments and displacements in an angular contact ball bearing.

ACKNOWLEDGEMENTS

The author wishes to record his thanks to Professor A. S. T. Thomson, D.Sc., Ph.D., A.R.C.S.T., M.I.C.E., M.I.Mech.E., F.R.S.E., for the use of laboratory and computing facilities.

He is also grateful to Mr. W. B. McHutchison for many helpful discussions and suggestions.

Thanks are also due to drawing office and laboratory staff for much willing help in the course of this work.

The author is particularly indebted to Dr. and Mrs. J. Follan for their hospitality during the composition of part of the thesis.

APPENDIX 1.

ATLAS AUTOCODE PROGRAMME FOR GYRO WITH SLACK ROTOR BEARINGS.

```
begin
routine spec aux (array name f, real t)
array y(1:9)
real t, o, J, I,omega, Mx, My, k, Rb,Rg,a,mu,E,IE,phi,F,z,dt,N,M
integer i
J=1.525
I=2.15
omega=2.514a3
k=2a7
o=1a-8
->3
2:new line
1065,0,0,5.125
3:read(y(1),y(2),dt,M);y(6)=-y(2)
y(3)=0
y(4)=0
y(5)=0
y(7)=0
y(8)=0
y(9)=0
new line;new line;t=0;N=0;read(Mx);stop if Mx<0;y(6)=0 if Mx>20
read(My,Rb,Rg,a,mu)
caption£Mx£=;print(Mx,2,1)
caption £My£=;print(My,2,1)
caption£Rb£=;print fl(Rb,2)
caption£Rg£=;print fl(Rg,2)
caption£a£=;print fl(a,1)
caption£mu£=;print (mu,1,2)
caption£initial£velocities£=;print(y(2),2,1);spaces(1);print(y(6),2,1)
new line;new line
caption c
£££t£££££phi£x£££thetap£x£££thetay£££rotor£x£££rotor£y£££c
log£E/IE£W+E/IE£££££££o;new line
1: new line
print fl(t,2);spaces(1)
cycle i= 1,2,7
print fl (y(i),2); spaces(1)
repeat
```

```
print fl(y(1)+y(5),2); spaces (1);print fl(y(3)+y(7),2); spaces (1)
phi=sqrt(y(1)↑2+y(3)↑2);F=0;F=phi-a if phi>a
E=(Mx*y(6)↑2+My*y(8)↑2+I*((y(2)+y(6))↑2+(y(4)+y(8))↑2)+k*F↑2)/2
IE=Ei1 t<1a-10;z=.4343*log(E/IE)
print fl(z,3);spaces(1);print fl((y(9)+E)/IE,3);spaces (1);print fl(e,2)
N=N+1
->2 if N>M or z<-3or z>3
kutta merson (y,t,t+dt,e,9,10,aux)
t=t+dt
->1


routine aux(array name f, real t)
real u,v
phi=sqrt(y(1)↑2+y(3)↑2);F=0;F=phi-a if phi>a
u= (1/Mx)(Rb*y(2)-Rg*y(6)+k*y(1)F/phi-mu*k*y(3)F/phi)
v= (1/My)(Rb*y(4)-Rg*y(8)+k*y(3)F/phi+mu*k*y(1)F/phi)
f(2)= -u- J*omega/I*(y(4) +y(8))-k*y(1)F/(I*phi) - Rb/I*y(2)+ mu**y(3)F/(phi*I)
f(1)= y(2)
f(4)= -v + J*omega/I*(y(2)+y(6))-k*y(3)F/(I*phi)-Rb/I*y(4) - mu*k*y(1)F/(phi*I)
f(3)=y(4)
f(6)=u
f(8)=v
f(5)=y(6)
f(7)=y(8)
f(9)= Rg*(y(6)↑2+y(8)↑2)+Rb*(y(2)↑2+y(4)↑2)+mu*k*F*(y(1)*y(4)-y(2)*y(3))/phi

end
end of program
```

MX = 1.0 MY = 1.0 RB = 2.15a 2 RG = 1.00a 2 A = 0.0a-99 MJ = 0.10 INITIAL VELOCITIES = -0.2 0.2

T	PHI X	PHI Y	THETA X	THETA Y	ROTOR X	ROTOR Y	LOG E/IE	H*E/IE	E
0.00a-99	1.00a -4	0.00a-99	0.00a-99	0.00a-99	1.00a -4	0.00a-99	0.000a-99	1.000a 0	1.00a -8
1.00a -3	7.09a -5	3.78a -5	8.64a -5	-2.83a -5	1.57a -4	9.49a -6	-1.052a -1	1.000a 0	1.00a -8
2.00a -3	-5.98a -6	4.82a -5	1.63a -4	2.43a -5	1.57a -4	7.25a -5	-1.121a -1	1.000a 0	1.00a -8
3.00a -3	-6.35a -5	-9.92a -7	1.58a -4	1.03a -4	9.41a -5	1.02a -4	-6.768a -2	1.000a 0	1.00a -8
4.00a -3	-4.50a -5	-6.74a -5	8.93a -5	1.26a -4	4.43a -5	5.81a -5	-1.558a -2	1.000a 0	1.00a -8
5.00a -3	3.18a -5	-7.61a -5	3.68a -5	7.49a -5	6.87a -5	-1.27a -6	4.153a -2	1.000a 0	1.00a -8
6.00a -3	8.35a -5	-4.60a -6	5.18a -5	5.75a -6	1.35a -4	1.15a -6	1.059a -1	1.000a 0	1.00a -8
7.00a -3	4.45a -5	8.09a -5	1.15a -4	-1.58a -5	1.59a -4	6.51a -5	1.725a -1	1.000a 0	1.00a -8
8.00a -3	-5.50a -5	8.58a -5	1.63a -4	2.57a -5	1.08a -4	1.12a -4	2.386a -1	1.000a 0	1.00a -8
9.00a -3	-1.09a -4	-8.03a -6	1.54a -4	8.89a -5	4.52a -5	8.09a -5	3.052a -1	1.000a 0	1.00a -8
1.00a -2	-4.64a -5	-1.08a -4	9.60a -5	1.17a -4	4.95a -5	8.65a -6	3.728a -1	1.000a 0	1.00a -8
1.10a -2	8.09a -5	-9.89a -5	3.88a -5	8.27a -5	1.20a -4	-1.62a -5	4.408a -1	1.000a 0	1.00a -8
1.20a -2	1.36a -4	2.77a -5	3.55a -5	1.24a -5	1.71a -4	4.01a -5	5.090a -1	1.000a 0	1.00a -8
1.30a -2	4.19a -5	1.44a -4	9.76a -5	-3.20a -5	1.40a -4	1.12a -4	5.774a -1	1.000a 0	1.00a -8
1.40a -2	-1.17a -4	1.13a -4	1.75a -4	-4.75a -7	5.79a -5	1.12a -4	6.461a -1	1.000a 0	1.00a -8
1.50a -2	-1.67a -4	-5.63a -5	1.91a -4	9.16a -5	2.34a -5	3.52a -5	7.150a -1	1.000a 0	1.00a -8
1.60a -2	-2.99a -5	-1.89a -4	1.11a -4	1.59a -4	8.10a -5	-3.03a -5	7.839a -1	1.000a 0	1.00a -8
1.70a -2	1.67a -4	-1.24a -4	9.43a -7	1.19a -4	1.68a -4	-4.73a -6	8.530a -1	1.000a 0	1.00a -8
1.80a -2	2.02a -4	9.82a -5	-2.06a -5	-1.04a -5	1.82a -4	8.79a -5	9.222a -1	1.000a 0	1.00a -8
1.90a -2	7.06a -6	2.44a -4	9.45a -5	-1.01a -4	1.02a -4	1.43a -4	9.914a -1	1.000a 0	1.00a -8
2.00a -2	-2.31a -4	1.29a -4	2.45a -4	-3.70a -5	1.41a -5	9.21a -5	1.061a 0	1.000a 0	1.00a -8

TYPICAL RESULTS FOR GYRO WITH SLACK BEARINGS.

APPENDIX 2.

ATLAS AUTOCODE PROGRAMME FOR GYRO WITH ECCENTRICITY AND STIFFNESS VARIATION IN THE SPIN AXIS BEARINGS.

```
begin
routine spec aux (array name f, real t)
array y(1:9)
real t, e, J, I,omega, Mx, My, k, Rb,Rg,a,mu,E,IE,phi,F,z,dt,N,M,e
om1,dk,eee,T,sumx
integer i

J=1.525
I=2.15
omega=2.514α3
k=1.51α7
e=1α-8
sumx=0
->3
2:new line
caption mean£LOG£E/IE=;print fl((sumx/M),3);sumx=0;new line
1065,0,0,5.125
3: cycle i=1,1,9;y(i)=0;repeat
read(om1,y(1),y(4),y(8),dt,M)
new line;new line;t=0;N=0;read(Mx);stop if Mx<0;y(6)=0 if Mx>20
read(My,Rb,Rg,a,mu,dk,eee,T)
captionMx£=;print(Mx,2,2)
caption  £My£=;print(My,2,2)
caption£Rb£=;print fl(Rb,2)
caption£Rg£=;print fl(Rg,2)
caption£a£=;print fl(a,1)
caption£mu£=;print (mu,1,2)
caption£dk/k£=;print (dk/k,1,2)
caption£eee£=;print fl(eee,1)
caption£om1/om£=;print (om1/omega,1,3);new line
caption£I.V.£=;print(y(2),2,1);spaces(1);print(y(6),2,1)
caption£T£=;print(T,4,1)
new line;new line
caption e
££££t£££££££phi£x£££££phi£y£££££theta£x£££theta£y£££rotor£x£££rotor£ye
£££log£E/IE ££W+E/IE£££££££e;new line
1: new line
print fl(t,2);spaces(1)
cycle i= 1,2,7
print fl (y(i),2); spaces(1)
repeat
```

```
print fl(y(1)+y(5),2); spaces (1);print fl(y(3)+y(7),2); spaces (1)
phi=sqrt(y(1)↑2+y(3)↑2);F=0;F=phi-a if phi>a
E=(Mx*y(6)↑2+My*y(8)↑2+I*((y(2)+y(6))↑2+(y(4)+y(8))↑2)+k*F↑2e
+dk*((y(1)↑2-y(3)↑2)*cos(2*om1*t)+2*y(1)*y(3)*sin(2*om1*t))e
-(k+dk)*ecc*(y(1)*cos(om1*t)+y(3)sin(om1*t)))/2
IE=Eif t<1α-10;z=.4343*log(E/IE);sumz=sumz+z
print fl(z,3);spaces(1);print fl((y(9)+E)/IE,3);spaces (1)
print fl(e,2)
N=N+1
->2 ifN>M or z<-3or z>3
kutta merson (y,t,t+dt,e,9,20,aux)
t=t+dt
->1


routine aux(array name f, real t)
real u,v

phi=sqrt(y(1)↑2+y(3)↑2);F=0;F=phi-a if phi>a
u=Rb*y(2)+k*y(1)F/phi-mu*k*y(3)F/phi-(k+dk)*ecc*cos(om1*t)e
+dk*(y(1)*cos(2*om1*t)+y(3)*sin(2*om1*t))
v=Rb*y(4)+k*y(3)F/phi+mu*k*y(1)F/phi-(k+dk)*ecc*sin(om1*t)e
+dk*(y(1)*sin(2*om1*t)-y(3)*cos(2*om1*t))
f(6)=(u-Rg*y(6))/Mx;f(8)=(v-Rg*y(8))/My
f(1)=y(2);f(2)=-f(6)-u/I-J*omega/I*(y(4)+y(8)) +T*cos(omega*t)
f(3)=y(4);f(4)=-f(8)-v/I+J*omega/I*(y(2)+y(6)) +T*sin(omega*t)
f(5)=y(6)
f(7)=y(8)
f(9)= Rg*(y(6)↑2+y(8)↑2)+Rb*(y(2)↑2+y(4)↑2)+mu*k*F*(y(1)*y(4)-y(2)*y(3))/phi

end
end of program
```

MX = 2.63 MV = 0.66 RH = 0.00E-99 RG = 0.00E-99 A = 0.0E-99 MU = 0.00 DK/K = 0.15 ECC = 0.0E-99 OM1/OM = 0.391
I.V. = 0.5 -0.5 T = 0.0

T	PHI X	PHI Y	THETA X	THETA Y	ROTOR X	ROTOR Y	LOG E/IE	W*E/IE	E
0.00E-99	1.00E -4	0.00E-99	0.00E-99	0.00E-99	1.00E -4	0.00E-99	0.000E-99	1.000E 0	1.00E -8
1.00E -3	-8.18E -5	-2.05E -5	-1.42E -4	-1.81E -4	-2.24E -4	-2.01E -4	-1.453E -2	9.671E -1	1.00E -8
2.00E -3	2.00E -4	-2.42E -5	-2.30E -4	-5.23E -4	-2.96E -5	-5.47E -4	5.558E -3	1.013E 0	1.00E -8
3.00E -3	-8.12E -5	-8.78E -5	1.32E -4	-6.61E -4	5.06E -5	-7.48E -4	2.832E -2	1.067E 0	1.00E -8
4.00E -3	-5.64E -5	-1.22E -4	3.66E -4	-4.38E -4	3.10E -4	-5.60E -4	5.263E -2	1.129E 0	1.00E -8
5.00E -3	-4.31E -5	-7.45E -5	3.89E -4	-1.77E -4	3.46E -4	-2.46E -4	7.593E -2	1.191E 0	1.00E -8
6.00E -3	-7.55E -5	-1.18E -5	1.90E -4	2.76E -5	1.14E -4	1.58E -5	5.586E -2	1.137E 0	1.00E -8
7.00E -3	3.61E -5	1.41E -4	-1.23E -4	-1.70E -4	-8.67E -5	-3.84E -5	7.047E -2	1.176E 0	1.00E -8
8.00E -3	9.82E -5	1.85E -4	-2.31E -4	-5.40E -4	-1.33E -4	-3.64E -4	8.077E -2	1.204E 0	1.00E -8
9.00E -3	-4.04E -5	1.67E -4	-1.59E -6	-7.98E -4	-4.20E -5	-6.29E -4	6.341E -2	1.157E 0	1.00E -8
1.00E -2	5.57E -5	2.01E -5	2.37E -4	-6.49E -4	2.93E -4	-6.29E -4	3.222E -2	1.077E 0	1.00E -8
1.10E -2	-7.35E -5	-1.99E -5	4.27E -4	-3.78E -4	3.53E -4	-3.90E -4	4.715E -3	1.011E 0	1.00E -8
1.20E -2	-5.55E -5	-1.13E -4	2.97E -4	8.09E -5	2.42E -4	-5.25E -5	-9.990E -3	9.773E -1	1.00E -8
1.30E -2	1.33E -4	-5.76E -5	-5.74E -5	2.47E -5	7.58E -5	-3.35E -5	-9.187E -3	9.791E -1	1.00E -8
1.40E -2	-9.43E -5	-4.71E -6	-1.45E -4	-2.58E -4	-2.40E -4	-2.63E -4	-4.248E -2	9.068E -1	1.00E -8
1.50E -2	1.86E -4	1.95E -5	-1.91E -4	-5.86E -4	-4.34E -6	-5.67E -4	-2.518E -2	9.437E -1	1.00E -8
1.60E -2	-6.80E -5	-7.80E -6	1.73E -4	-7.14E -4	1.05E -4	-7.22E -4	5.798E -4	1.001E 0	1.00E -8
1.70E -2	-7.40E -5	-1.18E -4	3.92E -4	-3.70E -4	3.18E -4	-4.97E -4	1.384E -2	1.032E 0	1.00E -8
1.80E -2	5.24E -6	-1.16E -4	3.46E -4	-1.01E -4	3.51E -4	-2.17E -4	3.096E -2	1.074E 0	1.00E -8
1.90E -2	-9.15E -5	-1.19E -4	1.51E -4	1.08E -4	5.98E -5	-1.11E -5	2.985E -2	1.069E 0	1.00E -8
2.00E -2	6.48E -5	3.32E -5	-1.62E -4	-1.47E -4	-9.69E -5	-1.14E -4	5.832E -2	1.144E 0	1.00E -8
2.10E -2	3.95E -5	1.36E -4	-1.93E -4	-5.65E -4	-1.53E -4	-4.29E -4	6.935E -2	1.173E 0	1.00E -8
2.20E -2	-3.12E -5	1.97E -4	3.61E -5	-8.29E -4	4.96E -6	-6.32E -4	5.340E -2	1.131E 0	1.00E -8
2.30E -2	2.04E -5	1.31E -4	2.83E -4	-6.94E -4	3.04E -4	-5.63E -4	4.651E -2	1.113E 0	1.00E -8
2.40E -2	-4.87E -5	6.83E -5	4.09E -4	-3.73E -4	3.60E -4	-3.04E -4	3.374E -2	1.081E 0	1.00E -8
2.50E -2	-5.57E -5	-5.66E -5	2.58E -4	3.24E -5	2.02E -4	-2.41E -5	1.357E -2	1.032E 0	1.00E -8
2.60E -2	1.49E -4	-1.08E -4	-1.00E -4	3.95E -5	4.87E -5	-6.84E -5	-8.860E -3	9.798E -1	1.00E -8
2.70E -2	-8.17E -5	-5.09E -5	-1.51E -4	-2.87E -4	-2.33E -4	-3.38E -4	-3.982E -2	9.124E -1	1.00E -8
2.80E -2	1.51E -4	-1.60E -5	-1.41E -4	-5.85E -4	9.99E -6	-6.01E -4	-2.859E -2	9.363E -1	1.00E -8
2.90E -2	-3.91E -5	3.98E -5	2.02E -4	-7.35E -4	1.63E -4	-6.96E -4	-2.354E -2	9.472E -1	1.00E -8
3.00E -2	-1.09E -4	-5.28E -5	4.18E -4	-3.70E -4	3.09E -4	-4.23E -4	-2.828E -2	9.370E -1	1.00E -8
3.10E -2	5.87E -5	-6.32E -5	2.96E -4	-1.01E -4	3.55E -4	-1.64E -4	-1.284E -2	9.727E -1	1.00E -8
3.20E -2	-1.09E -4	-1.45E -4	1.18E -4	1.16E -4	8.49E -6	-2.92E -5	8.420E -3	1.020E 0	1.00E -8
3.30E -2	1.01E -4	-9.29E -5	-1.95E -4	-9.79E -5	-9.32E -5	-1.91E -4	2.641E -2	1.063E 0	1.00E -8
3.40E -2	2.90E -6	1.21E -5	-1.57E -4	-5.26E -4	-1.54E -4	-5.13E -4	4.682E -2	1.114E 0	1.00E -8
3.50E -2	-3.19E -5	1.27E -4	7.72E -5	-7.77E -4	4.53E -5	-6.50E -4	3.726E -2	1.090E 0	1.00E -8
3.60E -2	-5.23E -6	1.92E -4	3.17E -4	-7.02E -4	3.12E -4	-5.10E -4	6.089E -2	1.151E 0	1.00E -8
3.70E -2	-5.79E -5	1.62E -4	3.97E -4	-3.81E -4	3.39E -4	-2.20E -4	5.692E -2	1.140E 0	1.00E -8
3.80E -2	-4.45E -5	6.01E -5	2.11E -4	-4.67E -5	1.67E -4	1.34E -5	3.369E -2	1.081E 0	1.00E -8
3.90E -2	1.47E -4	-8.28E -5	-1.30E -4	-7.35E -6	1.67E -5	-9.02E -5	8.883E -3	1.021E 0	1.00E -8
4.00E -2	-4.28E -5	-7.14E -5	-1.61E -4	-3.29E -4	-2.04E -4	-4.00E -4	-1.237 -2	9.719E -1	1.00E -8

MEAN LOG E/IE= 2.109E -2

TYPICAL RESULTS FOR GYRO WITH STIFFNESS VARIATION OF THE ROTOR BEARINGS

Appendix 3

Derivation of the periodicity conditions 8.9 and 8.36

A.3.1 - General form of periodicity conditions

Chapter II, section 4 of Malkin's book, reference (14) derives the conditions under which the set of equations:

$$\frac{dx_s}{dt} = a_{s1} x_1 + \text{----} + a_{sn} x_n + fs\ (t) \qquad A.3.1$$

$$s = (1, \text{----}, n)$$

have real periodic solutions of the same period as the periodic functions fs (t). The coefficients a_{sj} are constants.

Following through Malkin's analysis, he first defines the fundamental system of linearly independent solutions $x_{sj}(t)$ of the homogenous equations:

$$\frac{dx_s}{dt} = a_{s1} x_1 + \text{-----} + a_{sn} x_n \qquad A.3.2$$

these solutions being determined by the assumed initial conditions

$$x_{sj}\ (0) = \delta_{sj}\ \ (s, j = 1, \text{----}, n). \qquad A.3.3$$

δ_{sj} is the Kronecker delta ie $\delta_{sj} = 1$ for $s = j$, and $\delta_{sj} = 0$ for $s = j$.

The set of convolution integrals

$$x^*_s\ (t) = \int_0^t \sum_{\alpha=1}^{n} x_{s\alpha}(t - \tau)\ f_\alpha\ (\tau)\ d\tau \qquad A.3.4$$

is a particular solution of the original set of equations A.3.1 and if it is added to the general solution of equations A.3.2 we obtain a general solution of equations A.3.1 as follows:

$$x_s = C_1 x_{s1}\ (t) + \text{----} + C_n x_{sn}\ (t) + \int_0^t \sum_{\alpha=1}^{n} x_s\ \ (t - \tau)\ f_\alpha\ (\tau)\ d\tau \qquad A.3.5$$

C_1, -----, C_n are arbitrary constants equal to the initial values $x_s(0)$, and must be chosen in such a way that the solution is periodic, of period T equal to the period of the functions $f_s(t)$. This implies that

$$x_s(T) - x_s(0) = 0$$

Substituting this condition in A.3.5 gives

$$C_1 x_{s1}(T) + \text{----} + C_n x_{sn}(T) - C_s + \int_0^T \sum_{\alpha=1}^{n} x_s (T-\tau) f_\alpha(\tau)\, d\tau = 0 \qquad \text{A.3.6}$$

and for the case $f_\alpha(\tau) = 0$,

$$C_1^* x_{s1}(T) + \text{----} + C^*_n x_{sn}(T) - C^*_s = 0 \qquad \text{A.3.7}$$

Malkin now concentrates attention on the resonance case; that is, the case where the matrix $\lceil a_{11} \text{------} a_{nn} \rfloor$ has either zero eigen values or pairs of imaginary eigen values of the form $\pm \frac{2\pi p i}{T}$ (p any integer). He defines m periodic solutions $\varphi_{s1}(t)$, --------, $\varphi_{sm}(t)$ (period T) of the equations A.3.2. The number of solutions m will be equal to the number of zero or imaginary eigen values of the form $\pm \frac{2\pi p i}{T}$.

The equations

$$\frac{dy_s}{dt} + a_{1s} y_1 + \text{-----} + a_{ns} y_n = 0 \qquad \text{A.3.8}$$

are described as conjugate to equations A.3.2 and have eigen values opposite in sign to those of equations A.3.2. Hence they will also have m periodic

solutions $\psi_{s1}(t)$, -----, $\psi_{sm}(t)$ of period T.

Using a previously developed result, (eqn. 3.3 p. 110 of his book), Malkin writes:-

$$\sum_{\alpha=1}^{n} x_{\alpha j}(t-h)\,\psi_{\alpha i}(t) = A_{ji} = \text{constant} \qquad \text{A.3.9}$$

this being a general results for conjugate systems of equations, true for any h.

Putting t = h and using the assumed initial conditions A.3.3, the constants

$$A_{ji} = \sum_{\alpha=1}^{n} x_{\alpha j}(0)\,\psi_{\alpha i}(h)$$

i.e. $$\sum_{\alpha=1}^{n} x_{\alpha j}(t-h)\,\psi_{\alpha i}(t) = \psi_{ji}(h) \qquad \text{A.3.10}$$

Malkin now multiplies the sth equation of the set A.3.6 by $\psi_{si}(T)$ and sums over the index s from 1 to n. This gives:-

$$C_1 \sum_{s=1}^{n} x_{s1}(T)\,\psi_{si}(T) + \text{-----} + C_n \sum_{s=1}^{n} x_{sn}(T)\,\psi_{si}(T)$$

$$- \sum_{s=1}^{n} C_s \psi_{si}(T) + \int_0^T \sum_{s,\alpha=1}^{n} x_s(T-\tau)\,\psi_{si}(T)\,f_\alpha(\tau)\,d\tau = 0$$

A.3.11

Putting t = T, h = 0 in 4.11 gives the identity

$$\sum_{s=1}^{n} x_{sj}(T)\,\psi_{si}(T) = \psi_{ji}(0)$$

and for $t = T$, $h = \tau$

$$\sum_{s=1}^{n} x_{s\alpha}(T-\tau)\psi_{s\,i}(\tau) = \psi_{\alpha i}(\tau)$$

Substituting these in equations A.3.11 gives:-

$$C_1[\psi_{1i}(0) - \psi_{1i}(T)] + \cdots + C_n[\psi_{ni}(0) - \psi_{ni}(T)]$$
$$+\int_0^T \sum_{\alpha=1}^{n} f_\alpha(\tau)\psi_{\alpha_i}(\tau)\,d\tau = 0$$

Since the functions ψ are periodic the terms in square brackets vanish, leaving as the condition of existence of periodic solutions of equations 4.1:-

$$\int_0^T \sum_{\alpha=1}^{n} f_\alpha(\tau)\,\omega_{\alpha i}(\tau)\,d\tau$$

$$(i = 1, \cdots, m) \qquad \text{A.3.12}$$

A.3.2 Application to calculation of characteristic exponents

Turning to section 7, chapter V of Malkin's book we find the periodicity condition A.3.12 being applied to the equations

$$\frac{dy_s^{(p)}}{dt} = \lambda_0 \sum_{\alpha=1}^{n} a_{s\alpha}\, y_\alpha^{(p)} - \lambda_0\, i\omega_j\, y_s^{(p)}$$
$$+\mu \sum_{\alpha=1}^{n} (\sigma a_{s\alpha} + \lambda_0 f_{s\alpha} + \mu\sigma f_{s\alpha})\, y_\alpha^{(p-1)}$$
$$-\mu a^{(p)}\, y_s^{(p-1)} \qquad \text{A.3.13}$$

which equations represent the relationship between the pth and (p - 1)th approximation to the solution of:-

$$\frac{dy_s}{dt} = (\lambda_o + \mu\sigma) \sum_{\alpha=1}^{n} (a_{s\alpha} + \mu f_{s\alpha}) y_\alpha \qquad \text{A.3.14}$$

$$-(\lambda_o\, i\,\omega_j + \mu a)\, y_s$$

Comparing equation A.3.13 with equations A.3.1 and 3.2 the first two terms on the right hand side of A.3.13 correspond to the right hand side of A.3.2, while the remainder of the right hand side of A.3.13 corresponds to the term $f_s(t)$ in A.3.1.

Putting p = 1 in equation A.3.13 gives

$$\frac{dy_s^{(1)}}{dt} = \lambda_o \sum_{\alpha=1}^{n} a_{s\alpha} y_\alpha^{(1)} - \lambda_o\, i\,\omega_j\, y_s^{(1)}$$

$$+ \mu \sum_{\alpha=1}^{n} (\sigma a_{s\alpha} + \lambda_o f_{s\alpha} + \mu\sigma f_{s\alpha})\, y_\alpha^{(o)} \qquad \text{A.3.15}$$

$$- \mu a^{(1)}\, y_s^{(o)}$$

where $y_s^{(o)}$ is the solution of A.3.14 for $\mu = o$.

i.e. $$\frac{dy_s^{(o)}}{dt} = \lambda_o \sum_{\alpha=1}^{n} a_{s\alpha} y_\alpha^{(o)} - \lambda_o\, i\,\omega_j\, y_s^{(o)} \qquad \text{A.3.16}$$

The equations having been normalised by change of the time variable and the introduction of the factor λ_o, the functions $y_s^{(o)}$ can be written

$$y_s^{(o)} = M_o \varphi_{s1} + N_o \varphi_{s2}$$

where φ_{s1} and φ_{s2} are respectively constant and periodic, period 2π.

Applying the condition A.3.12 to A.3.15 and putting β for s, we obtain

$$\mu \int_0^{2\pi} \sum_{\alpha,\beta=1}^{n} (\sigma a_{\beta\alpha} + \lambda_0 f_{\beta\alpha} + \mu\sigma f_{\beta\alpha})(M_0 \varphi_{\alpha 1} + N_0 \varphi_{\alpha 2})\psi_{\beta i}$$

$$- a^{(1)} (M_0 \varphi_{\beta 1} + N_0 \varphi_{\beta 2})\psi_{\beta i} \quad dt = 0$$

for i = 1, 2.

hence

$$\Big[\sigma \int_0^{2\pi} \sum_{\alpha,\beta=1}^{n} a_{\beta\alpha} \varphi_{\alpha 1} \psi_{\beta i}\, dt + (\lambda_0 + \mu\sigma) \int_0^{2\pi} \sum_{\alpha,\beta=1}^{n} f_{\beta\alpha} \varphi_{\alpha 1} \psi_{\beta i}\, dt$$

$$- a^{(1)} \int_0^{2\pi} \sum_{\alpha,\beta=1}^{n} \varphi_{\alpha 1} \psi_{\beta i}\, dt \Big] M_0$$

$$+ \Big[\sigma \int_0^{2\pi} \sum_{\alpha,\beta=1}^{n} a_{\beta\alpha} \varphi_{\alpha 2} \psi_{\beta i}\, dt + (\lambda_0 + \mu\sigma) \int_0^{2\pi} \sum_{\alpha,\beta=1}^{n} f_{\beta\alpha} \varphi_{\alpha 2} \psi_{\beta i}\, dt$$

$$- a^{(1)} \int_0^{2\pi} \sum_{\alpha,\beta=1}^{n} \varphi_{\alpha 2} \psi_{\beta i}\, dt \Big] N_0 = 0$$

again for i = 1, 2.

Defining the matrices A and B by the expressions following Malkin's equation 7.6, p.414, reduces these two equations to:-

$$\Big(\sigma A_{11} + B_{11} + \frac{\mu\sigma}{\lambda_0} B_{11} - a^{(1)} \int_0^{2\pi} \sum_{\alpha,\beta=1}^{n} \varphi_{\alpha 1} \psi_{\beta 1}\, dt\Big) M_0$$

$$+ \Big(\sigma A_{21} + B_{21} + \frac{\mu\sigma}{\lambda_0} B_{21} - a^{(1)} \int_0^{2\pi} \sum_{\alpha,\beta=1}^{n} \varphi_{\alpha 2} \psi_{\beta 1}\, dt\Big) N_0 = 0$$

A.3.17

and

$$\Big(\sigma A_{12} + B_{12} + \frac{\mu\sigma}{\lambda_0} B_{12} - a^{(1)} \int_0^{2\pi} \sum_{\alpha,\beta=1}^{n} \varphi_{\alpha 1} \psi_{\beta 2}\, dt\Big) M_0$$

$$+ \Big(\sigma A_{22} + B_{22} + \frac{\mu\sigma}{\lambda_0} B_{22} - a^{(1)} \int_0^{2\pi} \sum_{\alpha,\beta=1}^{n} \varphi_{\alpha 2} \psi_{\beta 2}\, dt\Big) N_0 = 0$$

If Malkin's conditions 6.22 p.411 are now applied viz.

$$\sum_{\alpha=1}^{n} \varphi_{\alpha i} \psi_{\alpha i} = 1, \quad \sum_{\alpha=1}^{n} \varphi_{\alpha k} \psi_{\alpha i} = 0, \quad i \neq k$$

then equations A.3.17 reduce to Malkin's 7.6 p 414 except that a factor 2π must be applied to the exponent $a^{(1)}$.

APPENDIX 4.

ALGOL PROGRAMME FOR FREQUENCY RESPONSE OF GYRO WITH FLEXIBLE BEARINGS.

```
'begin''real' k,Rb,Rg,I,J,Mx,My,om,OM,fr,dfr;
'integer'i,j,N,run;
'array'A,B[1:4,1:4],FRR[1:1];


'procedure'carpol(x,y);'real'x,y;
'begin''comment'x and y become r and theta,
where theta is in degrees in the correct quadrant;
'real'z;
z:=sqrt(x*x+y*y);
y:=180.0*arctan(y/x)/3.14159265;
'if'x<0'then'y:=y+180.0;
x:=z;
'end'carpol;


'procedure'invert complex(n,A,B,error);
'value'n;'array'A,B;'label'error;
'integer'n;


'begin''comment' inverts the complex matrix A+iB,[n*n]
which should be available as two real [n*n] arrays A,B.
On exit A contains the real part and B the imaginary part
of the inverted matrix.error is a non-local label
indicating a failure.;

'array'C[1:n+n,1:n+n];'integer'i,j;
'for'i:=1'step'1'until'n'do'
'for'j:=1'step'1'until'n'do'
'begin'C[i,j]:=A[i,j];C[i+n,j]:=B[i,j];
      C[i,j+n]: =-B[i,j];C[i+n,j+n]:=A[i,j];
'end'i,j;
invert(C,n+n,error);

'for'i:=1'step'1'until'n'do'
'for'j:=1'step'1'until'n'do'
'begin'A[i,j]:=C[i,j];B[i,j]:=C[i+n,j];'end';
'end' invert complex;
```

```
'procedure' invert(A,n,error); 'value' n; 'array' A;
  'integer' n; 'label' error;
'begin' 'comment' inverts the matrix A in situ;
        'integer' i,j; 'array' X[1:n,1:n+n];
        'for' i← 1 'step' 1 'until' n 'do'
        'begin' 'for' j ← 1 'step' 1 'until' n 'do'
                'begin' X[i,j]← A[i,j];
                        X[i,j+n]←0.0
                'end';
                X[i,i+n]←1.0
        'end';
        Gauss(X,A,n,n,error)
'end'invert;

'procedure' Gauss(a,Y,n,r,L); 'value' n,r; 'array' a,Y;
  'integer' r,n; 'label' L;
'begin' 'comment' Solves the matrix set of linear equations AY=H
                  where A is an (n*n) matrix of coefficients,
                        H is an (n*r) matrix of right hand sides
                        Y is the (n*r) solution matrix.
                  a is the (n*(n+r)) partitioned matrix (A/H).
                  If the system has many solutions then a jump to
                  L is performed where L is a label outside the
                  procedure. The matrix a is destroyed;
        'integer' i,j,k,l; 'real' temp;
        'for' l←1 'step' 1 'until' n-1 'do'
        'begin' j←l; temp←abs(a[l,l]);
                'for' k←l+1 'step' 1 'until' n 'do'
                'if' abs(a[k,l])>temp 'then'
                'begin' temp←abs(a[k,l]); j←k 'end';
                'if' temp=0.0 'then' 'goto' L;
                'if' j#l 'then'
                'for' k←l 'step' 1 'until' n+r 'do'
                'begin'
                      temp←a[l,k]; a[l,k]←a[j,k]; a[j,k]←temp;
                'end';
                'for' j←n+r 'step' -1 'until' l 'do'
                a[l,j]←a[l,j]/a[l,l];
                'for' i← l+1 'step' 1 'until' n 'do'
                'begin' temp←a[i,l];
                        'for' j←l+1 'step' 1 'until' n+r 'do'
                        a[i,j]←a[i,j]-temp*a[l,j]
                'end'
        'end';
        'for' j←n+1 'step' 1 'until' n+r 'do'
        'for' i←n 'step' -1 'until' 2 'do'
        'begin' 'if' a[i,i]=0.0 'then' 'goto' L;
                Y[i,j-n]←a[i,j]/a[i,i];
                'for' k←i-1 'step' -1 'until' 1 'do'
                a[k,j]←a[k,j]-a[k,i]*Y[i,j-n]
        'end';
        'for' i ←1 'step' 1 'until' r 'do' Y[1,i]←a[1,n+i]/a[1,1]
'end' Gauss;
```

```
'procedure'create(channel number, file name);'value' channel number;
'integer' channel number;'string' file name;'external';

'procedure' use(channel number,file name);'value' channel number;
'integer'channel number;'string' file name;'external';

'procedure'data skip(channel number);'value'channel number;
'integer' channel number ;'external';

'procedure' write binary(channel number,array,array name);
'value'channel number; 'integer' channel number;
'array' array;'string' array name;'external';

'procedure' time now;'external';


use(40,'('LINFR')');
I:=0.83875;J:=1.525;Mx:=0.709125;My:=0.236375;Rb:-800.0;
Rg:=200.0;k:=&8;OM:=2514.0;
again:run:=0;
fr:=read;'if'fr<0'then''goto'finish;
dfr:=read;N:=read;
start:om:=fr*OM;
write text('('time%now')');time now;new line(1);
write text ('('frequency% ratio'('c')'')');
print(fr,2,2);
FRR[1]:=fr;
write binary (40,FRR,'('FRR')');

A[1,1]:=(k-om*om*I)/&4;A[2,1]:=0;A[3,1]:=-k/&4;A[4,1]:=0;
A[1,2]:=0;A[2,2]:=A[1,1];A[3,2]:=0;A[4,2]:=A[3,1];
A[1,3]:=0;A[2,3]:=-J*OM;A[3,3]:=Rg;A[4,3]:=0;
A[1,4]:=J*OM;A[2,4]:=0;A[3,4]:=0;A[4,4]:=Rg;

B[1,1]:=Rb*om/&4;B[2,1]:=J*OM*om/&4;B[3,1]:=-B[1,1];B[4,1]:=0;
B[1,2]:=-B[2,1];B[2,2]:=B[1,1];B[3,2]:=0;B[4,2]:=-B[1,1];
B[1,3]:=-om*I;B[2,3]:=0;B[3,3]:=om*Mx;B[4,3]:=0;
B[1,4]:=0;B[2,4]:=B[1,3];B[3,4]:=0;B[4,4]:=om*My;

write text('('('('c')'orig.%real%matrix'('45s')'
orig.%imag.%matrix%%-both%divided%by%J*OMEGA.')');

'for'i:=1'step'1'until'4'do''begin'
new line(1);
'for'j:= 'step'1'until'4'do''begin'
A[i,j]:=A[i,j]/(J*OM);
print(A[i,j],0,4);                    'end';
space(10);
'for'j:=1'step'1'until'4'do''begin'
B[i,j]:=B[i,j]/(J*OM);
print(B[i,j],0,4);                    'end';
'end' i;
```

```
write binary(40,A,'('ORREAL')');
write binary(40,B,'('ORIMAG')');

invert complex(4,A,B,error));
write text('('('('c')'real%matrix'('50s')'imaginary %matrix')');
'for'i:=1'step'1'until'4'do'
'begin' new line(1);
        'for'j:=1'step'1'until'4'do'
        print(A[i,j],0,4);space(10);
        'for'j:=1'step'1'until'4'do'
         print(B[i,j],0,4);
'end'i;

write binary(40,A,'('REAL')');
write binary(40,B,'('IMAG')');

'for'i:=1'step'1'until'4'do'
'for'j:=1'step'1'until'4'do'

carpol(A[i,j],B[i,j]);
write text('('('('c')'amplitude%matrix'('45s')'phase%matrix')');
'for'i:=1'step'1'until'4'do'
'begin'new line(1);
      'for'j:= 'step'1'until'4'do'
       print(A[i,j],0,4);space(10);
      'for'j:=1'step'1'until'4'do'
       print(B[i,j],3,1);
'end';

write binary(40,A,'('AMP')');write binary(40,B,'('PHASE')');

write text('('('('c')'decibel%matrix')');
'for'i:=1'step'1'until'4'do'
'begin' newwline(1);
      'for'j:=1'step'1'until'4'do'
       print(8.686*ln(A[i,j]),3,1);
'end';

write binary(40,A,'('DB')');

error:run:=run+1;fr:=fr+dfr;
'if'run>N'then''goto'again;
paper throw;'goto'start;
finish:'end'of program;
```

```
TIME NOW21/00/40
FREQUENCY RATIO
  2.00
ORIG. REAL MATRIX
 2.0553E  0    0.0000E  0    0.0000E  0    1.0000E  0
 0.0000E  0    2.0553E  0   -1.0000E  0    0.0000E  0
-2.6083E  0    0.0000E  0    5.2167E -2    0.0000E  0
 0.0000E  0   -2.6083E  0    0.0000E  0    5.2167E -2
REAL MATRIX
 3.9313E -1    1.2531E -2   -1.3220E -1   -1.4270E -4
-1.7859E -2    1.7891E -1   -6.2461E -3   -2.6350E -1
 4.2969E -2    8.6759E -1    4.0650E -2    4.7095E -1
-9.8551E -1    7.4352E -2   -4.7095E -1    8.9035E -2
AMPLITUDE MATRIX
 3.9378E -1    3.1006E -1    1.3232E -1    1.6884E -1
 1.1843E -1    1.8115E -1    5.6981E -2    2.6351E -1
 1.1036E  0    8.6894E -1    7.0275E -1    4.7318E -1
 9.8886E -1    1.5043E  0    4.7318E -1    9.9991E -1
DECIBEL MATRIX
  -8.1   -10.2   -17.6   -15.5
 -18.7   -14.8   -24.9   -11.5
   0.9    -1.2    -3.1    -5.5
  -0.3     3.5    -6.5    -0.0  TIME NOW21/00/42
FREQUENCY RATIO
  2.20
ORIG. REAL MATRIX
 1.9391E  0    0.0000E  0    0.0000E  0    1.0000E  0
 0.0000E  0    1.9391E  0   -1.0000E  0    0.0000E  0
-2.6083E  0    0.0000E  0    5.2167E -2    0.0000E  0
 0.0000E  0   -2.6083E  0    0.0000E  0    5.2167E -2
REAL MATRIX
 3.6159E -1    1.7148E -2   -1.5920E -1    6.0180E -4
-1.7075E -2    1.6214E -1   -4.3014E -3   -2.8270E -1
 1.8405E -2    6.7601E -1    2.6128E -2    3.0594E -1
-7.6718E -1    3.7287E -2   -3.0694E -1    4.4559E -2
AMPLITUDE MATRIX
 3.6252E -1    2.6534E -1    1.6934E -1    1.2091E -1
 1.0140E -1    1.6440E -1    4.0720E -2    2.8272E -1
 9.2427E -1    6.7633E -1    5.4462E -1    3.0819E -1
 7.6745E -1    1.2443E  0    3.0819E -1    7.6358E -1
DECIBEL MATRIX
  -8.8   -11.5   -15.4   -18.4
 -19.9   -15.7   -27.8   -11.0
  -0.7    -3.4    -5.3   -10.2
  -2.3     1.9   -10.2    -2.3
```

```
ORIG. IMAG. MATRIX  -BOTH DIVIDED BY J*OMEGA.
-1.0492E -1   -5.0280E -1    1.1000E  0    0.0000E  0
 5.0280E -1    1.0492E -1    0.0000E  0    1.1000E  0
-1.0492E -1    0.0000E  0    9.3000E -1    0.0000E  0
 0.0000E  0   -1.0492E -1    0.0000E  0    3.1000E -1
IMAGINARY MATRIX
-2.2548E -2    3.0980E -1    5.7797E -3    1.6884E -1
-1.1505E -1   -2.8405E -2   -5.6638E -2   -1.1467E -3
-1.1027E  0    4.8471E -2   -7.0157E -1    4.5465E -2
-5.1150E -2   -1.5024E  0   -4.5865E -2   -9.9752E -1
PHASE MATRIX
  -3.3    87.7   177.5    90.0
 261.2    -9.0   263.7   180.2
 -87.8     3.2   -86.7     5.8
 183.0   -87.2   185.8   -86.0
```

```
ORIG. IMAG. MATRIX  -BOTH DIVIDED BY J*OMEGA.
 1.1541E -1   -5.5308E -1    1.2100E  0    0.0000E  0
 5.5308E -1    1.1541E -1    0.0000E  0    1.2100E  0
-1.1541E -1    0.0000E  0    1.0230E  0    0.0000E  0
 0.0000E  0   -1.1541E -1    0.0000E  0    3.4100E -1
IMAGINARY MATRIX
-2.7262E -2    2.6479E -1    6.8544E -3    1.2091E -1
-9.9955E -2   -2.7174E -2   -4.0492E -2    3.1014E -3
-9.2409E -1    2.0821E -2   -5.4399E -1    2.7759E -2
-2.0581E -2   -1.2437E  0   -2.7758E -2   -7.8228E -1
PHASE MATRIX
  -4.3    86.3   177.7    89.7
 260.3    -9.5   263.9   179.4
 -88.9     1.7   -87.3     5.2
 181.5   -88.3   185.2   -86.6
```

BIBLIOGRAPHY

1. QUARTLEY, A.L.: "Self Sustained Oscillation in a Gyro" R.R.E. Memorandum No.1337, August 1957.

2. PRENTIS, J.M.: "On the Stability of a Gimbal mounted Gyroscope" J. Mech. Eng. Sci., Vol.3, No.1, p.1., March 1961.

3. MAGNUS, K.: "Beitrage zur Dynamik des Kraftefreien, Kardanisch gelagerten Kreisels" Z.A.M.M., Vol.35, p.23, 1955.

4. KHARLAMOV, S.A.: "On the theory of the Astatic gyro with electric drive and gimbal suspension" Isv. Ak. Nauk SSSR, Mekh.i.Mash. No.6, p.45, 1963.

5. YAMAMOTO, T.: "On the critical speeds of a shaft" Memoirs of the Faculty of Engineering, Nagoya University, Vol.6, p.116, 1954.

6. YAMAMOTO, T.: "On the vibrations of a rotating shaft" Memoirs of the Faculty of Engineering, Nagoya University, Vol.9, p.19, 1957.

7. STRATTON, A.: "Gyroscopes for Inertial Navigation" (James Clayton Lecture) Proc. Inst. Mech. E., Vol.178, Pt.1, p.1129, 1964.

8. HOLMES, J.: "Rotor Ball Bearings for Precision Gyroscopes". Proc. Inst. Mech.E., Vol.179, Part 3E., 1964 - 65.

9. KHARLAMOV, S.A.: "On the Rigidity of a Preloaded Angular Contact Ball Bearing" Isv. Ak. Nauk. SSSR, Mekh.i.Mash. No.5, p.139, 1962.

10. BUCKINGHAM, R.A.: "Numerical Methods" P.336

11. TEARE, B.R: "Theory of Hysteresis Motor Torque" Trans. A.I.E.E. Vol.59, p.907, 1940.

12. MAUNDER, L: "Natural Frequencies of a Free Gyroscope supported in Gimbals on an Elastic Shaft" J. Mech. Eng. Sci. Vol.3, No.4, p.318, Dec.1961.

13. FLOQUET, G.: "Sur les équations différentielles lineaires à coéfficients périodiques" Ann. Ecole Norm. Sup. Paris, Vol.12, p.47, 1883.

14. MALKIN, I.G.: "Some Problems in the theory of non-linear oscillations" U.S. Atomic Energy Commission translation No. AEC tr 3766, 2 vols.

15. LOWIS, O.J.: "The stability of a rotor blade flapping motion at high tip speed ratios" Aeronautical Research Council, 23, 371, O.1663, P.L.134, 1962.

16. PARKS, P.C.: "Discussion on Stability of Systems" Proc. I.Mech.E., Vol.178, Pt.3M, 1963 - 64.

17. WIPPELL, A.P.R., and MAUNDER, L.: "Vibration of a Free Gyroscope on a non uniform Elastic Shaft" J. Mech. Eng. Sci. Vol.5, No.3, p.227, 1963.